# Dynamics in Peptide Folding, Surface Activity and Self-assembly

by

Vikas Parasmal Jain

A Dissertation Submitted to the Graduate Faculty in Engineering in Partial Fulfillment of the Requirements for the Degree of Doctor of Philosophy

The City University of New York

2011

This manuscript has been read and accepted for the Graduate Faculty in Engineering in satisfaction of the dissertation requirement for the degree of Doctor of Philosophy.

| | |
|---|---|
| Date | Prof. Raymond S. Tu<br>Chair of Examining Committee |
| Date | Prof. Mumtaz Kassir<br>Executive Officer |
| | Prof. Charles Maldarelli |
| | Prof. Alexander Couzis |
| | Prof. Lane Gilchrist |
| | Prof. Scott Banta |

**Supervision Committee**

THE CITY UNIVERSITY OF NEW YORK

## Abstract

**Dynamics in Peptide Folding, Surface Activity and Self-assembly**

by

**Vikas P. Jain**

**Advisor: Prof. Raymond S. Tu**

Tunable amphiphilicity is an attractive tool for applications ranging from separation processes to drug delivery. We have designed an α-helical peptide containing 23 amino acids, incorporating hydrophobic residues on one side (leucines and alanines) and hydrophilic residues on the opposite side. Our model peptide shows switchable surface activity, where the folded form (α-helix) of the peptide is amphiphilic and the unfolded form (random coil) is not amphiphilic. Subsequently, we apply this dynamically folding peptide to examine DNA condensation, starting from a fundamental new understanding of biomolecular surface activity and ending with systems that fold, self-assemble, and condense to states relevant for drug delivery.

We demonstrate four properties to show that our model peptide can be applied in dynamic condensation processes. First, circular dichroism shows that our model peptide has transient secondary structure. We show that we can control the equilibrium structure and, thus, control the surface activity. Second, Pendant bubble tensiometry is used to characterize the dynamic amphiphilicity (surface activity) due to folding of the model

peptide. Together, the circular dichroism and pendant bubble tensiometer study shows that our model peptide responds to environmental stimuli with dynamic folding and surface activity. Third, modeling of the dynamic surface activity/amphiphilicity helps in understanding the effect of different factors on folding of the peptide and its transport to the air-water interface. The results indicate that the kinetic adsorption rate of the folded peptide onto air–water interface dominates the dynamic process, which contrasts many head–tail surfactants where diffusion typically dominates over kinetics in the adsorption to interfaces. Additionally, the numerical solution is compared with an asymptotic solution, showing agreement with our findings that the fundamental dynamics of the tunable surface-active peptide are indeed controlled by the adsorption step. Fourth, multi-angle light scattering is used to study the kinetics of DNA condensation. We quantify the rapid self-assembly of the DNA-peptide complex formation, corroborating our hypothesis that the kinetics of DNA condensation are controlled by the folding dynamics of the model peptide. We also compare the scattering data of our model peptide with a common non-folding condensing agent, Spermidine. This work shows our ability to engineer synthetic peptides where tunable amphiphilicity coincides with biomolecular binding, and these rationally designed systems can be used as a potential tool for applications ranging from gene delivery to separations.

# Acknowledgements

First and foremost, I am heartily thankful to my advisor, Prof. Raymond Tu, whose guidance and supervision from the initial to final level enabled me to develop an understanding of the subject. His perpetual energy, acute physical insight on problems and exceptional collaborative skills not only motivated me at every stage of this thesis work but also enriched my growth as a researcher. On many occasions, he shared his own experiences for my betterment. Without his guidance and persistent help, this dissertation would not have been possible. I am indebted to him more than he knows.

I would like to thank my PhD committee, Prof. Charles Maldarelli, Prof. Alexander Couzis, Prof. Lane Gilchrist and Prof. Scott Banta for their constructive comments on this thesis. A special thanks to Prof. Charles Maldarelli for all his help in the modeling of the interfacial transport. I would also like to thank Prof. Ilona Kretzschmar for letting us stay in her lab for the starting 6 months and for all the guidance throughout my PhD career.

In addition, I gratefully acknowledge Dr. Narasimhan Chakravarthy for giving me the opportunity to work on “Characterization of Thermal-stress induced Aggregates in Monoclonal Antibodies,” at Schering-Plough Corporation, New Jersey. I am also

thankful to Dr. Angela Mohs, Dr. Manoj Sharma, Dr. Amardeep Bhalla and Dr. Aniket Badkar for many stimulating discussions during my stay.

Many thanks go in particular to Dr. John Singh, Dr Ashish Gaikwad, Dr. Mahaprasad Kar and Dr. Pandurang Kulkarni for sharing their thoughts with me, which were very fruitful for shaping my career. Furthermore, I would like to thank my present and past group members: Lorraine, Angela, Karolin, Mellissa, Roham, Joseph, Sean, Tommy and Atin for providing a great work environment in the lab. To Andy, Xu and Lisa, thanks for all your help during these years.

I convey special acknowledgment to my friends: Anil, Amar, Shyam, Rohit, Nikhil, Chi, Kevin, Spyros, Gogo, Shripad, Prasad, Rajesh, Swapnil, Abhinav, Jayant, Vilobh, Pinky, Amit, DJ and Mayur. I feel extremely fortunate to have them around whenever I needed. Thank you everyone for making my stay at the City College of New York memorable.

Where would I be without my family? Words fail to express my gratitude to my family. I owe them for their love and inseparable support; this dissertation is simply impossible without them. I am thankful to my brothers, Manoj and Ansul, and my sister-in-law Deepaxi, who has always cheered, supported and motivated me whenever I needed. Finally, I would like to dedicate this thesis to my parents, Mrs. Leela Patni and Mr. Parasmal Patni, for their dedication, love and prayers. I am extremely indebted to them for providing the necessary stepping-stone to achieve my goals in life.

Vikas Parasmal Jain

# Contents

# List of figures

# List of tables

# Chapter 1

# Introduction

Transient folding of proteins is a common natural phenomenon that facilitates the protein's ability to bind targets with unparalleled specificity and time scales on the order of seconds in environments full of similar targets. This process is not possible with the classic static 'lock-and-key' perspective; rather, dynamic structural transitions may be required for the selectivity and kinetics observed in nature [2, 9-15]. The goal of this work is to rationally design a peptide that captures this behavior by coupling folding to surface activity, resulting in dynamic amphiphilicity of peptide-based helices and how it can be used for different applications like gene therapy and DNA separations. We explore the rational design of model peptides that can serve as templates for future designs that will incorporate selectivity inherent in helical biological molecules. The primary structure of our peptides is designed in such a way that upon folding the hydrophobic and hydrophilic domains become spatially disjoint, leading to amphiphilic behavior.

Moreover, we are inspired by biological systems where the folding can be coupled to an external stimulus.

The peptide design that couples folding and amphiphilicity can be contrasted to the typical mode of protein adsorption, where adsorption of a natural protein to an interface (solid or air) is typically coupled to unfolding event, where the hydrophobic core is exposed to the interface. Miller et al. review this process for proteins, describing the dynamic and equilibrium adsorption of protein–surfactant systems [16]. In contrast, our peptide system mimics nature's ability to stabilize secondary structure on binding. Many proteins found in nature are natively disordered, but when they bind to the protein's specific target, the disordered structure folds into a more ordered state. From this, we know that folding and binding are often cooperative processes leading to enhanced kinetics of binding to macromolecular targets. Applying these dynamics to peptide design, one can create novel peptide sequences that have dynamic surface activity by folding in response to environmental cues.

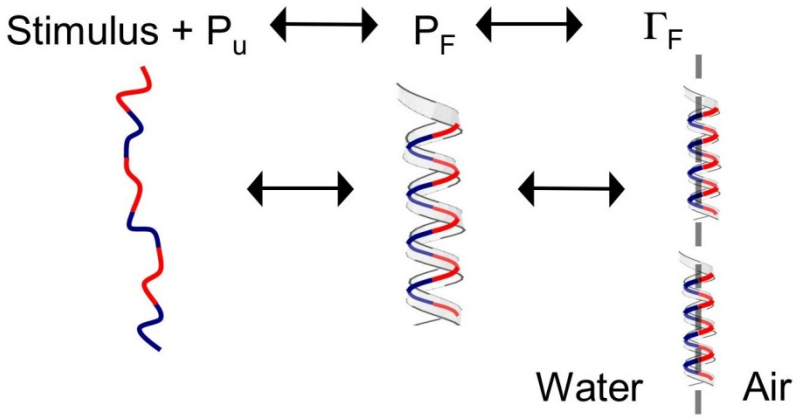

**Figure 1-1.** Folding initiated interfacial dynamics. The peptide (red = hydrophobic, blue = hydrophilic) is ensemble average unfolded ($P_U$). The sequence folds in the presence of a stimulus into an α-helical conformation ($P_F$). The α-helical conformation is amphiphilic. Folding will promote interfacial adsorption ($\Gamma_F$, concentration of folded peptide at interface).

Figure 1-1 shows the concept behind the design of our model dynamic surface-active peptide, where folding is a consequence of some environmental cue. In contrast to designing for static binding with a fixed target site, the novelty of our design approach is that binding behavior results in structural transition and, therefore, a transition in surface activity. Such a peptide with tunable surface activity can be designed to bind to a wide range of targets, coupling dynamic surface activity to selective binding.

## 1.1 Outline

In the second chapter, we introduce the fly-casting mechanism and discuss its advantages over the static 'lock n key' method. We will look at the different DNA and RNA binding system reported in the literature where binding is coupled to folding i.e. fishing mechanism is observed. In the same chapter, we will also introduce the process of DNA condensation, different condensing agents used and the challenges faced in the process of DNA condensation.

In the third chapter, we will discuss how new sequence designs can be developed based on a set of simple design "rules" for defining the thermodynamics of a synthetic helical peptides. In the same chapter, we will discuss the ability to use these rules in

combination with native binding sequences to engineer new amphiphilic peptide analogues. We will also look at the model peptide designed by us using the rules discussed in the previous section. Finally, we will briefly summarize the solid phase peptide synthesis process used to precisely synthesize the model peptide.

In the fourth chapter, we will characterize the model peptide in bulk by using circular dichroism and at air-water interface by using pendant bubble apparatus. In this chapter, we will show that our model peptide exhibit the phenomena of folding coupled to surface activity/amphiphilicity.

In the fifth chapter, we model the dynamic surface activity due to folding of the peptide and get the different parameters involved in transporting the peptide from bulk onto air-water interface. In this chapter, we will look that the effects of different parameters ($\sigma$, $\omega$ and $\varepsilon$) on the folding dynamics and dynamics in surface activity. We also compare our numerical solution to the asymptotic solution to confirm the results obtained from the numerical solution.

In the sixth and seventh chapter, we will look at using this system where folding is coupled to surface activity/amphiphilicity in different applications. In sixth chapter, we examine the kinetics of DNA condensation by using our model peptide. In the seventh chapter, we perform liquid crystal experiments and show how one can use the dynamic folding and amphiphilicity for the biosensing application. In the final chapter, we summarize our findings and point to future directions where rationally design peptides constructed to be dynamically amphiphilic could be applied.

# Chapter 2

# Background – coupled folding and binding

In this chapter, we discuss the idea behind the design of our model peptide i.e. folding coupled to surface activity/amphiphilicity. We will look at the fly-casting mechanism and discuss how this mechanism helps in controlling the kinetics, stability and selectivity of the overall binding process. We will also look at different proteins and other biologically inspired molecules that binds to DNA/RNA where folding is coupled to binding. In the end we introduce the process of DNA condensation and different challenges faced in understanding this condensation phenomenon.

Configurational dynamics in proteins have been found to be critical to a variety of physiological processes [10, 35] such as transcription and translation regulation [36], cellular signal reduction [37], protein phosphorylation [38] and molecular assemblies [39]. The cooperative processes of folding and binding are important to many of these biological processes and include several intra- and inter-molecular factors that

determine the interaction dynamics between the proteins and their targets [40]. Due to complexities involved in these interactions and protein folding, engineering simple hybrid peptide designs has emerged as an attractive tool to understand protein/peptide structure, function and dynamics.

Amphiphilic α-helices are a commonly observed structural feature found in many proteins and biologically active peptides. This structural motif has been found to play multiple roles in protein folding, protein-protein recognition, protein-membrane interactions, and protein and peptide biological activity [41]. The amphiphilic architecture is also important for the stabilization of the secondary structure of peptides/proteins when they bind to apolar surfaces such as phospholipids membranes, air etc [42, 43]. While a plethora of studies have examined the structural role of these helices in proteins, there remains a paucity of studies that examine the critical role of dynamics in the functional role of amphiphilic α-helices.

Designing biomimetic peptides from natural analogues requires a lucid perspective on naturally occurring protein folding and binding as cooperative processes [9, 11, 14, 35], where the protein searches for favorable intramolecular or intermolecular interactions [44-46]. There are many proteins in nature that are disordered in their physiological condition, but when they bind to the specific target or site, they become more ordered [12, 14, 15, 47]. This phenomenon of coupled folding to binding has been shown to enhance the binding kinetics and the selectivity of the overall binding process [46, 48]. Induced folding of the protein has some biological advantages over the static ‘lock-and-key’ method. First, flexible unstructured domains have an intrinsic plasticity that allows them to accommodate targets of various size and shape; and second,

free energy of binding is required for compensation for the entropic cost of ordering of the unstructured region. A site that does not provide enough binding free energy cannot induce folding and, hence, cannot form stable complex. Shoemaker et al showed that relatively disordered proteins molecule has a bigger capture radius as compared with the ordered protein molecule and the mobility of the folded protein is restricted due to conformation that is not the case with the unfolded protein. In this scenario, unfolded protein binds weakly to its target site at a relatively large distance followed by the folding of the protein as it approaches the specific binding site. This mechanism has been coined the "Fly-casting mechanism" (figure 2-1) [2, 13].

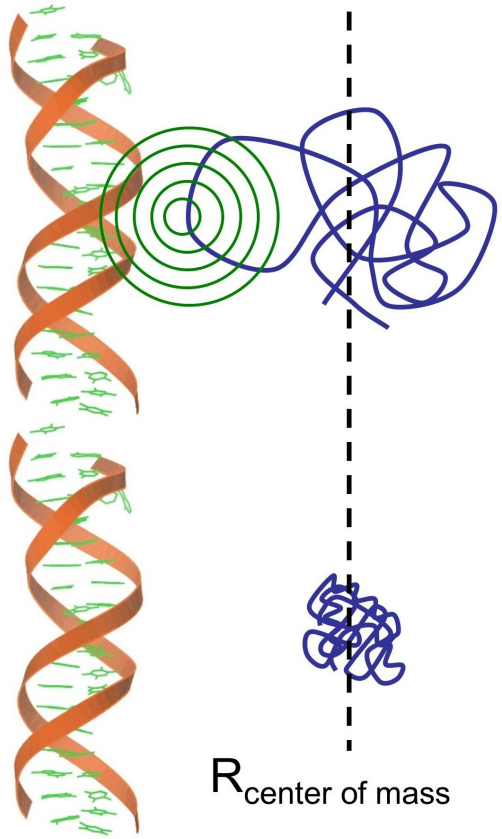


**Figure 2-1.** A cartoon representing the increase in the kinetics of the binding process due to fly-casting mechanism (adapted from Shoemaker et al [2]).

Engineering synthetic peptides with controllable molecular architectures that mimic the natural phenomena observed in this class of proteins requires careful consideration of the dominant inter- and intramolecular interactions. The goal of this work is to rationally design a peptide that captures this behavior by coupling folding to surface activity, resulting in dynamic amphiphilicity of peptide-based helices. In the following section, we will look at several protein systems and biologically inspired peptide systems that have the ability to bind DNA and RNA, changing states from intrinsically disordered to ordered on binding

## 2.1 DNA/RNA binding intrinsically disordered proteins as motivation

### 2.1.1 DNA binding proteins

A handful of researchers have attempted to use these intrinsically disordered proteins as the models for their peptide design, where peptides are constructed to mimic the dynamics of the binding process observed in nature. These authors are motivated to design peptides that explore the fundamental relationship between the dynamics of the folding and the kinetics of the selective binding that will allow to better understanding of the overall process. Such peptides with accelerated kinetics can be used for designing new generation of molecules that can be used as rapid acting diagnostic tools. For example, the basic leucine zipper family (bZIP), one of the best characterized family of DNA binding motif, consist of a N-terminal basic region that binds to a specific sequence of DNA and C-terminal leucine zipper that is responsible for dimerization [49-51]. In the

absence of DNA, leucine zipper is helical and dimeric while basic region is flexible and partially disordered. In presence of sequence specific DNA, the basic region is fully helical which shows that the folding of the protein is coupled with the binding to its DNA. O'Neil et al designed different peptides based on leucine zipper motif that helps in understanding the interaction of DNA with this class of proteins [52]. An induced helical fork model has been devised suggesting that the role of the leucine zipper is to position the basic region so that the zipper can both interact with DNA and promotes the helix formation in the basic regions, where helicity is induced in basic region only in presence of the target DNA. The helical fork model also identifies the residues that are important for helix stability but do not help in DNA recognition.

O'Neil et al replaced these residues with the small, neutral, helix favoring amino acids and designed different peptides and observed that the basic region forms the helix that binds to the major groove of DNA. The authors also showed that the specificity is maintained as the binding with non-specific DNA do not show rise in helicity of basic region as compared to that with specific DNA. Talanian et al showed that the basic region of the yeast transcriptional activator GCN4, which belongs to the bZIP family, retains the sequence specificity even when the leucine zipper is removed [53]. A peptide was synthesized with the basic region corresponding to the residues 222-252 of GCN4 and the leucine zipper was replaced with the Gly-Gly-Cys liner at the C-terminal. This peptide was then dimerized to give disulphide-bonded dimer and by using DNase I footprinting showed that it retains the sequence specificity by comparing the results with the basic region attached to leucine zipper. The minimum length for the basic region sequence for specific binding was also determined [53, 54]. Peptides of different sizes of basic region

were synthesized with the GGC linker attached to give disulphide-bonded dimer after dimerization. DNase I experiments were conducted, and it was found that the peptides containing 20 residues of GCN4 basic region show the same sequence specificity as that of intact protein. Also, circular dichroism experiments showed that 15 residues from the basic region of GCN4 (231-245) for a helix when contacting the specific DNA target. This sequence provides a template for peptide designs to study the interactions of a class of DNA-binding peptides where folding and binding are cooperative.

Other authors have taken advantage of this inherent modularity of DNA-binding sequences, combining dimerization domains with DNA binding domains. Kim et al designed a peptide consisting of alternate lysines (KGKGKGK) and the leucine zipper as a dimerization domain. This peptide sequence has been shown to bind specifically to Z-DNA [55]. Tu et al modified the bZIP sequence by adding alkyl tails to the C-terminus that formed mono- and dialkyl bZIP peptide-amphiphiles and investigated the effects of this modification on secondary structure and self-assembly formation [56]. Tu *et al*. observed that the peptide amphiphiles combines the characteristic of the basic zippers and cationic amphiphiles, capturing the functional behavior of both. The peptide amphiphiles enhance secondary structure and form hierarchical structures as they bind to DNA in helical conformation. Peptide amphiphiles, in general, are capable of forming hierarchical assemblies, making them an interesting choice to use as functional building blocks for different systems like gene delivery and artificial transcriptional factors [57, 58].

### 2.1.2 RNA binding proteins

RNA-protein interactions have also gathered attention [59, 60]. During the

interactions, folding can be induced in RNA alone, protein alone or in both RNA and protein [61-63]. For example, folding is induced in RNA when ribosomal S15 protein binds to rRNA [61], while binding of antitermination protein N of bacteriophage λ with its cognate RNA induces folding in the completely disordered protein [64]. Binding of neuleolin protein with its cognate stem loop RNA, induces folding of RNA hair loop and the ordering of the two RNA binding domains of the protein [63, 65]. Here, flexibility in both RNA and protein is essential for tight binding and also for RNA sequence recognition. In another example, the TMV (Tobacco Mosaic Virus) coat protein has a 25-residue loop that is disordered which undergoes a disorder-to-order transition upon RNA binding during the assembly of the capsid [66-69].

Several authors have shown that Rev protein, an essential regulatory protein encoded by human immunodeficiency virus (HIV) has arginine-rich binding regions that are found in many viruses [70-72]. In this case, specific binding of Rev protein to RNA not only stabilizes the complex but there is change in conformation of RNA [73]. At low temperature, an increase in the helicity of Rev peptide is observed when it binds selectively to IIB RNA, which again suggest that the binding is coupled to the folding [74]. Tan et al showed that the peptide consisting of residues from this region (corresponding to amino acids 34-50 of HIV Rev protein) is not only responsible for target specificity, but also retains binding affinity as tight as that of the isolated intact protein. It is also showed that the peptide is able to bind the rev responsive element (RRE) specifically and is sufficient for a high binding affinity, comparable to that of Rev [74-76].

The examples described above represent scenarios where researchers have used

intrinsically disordered proteins as models for the design of their peptides. The motive behind the design of these peptides is to mimic the original protein, but engineering synthetic peptides that will mimic the dynamics observed in nature requires careful consideration of the dominant inter- and intra-molecular interactions. Defining the thermodynamics of secondary structure stability will help in understanding the structure-function relationship, leading to better understanding of the overall dynamics observed in nature. In the following section, we will look the phenomenon of DNA condensation, different condensing agents used to study DNA condensation and challenges faced in understanding this phenomenon. We plan the control the kinetics of DNA condensation by controlling the dynamics of folding of our model peptide.

## 2.2 DNA condensation

DNA condensation has received careful consideration over the last few decades [17, 18]. The phenomenon of counterion-mediated DNA-condensation is fundamental to most DNA related activity in the cell, from chromosome packaging to control over translational mechanisms. Developing synthetic systems to manipulate DNA-condensation is essential for the development of biotechnologies for gene encapsulation and DNA-separation. Cellular DNA condensation into histone complexes requires that the DNA collapse from extended chains into compact, well-ordered self-assemblies called chromatin. Genomic DNA is a long polyelectrolyte that must fit into exceptionally small spaces such as the inside a cell nucleus or viral capsid. The average person's DNA (3 billion base pairs per cell) covers a total linear distance of approximately $2x10^{10}$ kilometers or about 2 meters per cell, which is 200,000 times the

average cellular diameter. So, to fit such large DNA of our twenty-three chromosomes into the nucleus (~1 um in diameter) requires an extraordinary degree of hierarchical packaging. Forces involved in the DNA condensation process have been identified [17-20]. The energetic barriers to such tight packaging are the loss of configurational entropy of the long DNA molecule, the tight bending of the stiff double helix and the electrostatic repulsion of the negatively charged phosphates in the DNA backbone. All of which contribute to a persistence length of DNA ~50 nm or ~150 base pairs. The phenomenon of DNA condensation is not only significant from biological application point of view but it also poses challenging questions for physical understanding of the condensed matter. We know that the condensing agent should neutralize 89-90% of the charge on the DNA for the condensation phenomenon to occur. Additionally, the final state of the condensate is known to be kinetically controlled and not thermodynamically [17, 18].

In nature, positively charged histone faces the negatively charged (phosphate) groups of the DNA's backbone. From electrostatics point of view, binding is due to the association of fixed multivalent positive and negative charges, so one would expect the binding of proteins to DNA to be dominated by an enthalpy decrease. But thermodynamic studies of the enthalpic and entropic contributions to the binding free energy indicate that protein-DNA binding is dominated by an entropy increase that depends logarithmically on the ambient salt concentration [21].

The primary driving force behind this interaction is counterion-mediated condensation. When two oppositely charged ions are far apart, a large part of their charges are already compensated by their counterions. Consequently, the enthalpy change that accompanies oppositely charged multivalent-ion association is modest. However,

when the oppositely charged multivalent-ions do associate, a number of opposite charges on the respective ions are brought in close proximity and a proportional number of counterions are released to the solution phase (this is a long ranged interaction resulting from correlated fluctuations). The resulting entropy gain of these released counterions is largely responsible for the binding process [22, 23]. Our initial studies explore the nonspecific electrostatic interaction between amphiphilic peptides and DNA, but future work will examine more specific interactions. Figure 2-2 depicts this process, showing a negatively charged DNA (orange), condensing into a well-packed nucleosomes (blue) in the presence of multivalent positively charged proteins (histone). This general process occurs in every living organism.

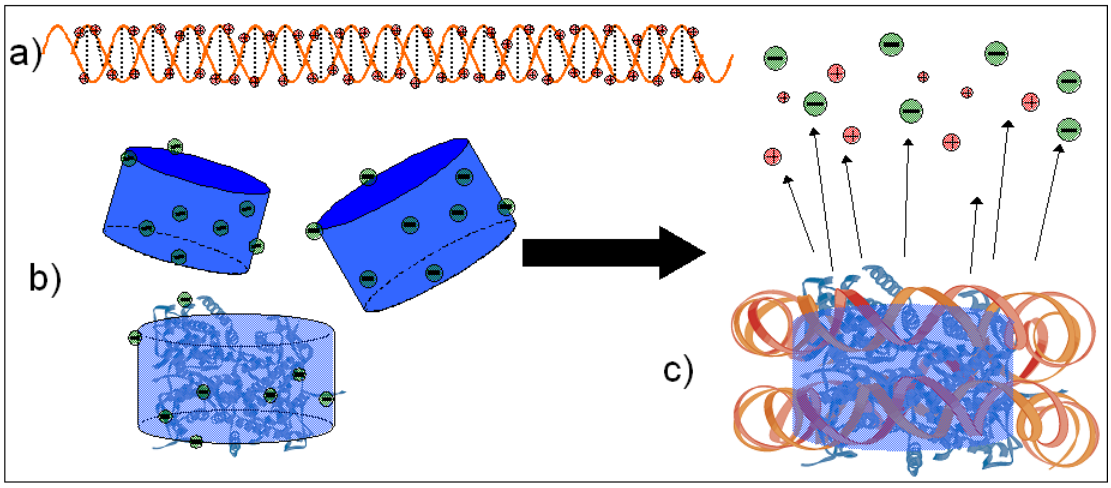


**Figure 2-2**. a) Negatively charged DNA (orange) with positively charged monovalent counterions condenses onto b) positively charged histones (blue) with negatively charged counterions. c) nucleosomes are formed by counter-mediated condensation, where the counterion release results in a significant increase in entropy.

The phenomenon of DNA condensation is a critical step in the formulation of gene

therapy delivery vectors. Genes are carried on chromosomes, and these chromosomes are the basic functional units of heredity. Gene therapy is a technique for correcting defective genes responsible for disease development. Carrier molecules, called vectors, are used to deliver the therapeutic gene to the target cells. In the beginning viral based carriers were used for gene delivery. Viruses have evolved a way of encapsulating and delivering their genes to human cells in a pathogenic manner. So, one can take advantage of this capability and manipulate the virus genome by removing disease-causing genes and inserting therapeutic genes. Some of the different types of viruses used as gene therapy vectors are retroviruses, adenoviruses, adeno-associated viruses (AAV) and herpes-simplex viruses. Due to toxicity and immunogenicity associated with the viral vectors, focus has shifted towards the non-viral based gene carrier.

Non-viral based carriers have advantages over viral based carrier for a number of reasons, but primarily because they present fewer toxicity and safety issues [24]. Additionally, longer DNA can be delivered with non-viral based vectors. Cationic liposomes have become the standard for non-viral based carriers, and they can be used to transfer ~ 1Mbp sections of the human artificial chromosomes. The drawback is that the transfection efficiency is low for non-viral based carriers as compared with viral based carriers [24, 25]. In addition to cationic lipids [24-29], other synthetic vectors include naturally occurring polyamines [30, 31] spermidine$^{3+}$ and spermine$^{4+}$, inorganic cation $Co(NH_3)_6^{3+}$ [17, 32], cationic polypeptides [33] such as poly L-lysine [34] and basic protein such as histone H1 and H5. Understanding how these common synthetic vectors condense DNA and how the nanostructure influences efficacy has been critical in the design of new molecules for non-viral gene therapy.

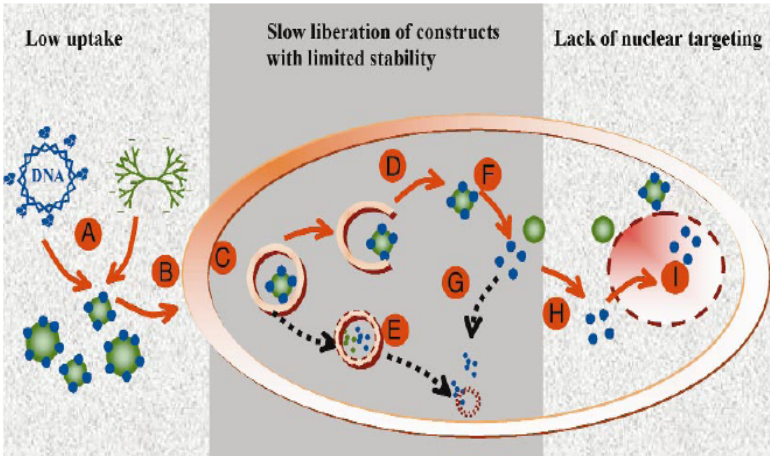


**Figure 2-3**. Schematic drawing of DNA delivery pathways with three major barriers. A. DNA complex formation B. Uptake C. Endocytosis D. Escape from endosomes E. Degradation F. Intracellular release G. Degradation (cytosol) H. Nuclear targeting I. Nuclear entry and expression [1].

Most DNA delivery systems operate at three levels: DNA condensation and complexation, endocytosis and nuclear targeting/entry (figure 2-3). After DNA condensation, the complex formed is taken up by cells usually through endocytosis. Endocytosis is a multistep process involving binding, internalization, and formation of endosomes, followed by fusion with lysosomes. There is degradation of entrapped DNA and associated complexes due to extremely low pH and enzymes within endosomes and lysosomes. Finally, the remaining DNA must then dissociate from the condensed complexes either before or after entering the nucleus. Once inside the nucleus, the transfection efficiency of the delivered DNA is mostly dependent on the composition of the gene expression system [1]. There are three major barriers in effective DNA delivery: low uptake across the plasma membrane, inadequate release of DNA molecules with limited stability and lack of nuclear targeting, see figure 2-3. Overcoming these barriers

will improve the transfection efficiency dramatically.

In our work, we describe a new condensation approach that addresses several of these issues. Stability of complex is a problem related to kinetics as DNA condensation is a reversible process, and condensation depends on the association of sufficient multivalent counterions to the DNA. Additionally, decomplexing of DNA before or after it enters the target nucleus is a biomolecular separation problem. Nanostructure is critical because DNA complex uptake by the cell is the transport problem that has been shown to be related to the nanoscale organization of the complexed assembly [24]. The work described here will explore the kinetics of the condensation phenomena with our rationally designed model peptide. We show that one can control the kinetics of DNA condensation by controlling the dynamics of peptide folding. Compared with other condensing agent, peptides offer a unique parameter to manipulate DNA-peptide complex structure at the molecular level: the ability of these peptides to fold into intramolecular secondary structure, α-helix and β-sheet. In addition, other parameters that can be used to manipulate the final DNA complex structure are the length of the peptide chain and the overall charge on the peptide sequence. Systematic design algorithms can be applied to improve understanding of condensation related mechanism at the molecular and self-assembled levels. Here we do not study DNA transfection across a membrane, but we investigate the first stage of the transfection process i.e. DNA-protein binding and DNA condensation. In third chapter, we will examine simple "rules" that one could apply to design an amphiphilic α-helix.

# Chapter 3

# Designing amphiphilic α-helix peptides

In this chapter, we will look at the different parameters to be taken into consideration to engineer a synthetic peptide with well-defined secondary structure. We will discuss the 'rules' of periodicity and propensity that are used to design the synthetic peptide and also the other parameters that help in stabilizing the α-helix. We will also look at various efforts reported in literature to understand structure-function relationship of the processes observed in nature by synthetic peptides whose designs are based on the secondary structure. In the end, we report the design of our model peptide and solid phase peptide synthesis process used to synthesize the model peptide.

In order to better understand the fundamental thermodynamics that described the cooperative phenomenon, a variety of strategies have been successfully employed to define a dynamically folding helix whereupon one can build rapid binding selectivity [77-84]. One simple strategy is to design an amphiphilic α-helix peptide based on a two-part

algorithm, where (1) intrinsic propensity and (2) periodicity define helical stability. We will be using these two rules to rationally design our model peptide. Before we discuss the design of our model peptide, we will discuss the different parameters to be taken into consideration for designing amphiphilic α-helix.

## 3.1 Helical Propensity and Periodicity

In 1974, Chou and Fasman [85] defined intrinsic propensity by calculating the conformational parameters of the 20 amino acids from the frequency of occurrence of these different amino acids in α-helix, β-sheets and random coil in 15 proteins (Table 3-1). This conformational parameter refers to the intrinsic inclination of individual amino acids to a given secondary structure, where side-group, van der Waals and steric interactions tend to restrict an amino acid to particular Φ and Ψ conformations.

DeGrado and Lear defined periodicity by investigating the role of hydrophobicity in the peptide sequence in determining the secondary structure in bulk and at apolar/water interfaces [4]. These nonlocal interactions are "programmed" into the sequence with a recurring pattern that defines a particular secondary structure where α-helices have a periodicity of 7 (35 amino acid per turn), meaning that the amino acids at i and i+7 define the refrain and β-sheets have 2 residues per turn (figure 3-1). The study was based on the design of three synthetic peptides comprising of only leucine (L) and lysine (K) with different hydrophobic periodicity and chain length. As all the three peptides consist of only two amino acids, intrinsic propensity for each peptide is the same and the only difference is the effect of hydrophobic periodicity on the secondary structure (Table 3-2).

**Table 3-1.** Chou and Fasman' conformation parameters of the 20 amino acids.

| **Helical Residues** | **Pα** | **β-Sheet residues** | **Pβ** |
|---|---|---|---|
| $Glu^{(-)}$ | 1.53 | Met | 1.67 |
| Ala | 1.45 | Val | 1.65 |
| Leu | 1.34 | Ile | 1.60 |
| $His^{(+)}$ | 1.24 | Cys | 1.30 |
| Met | 1.20 | Tyr | 1.29 |
| Gln | 1.17 | Phe | 1.28 |
| Trp | 1.14 | Gln | 1.23 |
| Val | 1.14 | Leu | 1.22 |
| Phe | 1.12 | Thr | 1.20 |
| $Lys^{(+)}$ | 1.07 | Trp | 1.19 |
| Ile | 1.00 | Ala | 0.97 |
| $Asp^{(-)}$ | 0.98 | $Arg^{(+)}$ | 0.90 |
| Thr | 0.82 | Gly | 0.81 |
| Ser | 0.79 | $Asp^{(-)}$ | 0.80 |
| Arg | 0.79 | $Lys^{(+)}$ | 0.74 |
| Cys | 0.77 | Ser | 0.72 |
| Asn | 0.73 | $His^{(+)}$ | 0.71 |
| Tyr | 0.61 | Asn | 0.65 |
| Pro | 0.59 | Pro | 0.62 |
| Gly | 0.53 | $Glu^{(-)}$ | 0.26 |

**Table 3-2.** Peptide sequence with hydrophobic periodicities, intrinsic propensity of the sequence and the observed conformation in bulk.

| Peptide | Repeat period | Intrinsic propensity | Results |
|---|---|---|---|
| LKKLLKL (A) | 3.5 | α (Pα = 1.19, Pβ = 1.06) | Too short |
| $(LKKLLKL)_2$ (B) | 3.5 | α (Pα = 1.19, Pβ = 1.06) | α |
| LKLKLKL (C) | 2.0 | α (Pα = 1.19, Pβ = 1.06) | β |

Chou-Fasman parameters for all the three peptides are Pα = 1.19 and Pβ=1.06, yielding an intrinsic inclination towards α-helix. The hydrophobic periodicity for peptides A and B matches to that of α-helix, and the periodicity for peptide C matches to that of a β sheet. Circular dichroism was used to measure the secondary structure in bulk, and Langmuir Blodgett technique was used to study the properties of peptides at an air-water interface. Peptide conformation at the air-water interface was determined by compressing the peptide monolayers and transferring them to solid substrate by using Langmuir Blodgett, and the degree of secondary structure was quantified by using infrared and circular dichroism spectroscopy. Circular dichroism in bulk solution showed that the peptide A was too short to form α-helices while peptide B showed α-helix secondary structure, while peptide C formed β-sheets. In Peptide C, the presence of the hydrophobic periodicity (2.0) appears to override the short-range interactions and forms β-sheets, despite the helical propensity. This shows the periodicity of the polar/non-polar residues dominates the intrinsic propensity.

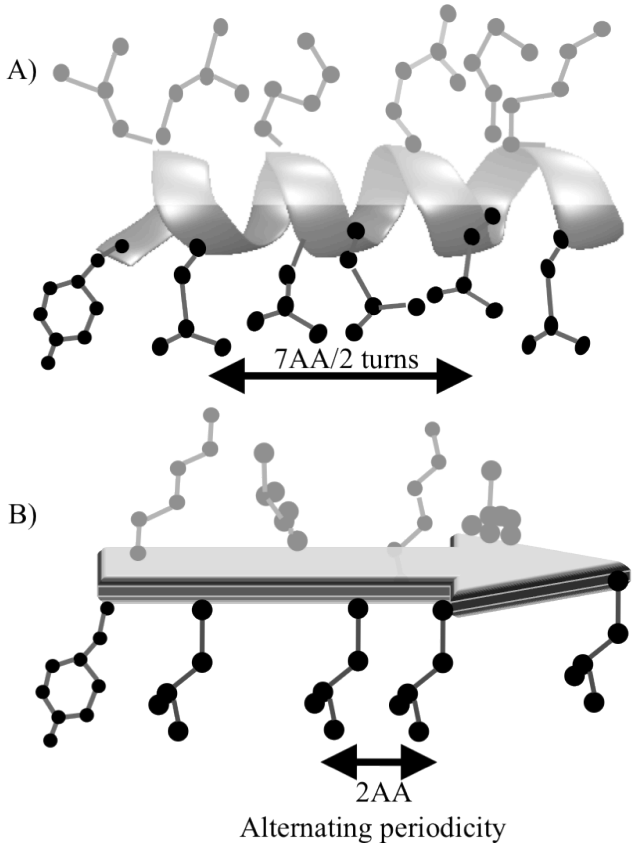


**Figure 3-1.** Peptide in α-helix (A) and β-sheet (B) conformation with polar side chains showed in gray color while non-polar in black color. Amino acid sequence matches the periodicity requirement for α-helix and β-sheet making it amphiphilic (adapted from Xiong et al [3]).

Langmuir Blodgett experiments showed that peptides B and C formed more stable monolayers as compared with peptide A. Due to hydrophobic periodicity, peptides B and C form a more stable secondary structure such that the hydrophobic residues are segregated on one side, forming an apolar surface (Figure 3-2). At air-water interface, the apolar surface of the peptide will partition into air phase, where the free energy of dehydration of the hydrophobic side chains is the driving force for separation, stabilizing

the amphiphilic secondary structure of the peptide.

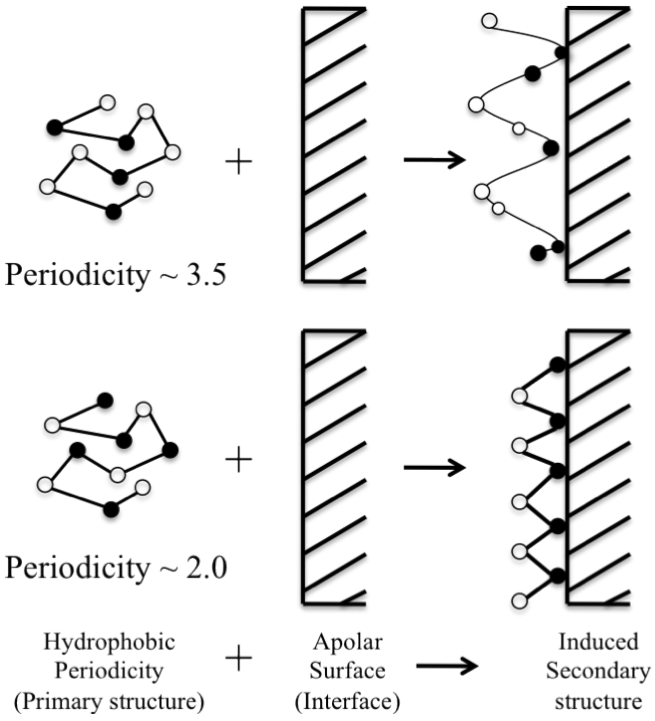


**Figure 3-2**. Schematic diagram for showing the effect of hydrophobic periodicity on the secondary structure at interfaces. Filled circles are hydrophobic residues and open circles are hydrophilic residues.

Peptide at apolar/water interface arranges in such a way that will maximize the contact between hydrophobic residues and apolar surface and the contact between hydrophilic surface and aqueous environment (adapted from DeGrado et. al [4]).

Xiong et al [3] observed the similar results, showing that the periodicity of polar and non-polar residues that determines the secondary structure of the given amino acid sequence by comparing the intrinsic propensities of amino acids to polar/non polar periodicity by direct competition. Two groups of peptides (Figure 3-3) were designed, where group A consisted of Leu, Lys and Glu, and group B consisting of Ile, Arg and

Asp. Each group has one hydrophobic residue, one negatively charged residue and one positively charged residue. Amino acids in group A has a intrinsic inclination towards α-helix secondary structure while that in group B have tendency to form β-sheets. In group A, peptide I is 'programmed' such that it favors the α-helix secondary structure predicted by intrinsic inclinations while periodicity of peptide II opposes the α-helical secondary structure. Similarly, in group B, peptide III is 'programmed' such that it favors the α-helix secondary structure, which is opposed by the intrinsic inclinations of the amino acids in the group, while periodicity of peptide IV favors the β-sheet secondary structure. Thus, there are two sets of peptides where the intrinsic inclination and periodicity favor each other or they oppose each other.

Group A (amino acids with α-helix intrinsic propensities)

Peptide I (α-helical periodicity)

Tyr-Leu-Glu-Glu-Leu-Leu-Lys-Lys-Leu-Glu-Glu-Leu-Leu-Lys-Lys-Leu

• • − − • • + + • − − • • + + •

Peptide II (β-strand periodicity)

Tyr-Lys-Leu-Glu-Leu-Lys-Leu-Glu-Leu

• + • − • + • − •

Group B (amino acids with β-sheet intrinsic propensities)

Peptide III (α-helical periodicity)

Tyr-Ile-Asp-Asp-Ile-Ile-Arg-Arg-Ile-Asp-Asp-Ile-Ile-Arg-Arg-Ile

• • − − • • + + • − − • • + + •

Peptide IV (β-strand periodicity)

Tyr-Arg-Ile-Asp-Ile-Arg-Ile-Asp-Ile

• + • − • + • − •

**Figure 3-3.** Group A is composed of amino acids with α-helix intrinsic propensities and Group B is composed of amino acids with β-sheet intrinsic propensities. + and -: Polar amino acids and •: non-polar amino acids (Xiong et al [3]).

Using circular dichroism, they showed that peptide I that has intrinsic inclination

(Pα=1.28, Pβ=0.90) towards α-helix forms an α-helix while peptide III that has intrinsic inclination towards β-sheet (Pα=0.97, Pβ=1.14) also forms an α-helix despite the sheet-forming propensity of the group. These Pα and Pβ values were calculated using the method described in Chou and Fasman [85]. Similarly, peptide II has intrinsic inclination towards an α-helix but forms a β-sheet. Their work corroborates the idea that periodicity of polar and non-polar residues dominates the secondary structure of the sequence.

## 3.2 Stability

Stability of the secondary structure is also an important aspect in designing synthetic peptides. The Hodges group investigated the effect of hydrophobicity of amino acids side chains and intrinsic propensities on the stability of an amphiphilic α-helix [86]. It was found that even though hydrophobicity and intrinsic propensities are not correlated with each other, they do contribute to the stability of amphiphilic α-helix. These experiments show that the synergistic effect of intrinsic propensities and hydrophobicity drives the formation of stable helices. DeGrado and O'Neil determined the thermodynamic stabilities of the naturally occurring amino acids in α-helix as against random coil [87] while Lyu *et al*. determined the role of amino acids side chains in stabilizing/destabilizing α-helix [88]. Lyu *et al.* designed the synthetic peptide with the block sequence $YSE_4K_4X_3E_4K_4$, where X is any amino acid residue. The extent of helicity of the different peptides was determined by using circular dichroism and the order for neutral amino acids stabilizing the α-helix is found to be Ala > Leu > Met > Gln > Ile > Val > Ser > Thr > Asn > Gly. DeGrado and O'Neil observed similar results for

helix stabilizing tendencies that is Ala > Leu > Phe > Ile > Val. Another important aspect in designing a stable α-helix peptide is the chain length of the sequence. DeGrado and Lear [4] found that helix formation requires 14 residues while β-sheet requires 7 residues. This was proven by the LK peptides described above. Peptide A does not form helices as the periodic sequence becomes shorter, but peptide B forms stable α-helices with two septet repeats. Narita *et al*. observed the similar results for the critical chain requirement for α-helix and β-sheet [89]. Under forcing conditions, low dielectric solvents that favors the secondary structure formation, critical chain length for α-helix is approximately 13, and the critical chain length is four residues for β-sheets.

These studies together show that the primary structure of a peptide can be designed by using intrinsic propensity and periodicity of polar/non-polar amino acids, where upon folding the hydrophobic and hydrophilic domains become spatially disjoint, leading to amphiphilic behavior. Still, the activity of these amphiphilic sequences captures only one aspect discussed in the introduction, namely, conformational selection and not fly-casting. The following section discusses the potential to apply these dynamics to peptide design for selective binding, where one can create novel peptide sequences that have dynamic amphiphilicity by folding in response to environmental cues. Such a peptide with tunable amphiphilicity can be designed to bind to a wide range of targets, coupling dynamic amphiphilicity to selective binding. Moreover, these peptides can take advantage of the accelerated kinetics inherent in natively unfolded structures and applied as a template for next generation biologically inspired molecular designs.

## 3.3 Engineered synthetic peptides

### 3.3.1 Membrane mimics

Amphiphilicity is an important characteristic of many membrane bound peptides and proteins such as apolipoproteins, peptide hormones, and signal peptides. Plasma Apolipoprotein (Apo-I) consists of six highly homologous 22 amino acid segments, each containing amino acids with a high α-helix propensity and periodicity [90] (Figure 3-4A). A model docosapeptide is designed by equally distributing acidic and basic residues on the hydrophilic side and amino acids were selected such that the model peptide is different from the repeating Apo-I peptide sequence. The Apo-I mimic peptide has the potential to form an amphiphilic α-helix and has the similar binding characteristic of apolipoprotein A–I by comparing the different criteria such as binding to phospholipid single bilayer vesicles, surface activity and ability to activate lecithin:cholesterol acyltransferase [91, 92].

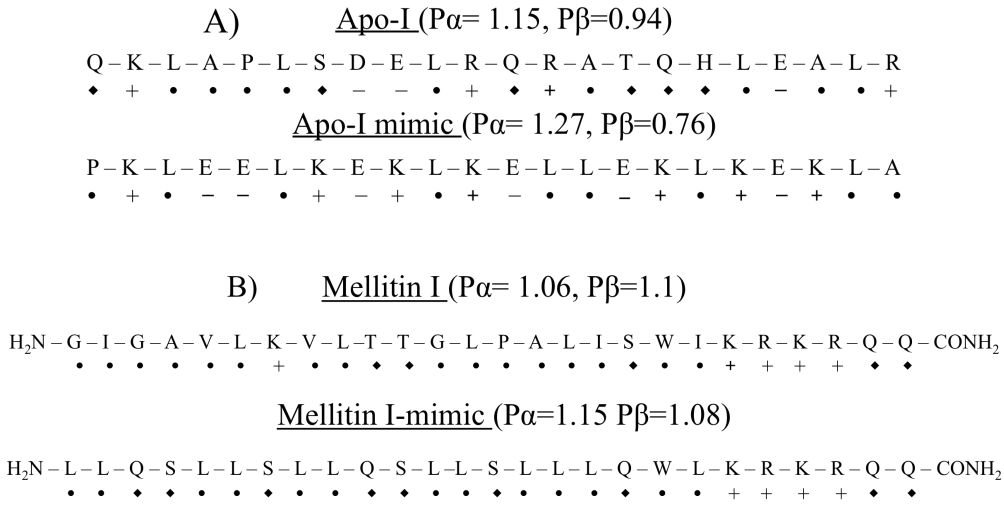


**Figure 3-4.** (**A**) Amino acid sequence of Apo I and its analogous synthetic amphiphilic peptide; (**B**) Amino acid sequence of Melittin I and its analogous synthetic amphiphilic peptide. + and −: Polar amino acids; ◆: polar neutral amino acids; •: non-polar amino acids.

Melittin, a toxic component from bee venom, is a hexacosapeptide in which the *N*-terminal region is predominantly hydrophobic (residues 1–20) and *C*-terminal is predominantly hydrophilic (residues 21–26) (Figure 3-4B). It has many properties similar to the apolipoproteins as it also binds to phospholipids bilayer, forms stable monolayer at the air-water interface and forms α-helix upon tetramerization or when bound to sodium dodecyl sulphate micelles or phospholipids bilayers [93]. The membrane interface has a potent ability to induce the secondary structure in melittin, and this folding of the peptide is coupled with its partitioning in the membranes. It has been shown that the amphiphilic structure is important for the hemolytic activity of mellitin [94]. DeGrado *et al*. designed the non-homologous analogous amino acid sequence, with hydrophobic:hydrophilic ratio

of 2:1, which provides valuable information about the role of hydrophobic-hydrophilic balance in the interaction of amphiphilic peptides with mono- and bilayers. Leucine is selected in the melittin mimic-I sequence because of its hydrophobicity and high α-helix forming tendency, and the leucine is placed on the hydrophobic face of the α-helix while glutamine is selected for the hydrophilic face. Serine residues are included to increase the hydrophobicity of the model peptide such that the amphiphilicity is equivalent to native peptide. This synthetic peptide has higher potential to form amphiphilic α-helix, and the authors found that both peptides, Melittin I and Melittin I-mimic, binds to the unilamellar egg lecithin vesicles and both are capable of disrupting phospholipids bilayer [95, 96].

These synthetic analogous amphiphilic helical peptides of simple sequence are a powerful tool for the systematic study of the structure-function relationship of lipid-associated proteins and the construction of water-soluble lipid-peptide complexes of desirable physical and physiological properties. These results also suggest that the rational design of peptides based on secondary structure considerations is a useful tool to elucidate the structure-function relationship in biologically active peptides.

### 3.3.2 *de* Novo designs

Engineering synthetic peptides that captures both the dynamics of folding without disrupting the selectivity of binding requires careful design considerations. To this end, the Szoka's group has designed the GALA peptide [97], a 30 amino acid synthetic peptide comprising of glutamic acid-leucine-alanine repeat that mimics the viral activity of hemagglutinin. This peptide switches to a random coil from an amphiphilic α-helix when the pH of the solution is changed from 7 to 5. Glutamic acid is selected as a

titratable residue that destabilizes the helix while at low pH and promotes the helix formation at high pH. The hydrophobic face has enough hydrophobicity to interact with the neutral bilayer membranes at low pH [98, 99]. There are several papers that investigate the mechanism of pore formation, rates of membrane permeabilization and the role of sequence [100-105]. LAGA peptide is designed from the same amino acids where the only difference is in the positioning of the leucines and glutamic acids (figure 3-5). LAGA peptide also shows the transition from random coil to α-helix with decreases in pH from 7.5 to 5, but the LAGA peptide does not form an amphiphilic α-helix. When the two peptides were compared, GALA partitions into membrane more effectively than LAGA. Therefore, the GALA peptide can initiate leakage of vesicle contents and membrane fusion [5].

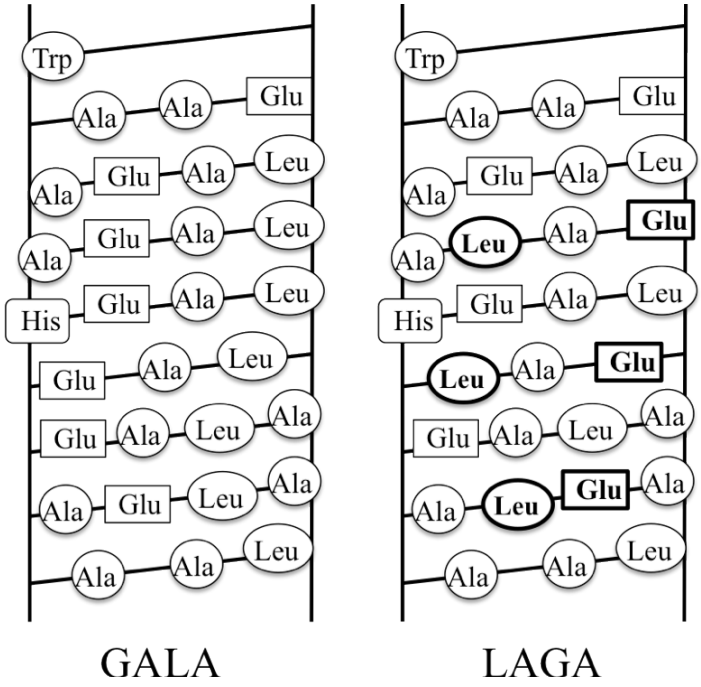


**Figure 3-5.** Helical grid representation of the GALA and LAGA peptides designed by Szoka's group. Difference between these two peptides is the aligning of the glutamic acid and leucines. They are on the different faces of the helix making GALA amphipathic (adapted from Parente *et al*. [63]).

Since GALA peptide can destabilize the bilayer at low pH, it has been used as a carrier for gene delivery. GALA peptide as such cannot bind directly to DNA as both have net negative charge, but when GALA is used with other synthetic amphipathic components, it can be used for DNA or ODN (oligonucleotide) delivery. Various components like polylysine [106], dendrimer [107] and cationic liposomes [108-110] have been used with GALA peptide and transfection efficiency of the DNA delivery has been studied. Design of KALA peptide, a synthetic cationic peptide, is based on GALA

where the negatively charged glutamic acid is replaced with positive charge lysine in the similar position in the peptide backbone while maintaining the other properties [111]. The KALA peptide has been designed to deliver DNA without using other amphipathic components. In contrast to the GALA peptide, the KALA peptides goes from an α-helix to a random coil when the surrounding pH is changed from 7.5 to 5. The reason for this behavior is the net increase in positive charge of the peptide that destabilizes the α-helix when the pH is decreased. Positive charges on KALA peptide can bind directly to DNA, and the hydrophobic fraction of the peptide can interact with the lipid packing of a membrane [112]. These engineered synthetic peptides are capable of interacting with DNA, and they represent a starting point for generating new synthetic molecules that are capable of binding selectively to DNA.

## 3.4 Model peptide design

In this section, we will look at the model peptide designed by using the 'rules' discussed in previous chapter. Our model peptide design (Figure 3-6) follows from the work in DeGrado's lab, where they examined the role of hydrophobic periodicity in the leucine-lysine (LK) peptides that defines the secondary structure, in bulk and at air-water interface, and the amphiphilicity. As discussed above, leucine–lysine (LK) peptides shows that the correct periodicity can stabilize amphiphilic secondary structure at hydrophobic interfaces [4]. We [6] have used amino acids that have inclination to form α-helix secondary structure, and we 'programmed' the sequence so that the peptide will form amphiphilic α-helix (Figure 3-7). Central to our design is the ability to tune the

amphiphilicity of our molecule as a function of environmental cues. Our model peptide is 23-chain amino acid with 8 positive charges and 5 negative charges (Figure 3-6).

Tunable amphiphilicity is an attractive tool for applications ranging from separation processes [113] to drug delivery [114, 115]. Over the last decade, the Abbott lab has explored a redox-based switch to control the hydrophobicity of the surfactant-like systems. These ferrocene-containing amphiphiles tune the oxidation state to yield an amphiphilic architecture [116, 117]. Another tunable system involves photoresponsive surfactants, where an azobenzene group defines the hydrophobic region, allowing UV light to control the cis- and trans- conformations [118-120]. Recent insightful studies Cicciarelli apply the pendant bubble technique to illuminate the reaction dynamics and transport phenomena of several molecular variations in the azobenzene system [121, 122]. The work presented here also uses the pendant bubble technique to examine dynamic surface activity of our model amphiphilic peptide α-helix, where we tune the chemical potential by a folding 'reaction' instead of redox reactions or light.

Our model peptide design is analogous to antibacterial [123] and hemagglutinin peptides [124] found in nature. It has been hypothesized that both these systems use structural transformations based on an α-helical motif to selectively penetrate the cell membrane. A variety of authors have designed synthetic peptide based analogues for these systems. These peptide sequences focus the ability of rationally designed sequences to penetrate cell walls, while our work focuses on the development of a simple model peptide to study the dynamics of folding coupled to amphiphilicity, where the long-term objective is a molecular architecture that possess tunable surface activity coupled to specific binding.

His-Glu-Ala-Lys-Glu-Leu-Leu-Lys-Glu-Trp-Ala-Lys-Leu-Leu-Lys-Lys-Leu-Leu-Lys-Glu-Ala-Lys-Glu
\+ − • + − • • + − • • + • • + + • • + − • + −

**Figure 3-6.** Model peptide sequence. Grey colored region shows the positive charge present in the peptide that prevents it from folding in the aqueous solution. + and -: Polar amino acids and •: non-polar amino acids [6].

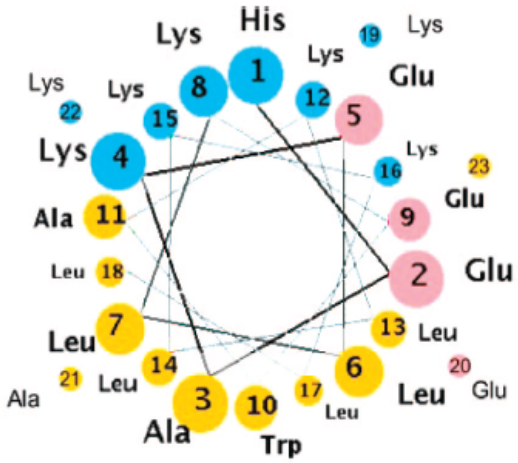


**Figure 3-7.** Helical Wheel for the model peptide system, where hydrophobic (yellow), basic (blue) and acidic (red) are highlighted. Axis is perpendicular to the plane and amino acids are going spirally downwards.

### 3.4.1 Selection of amino acids

The most hydrophobic amino acids that are strong α-helix formers are leucine and alanine (Table 1. Appendix). Leucine is much more hydrophobic than alanine, but alanine is a stronger α-helix former [85]. Three alanines are placed on the hydrophobic side in order to enhance the helical propensity. These alanines flank the more hydrophobic leucines, and the leucines form a stripe down the axis of the peptide helix.

As alanine is less hydrophobic, it will reduce the interaction of the peptide with the hydrophobic regions of the polyelectrolyte (DNA), and peptide will be able to maintain its secondary structure. A tryptophan is also placed on the hydrophobic side in order to quantify the concentration of peptides that has been complexed with the DNA. Tryptophan is a fluorophore that excites with UV-light (~280nm) and fluoresces at 350nm. Tryptophan is also a hydrophobic α-helix former. The most hydrophilic amino acid that is a strong α-helix former is a negatively charged glutamic acid. Lysine is also used as a hydrophilic amino acid, because Lysine has a positive charge and a greater helical propensity over Arginine, the other amino acid showing positive charge. Since the peptide is designed to have an overall positive charge for DNA-condensation there are 7 lysines and 5 glutamic acids on the hydrophilic side. Histidine is positively charged depending on the pH. Histidine is a neutral amino acid at pH 8, but histidine takes on a positive charge in acidic solutions (pI = ~7). Histidine is also a strong α-helix former. Histidine is placed in the N-terminal as a mechanism to control assembly with metal ions (chelation). Again, having strong α-helix former at the end will reinforce order, and the addition of metal ions in the subphase can be used to help to co-ordinate structure at the interface.

### 3.4.2 Solid Phase Peptide Synthesis (SPPS)

Synthesis by SPPS method [7] consist of the four steps (Figure 3-8). The first step is to attach an amino acid to the polymer or "solid phase". Peptide chain has two ends, N-terminus and C-terminus. The C-terminus is attached to the 'solid' phase, the surface of the polymeric beads. The first protected amino acid is reacted to the surface, where only

one amino acid covalently links to the surface because the amine group of the amino acid is protected, preventing uncontrolled condensation polymerization. This means that the peptide polymer link will not get hydrolyzed during the subsequent peptide reaction.

The second step is the deprotection where the protecting group, FMOC (9-fluorenylmethoxycarbonyl), is removed from the N-terminus so the amino acid can react with the subsequent amino acid in the sequence. The third step is the coupling. The next FMOC protected amino acid is then reacted with the amino acid attached to the polymer to begin building the peptide chain. The reaction is carried out in the solvent Dimethyl formamide (DMF). Steps 2 and 3 are repeated until the desired sequence is generated.

In the fourth step, the peptide sequence is cleaved from the solid phase. The complete peptide sequence is cleaved from the solid surface by breaking the bond between the peptide and the solid phase with trifluoroacetic acid. All the other impurities are removed by recrystallizing the peptide in ether (MTBE). MTBE is used because the protecting groups are typically soluble in ether. The two layers are separated by centrifugation, and the peptide is retained for further purification.

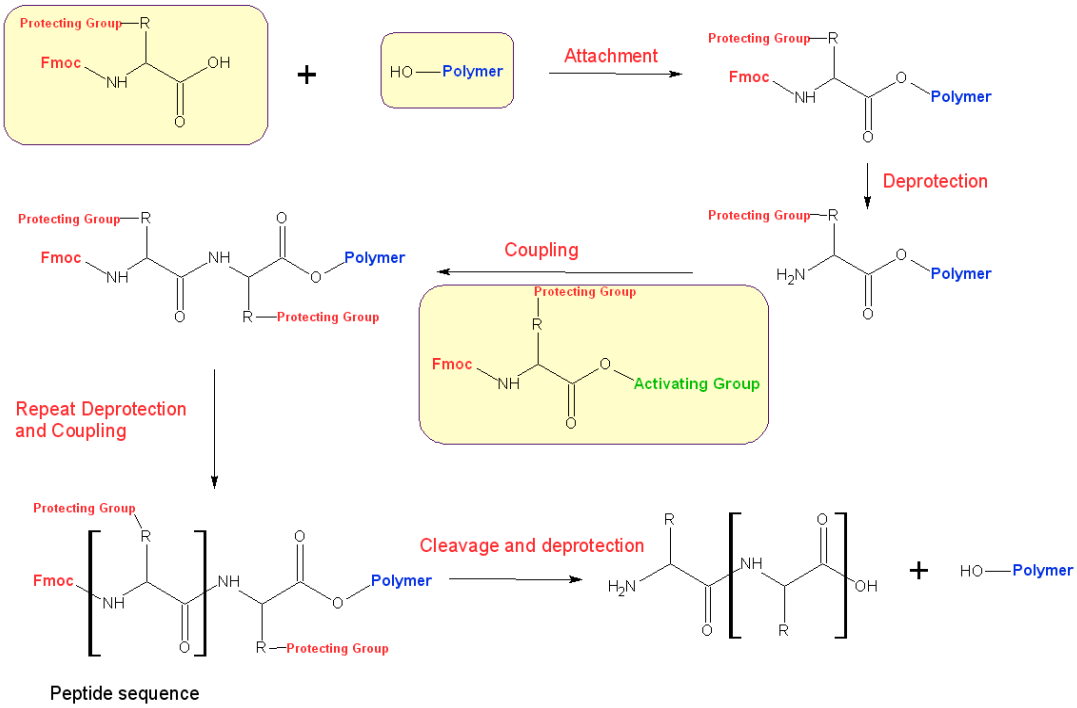


**Figure 3-8**. Solid Phase Peptide Synthesis [7].

In this synthesis, peptide is "immobilized" on the solid phase and can be retained during the filtration process, whereas liquid phase reagents and by-products of synthesis are flushed away. Since the peptide is immobilized and protected from side reactions, we have better control over the reaction and hence over the overall process. This also allows us to precisely synthesize peptides containing up to 50 residues. This scheme provides control over the sequence and can be varied to give new structures and constituent molecules that self assemble, including non-linear sequences, highly alkylated sequences and atypical amino acids. SPPS offer many advantages over the biological methods in terms of efficiency, purification procedures and well-defined control experiments.

# Chapter 4

# Tunable surface activity and dynamics

In this chapter, we demonstrate that a peptide can fold and unfold to control surface tension and the pendant bubble technique can be used to measure the dynamics. We use circular dichroism to characterize the bulk-phase ensemble average folded state as a function of salt concentration, and we use the pendant bubble method to characterize the dynamics of the process, namely, surface activity with folding. These tools provide a proof of concept for a simplified peptide design that couples folding to amphiphilicity. The model peptide can serve as a platform for future designs that will incorporate the selectivity inherent in helical biological molecules.

Our peptide is designed to exhibit a two state equilibrium. The folded peptide is assumed to be in equilibrium with the unfolded one in the aqueous solution (figure 4-1) and folded peptide is amphiphilic while unfolded is not. We plan to control the kinetics of DNA condensation by controlling the folding dynamics of the peptide. Before we introduce DNA in the system, we will first characterize the secondary structure of the

peptide and surface activity/amphiphilicity in salt solution. We use circular dichroism to characterize the secondary structure and pendant bubble apparatus to characterize the surface activity/amphiphilicity.

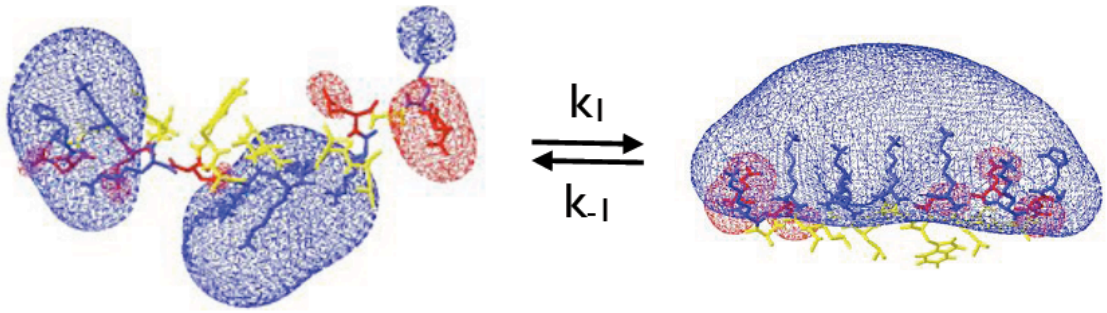


**Figure 4-1.** Cartoon showing transient secondary structure and amphiphilicity.

## 4.1. Circular dichroism

Circular dichroism (CD) spectroscopy is used for determining the ensemble average secondary structure of the peptide. The measurement is applied to estimate the fraction of a molecule in a given secondary structure conformation. This is done by passing circularly polarized light through a solution containing an optically active substance and measuring the difference in the absorption of left circularly polarized (LCP) light versus right circularly polarized (RCP) light. Transmission of circularly polarized light is absorbed due to the periodic structure of a chiral molecule as a function of wavelength. The instrument then detects the resulting ellipticity of the transmitted light.

For any given wavelength, if ΔA is the difference in the absorbance between LCP light and RCP, then by Beer's law we have

$$\Delta A = \left(\varepsilon_L - \varepsilon_R\right) C l \qquad (1)$$

Where, $\varepsilon_L$ and $\varepsilon_R$ are the molar extinction coefficient for LCP light and RCP light, C is the molar concentration and l (in cm) is the path length of the sample cuvette.

$$\Delta\varepsilon = \varepsilon_L - \varepsilon_R \qquad (2)$$

This difference in the molar extinction coefficient is the molar circular dichroism of the substance. Molar ellipticity (θ) and molar circular dichroism are related by the equation

$$[\theta] = 3298\Delta\varepsilon \qquad (3)$$

Unit of [θ] is degrees deciliter $mol^{-1}$ $decimeter^{-1}$ and for Δε is liter $mol^{-1}$ $cm^{-1}$.

$$[\theta]_{MRE} = \frac{100\theta}{C * l * n} \qquad (4)$$

Where, $[\theta]_{MRE}$ is the mean residue ellipticity (degree $cm^2$ $dmol^{-1}$) and n is the number of residues in peptide.

Secondary structure is determined by the CD spectroscopy in the far-UV region (190-250nm). At this wavelength, the peptide bond is the chromophore. The absence of chiral molecules results in zero CD intensity because all the signals cancel each other, while an ordered chiral structures result in a spectrum that contains both positive and negative signals. To fit secondary structure, method of least squares is used (linear regression). To determine the amount of α-helix, β-sheet and random coil in the secondary structure, one should have the basis set of standard conformations of known polypeptides

Using this technique, peptide is characterized as a function of salt (sodium chloride). Peptide solution of 0.5 g/l is prepared in water, and it is titrated with a 2M

NaCl solution. After adding an adequate amount of NaCl in the solution, CD experiment is conducted. This allows us to calculate the equilibrium constant of the reaction between folded and unfolded peptide. This is repeated for NaCl concentration in the solution ranging from 0M to 1M.

CD for the model sequence is shown in figure 4-2A. As stated earlier, our model peptide is designed to exhibit a two state equilibrium, random coil and α-helix. The characteristic CD spectrum for an α-helix shows minima at 208 and 222 nm. CD for deionized water (blue) shows a typical spectrum for a random coil (10% α-helical). The predominantly populated state is natively disordered. The overall charge on this peptide is +3, and, therefore, the intramolecular electrostatic repulsion results in an elongated state in deionized water. As the charges are screened by electrolytes (550 mM NaCl), decreasing the Debye length from ~300 nm to 0.4 nm, an ordered structure emerges (red, 70% a-helical). At approximately physiological electrolyte concentrations of 95 mM NaCl, the peptide shows a 63% helical structure. This value was predicted using established secondary structure predictors, such as GOR4 (65.4% α-helical) [125] or JUFO (70.4% α-helical) [126]. This data corroborates the hypothesis that one can design a peptide-sequence that can be programmed to fold under specific conditions. Still, the consideration of a percentage value for helicity can be deceptive, as the value represents the mean helicity of an ensemble of fluctuating conformations with time.

The thermodynamics of the equilibrium structural population can be established in the following manner. For the model sequence, one can plot the ellipticity at 222 nm as a function of salt concentration (figure 4-2B). Shifts in the populations of the folded and unfolded states are described by the following equations:

$$\sigma = \frac{F_n}{F_u} = \frac{\eta_u - \eta_x}{\eta_x - \eta_n} \qquad (5),$$

where the equilibrium constant, s, is the ratio of folded peptide to unfolded peptide, $F_n/F_u$, determined from the ellipticities, $\eta_n$ (folded), $\eta_u$ (unfolded) and $\eta_x$ (intermediate). By performing the same measurement as a function of salt concentration, Figure 4-2B, we can approximate the equilibrium constant for our model peptide. Moreover, future systematic variations in sequence can be applied to establish the free energy of folding with regard to the position of the charged groups or the concentration of specific targets.

From our CD experiments, we have shown that we can control the secondary structure of the peptide by controlling the salt concentration in the solution. Thus, our peptide has transient secondary structure. Next step is to characterize the amphiphilicity, which results due to folding of the peptide. We use pendant bubble apparatus to characterize the amphiphilicity/surface activity.

A)

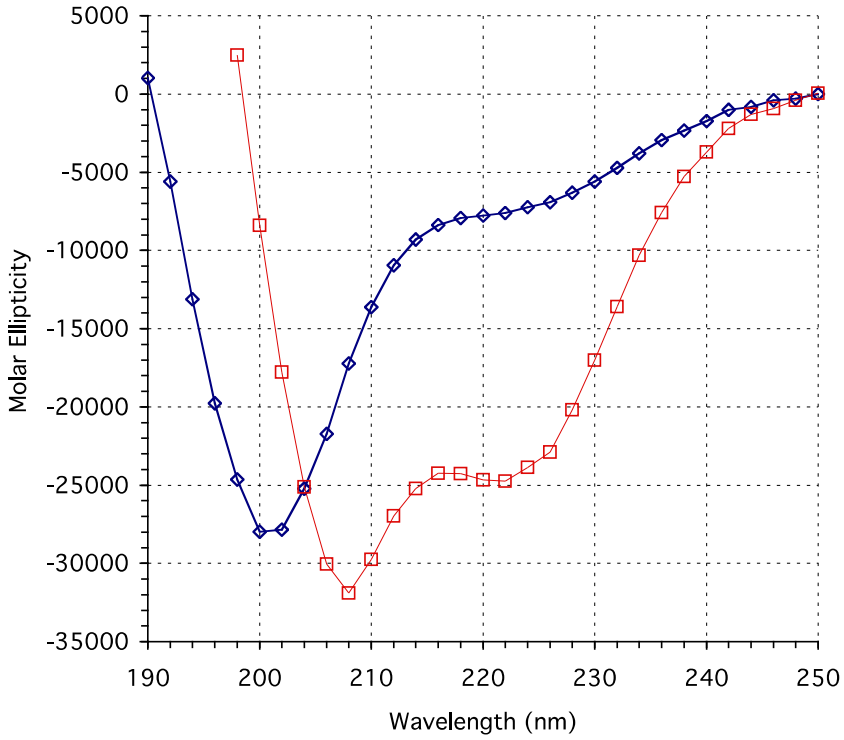
5000
0
-5000
-10000
-15000
-20000
-25000
-30000
-35000
Molar Ellipticity
190
200
210
220
230
240
250
Wavelength (nm)

B)

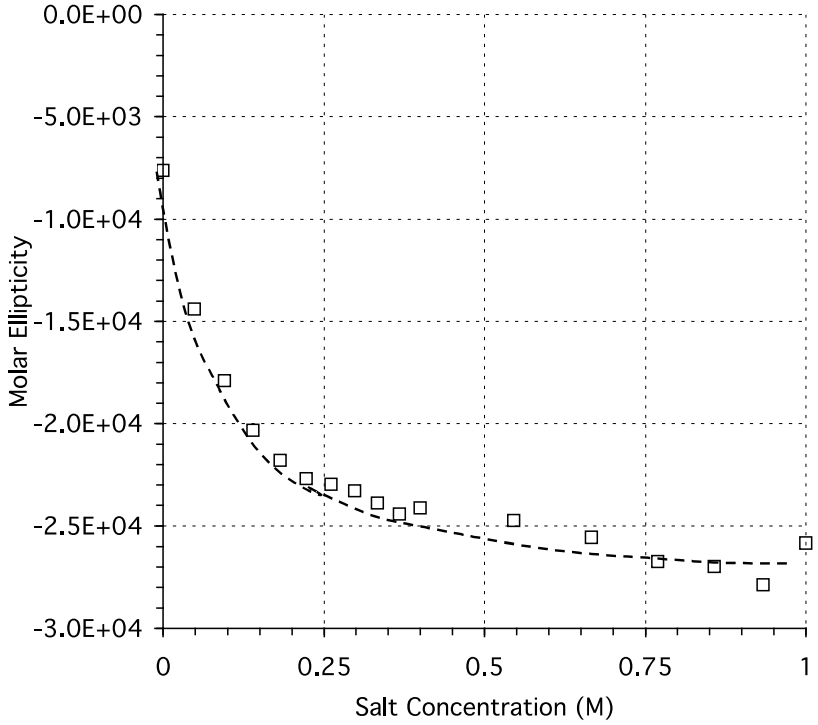
0.0E+00
-5.0E+03
-1.0E+04
-1.5E+04
-2.0E+04
-2.5E+04
-3.0E+04
Molar Ellipticity
0
0.25
0.5
0.75
1
Salt Concentration (M)

**Figure 4-2.** CD of the model peptide. (a) Solid blue line - the disordered peptide in DI water. Dashed red line - the helical amphiphilic peptide in 550 mM salt solution. (b) CD @ 222 nm. Mean residue ellipticity at 222 nm as a function of salt concentration. Lower values represent increased helicity.

## 4.2. Pendant bubble:

Pendant bubble tensiometry with video digitization is employed for the measurement of dynamic surface tension relaxation and equilibrium tensions. The system creates a silhouette of a pendant bubble, video images the silhouette, and digitizes the image. A beam with constant light intensity passes perpendicular to the sample cuvette through the pendant bubble and forms a silhouette of a bubble on a solid-state video camera. The pendant bubble is generated in an aqueous solution with peptide at a fixed bulk concentration, which is put inside a quartz cell (figure 4-3).

A 14-gauge stainless steel inverted needle (0.063 in. i.d.; 0.083 in. o.d.), which is connected to the normally closed port of a three-way miniature solenoid valve, is used for the bubble generation. The common port of the valve, controlled by a computer, is connected to a gas-tight Hamilton syringe placed in a syringe pump. The silhouette image is digitized into 480 x 640 with a level of gray with 8-bit resolution.

The experimental protocol is as follows: the quartz cell of 20x10x45 mm inside diameter is initially filled with the peptide aqueous solution in NaCl, and the bubble-forming needle is positioned in the quartz cell through which light beam passes perpendicularly. The solenoid valve is energized, and the air is allowed to pass through the needle, thereby forming a bubble of air. The valve is then closed when the bubble of

sufficient diameter (approximately 2.5mm) is formed. The time required to create an air bubble of this size is about 0.5 s. After the solenoid valve is closed, and the bubble is formed, sequential digital images are then taken of the bubble, which depends on the concentration of peptide. For high concentration (0.1-0.01 g/l) range time interval is around 5sec to 15sec while for lower concentration interval is around 20-30sec. All these images are saved to form a single movie. Each image is processed to determine the bubble edge coordinates, bubble volume, bubble surface area, and the surface tension for studying the formation of bubble. The theoretical shape of the pendant bubble is derived according to the classical Laplace equation that relates the pressure difference across the curved fluid interface

$$\gamma\left(\frac{1}{R_1}+\frac{1}{R_2}\right)=\Delta P \qquad (6),$$

where γ is the surface tension, R1 and R2 are the two principal radii of curvature of the surface, and ΔP is the pressure difference across the interface.

The pendant bubble system can also be used as a Langmuir trough. A bubble is formed on the tip of the inverted needle and is allowed to reach the equilibrium. Once equilibrium is reached, the bubble is expanded by opening the solenoid valve for 0.2s to 0.4s. Readings are taken for the new bubble having a higher surface area.

Using this technique, the peptide is characterized as a function of its concentration in 1M NaCl solution. As stated earlier, we assume that only folded peptide is adsorbed at the air water interface. Also, the peptide is characterized as a function of salt in 0.32g/l peptide solution.

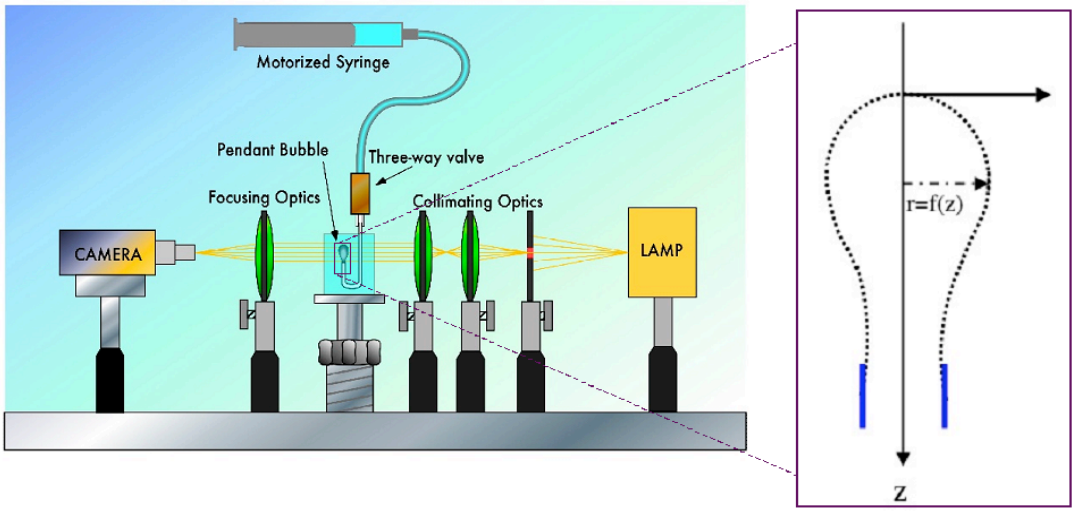


**Figure 4-3**. Pendant bubble apparatus

Data on the model peptide verifies that the pendant bubble is capable of detecting changes in surface activity as a function of time, where the formation of a depletion layer near the bubble interface gives non-equilibrium behavior. Figure 4-4A shows these results with increasing peptide concentration. Each line shown here represents a separate concentration of peptide at a constant salt concentration of 1 M NaCl. At this salt concentration the equilibrium constant is given by $\sigma = 25$. This experiment was done both dynamically and at very long times to establish equilibrium. As we increase concentration we see a faster decrease in surface tension, while longer time studies shows us that the equilibrium values are not concentration dependent. We tested three decades of peptide concentrations and observed no variation in the equilibrium surface tensions, implying near irreversible adsorption.

Dynamic pendant bubble experiments are also taken with changing salt concentration, Figure 4-4B. As expected from the equilibrium bulk phase folded populations, Fig 4-2, we see an increase in the adsorption rate of the peptides at higher

salt concentrations. Again, this agrees with the hypothesis that the folded structures are surface active, but the less folded populations are not. In contrast to the fixed salt concentration data, Fig 4-4A, at longer times, this data does show decreasing values of equilibrium surface tension with increased salt concentration. The equilibrium results suggest that there is also screening at the interface, where amphiphilic helical peptides are capable of packing closer at the interface, because of a shorter Debye length.

A)

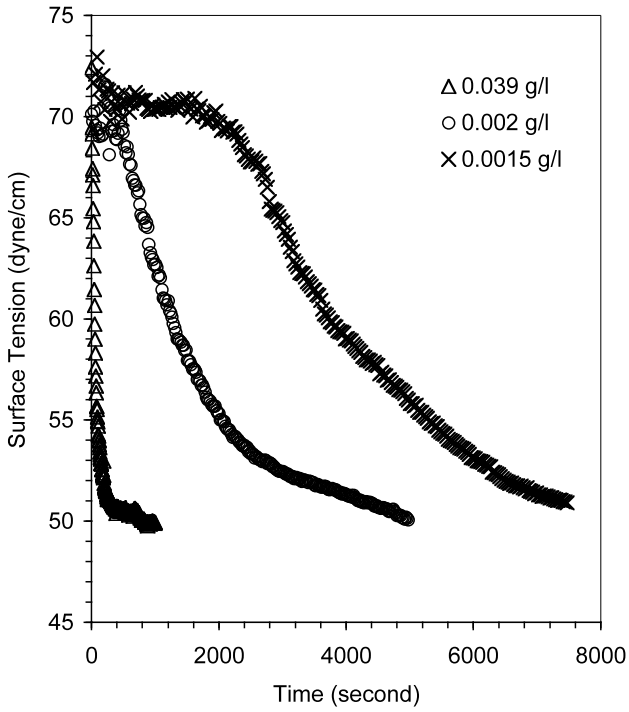
75
70
65
60
55
50
45
0
2000
4000
6000
8000
Surface Tension (dyne/cm)
Time (second)
△ 0.039 g/l
○ 0.002 g/l
× 0.0015 g/l

B)

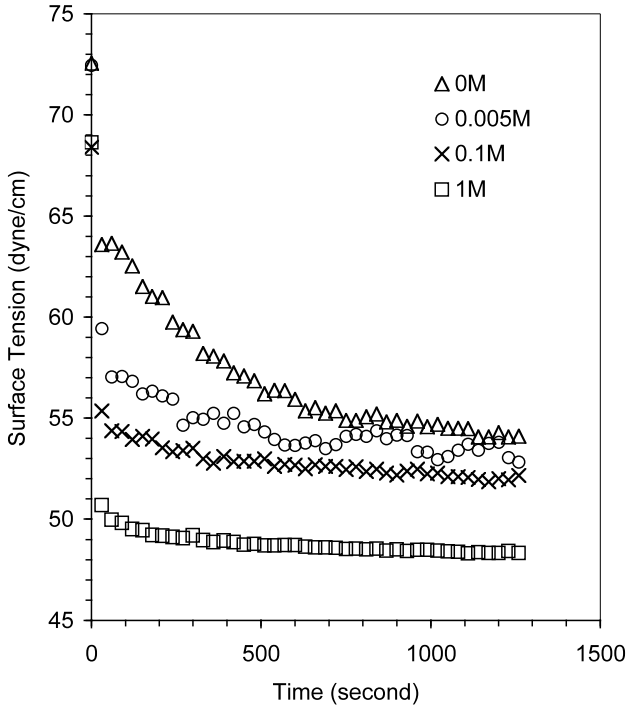
75
70
65
60
55
50
45
0
500
1000
1500
Surface Tension (dyne/cm)
Time (second)
△ 0M
○ 0.005M
× 0.1M
□ 1M

**Figure 4-4.** Pendant bubble. Surface tension as a function of time is plotted at various total peptide concentrations (a) and salt concentrations (b).

We quantify the nature of the dynamics by evaluating how quickly the interface reaches 90% of the equilibrium surface tension. We define this time as $t_{90}$. The evaluation of $t_{90}$ allows us to estimate that relative contributions of diffusion compared to adsorption dynamics. The folding time scales do not define the dynamics of this system are not rate limiting as short peptide will fold and unfold on time scales O ~ milliseconds [127], and the phenomenon observed here is limited by time scales O ~ seconds to thousands of seconds. Figure 4-5 shows log $t_{90}$ plotted against the log of the total peptide concentration, Co, in the pendant bubble experiment. Far from the bubble, the folded peptide concentration is simply the total peptide concentration multiplied by the folded population from equation 2, $\sigma$Co.

The slope for figure 4-5 is ~1.35. Surface tensions are found to increase with surface concentration according to pendant bubble expansion experiments. Using the assumption of irreversible Langmuir adsorption as described above, we assume the adsorption limited dynamics will follow $d\Gamma/dt = \beta\ Cs\ (\Gamma-\Gamma_\infty)$, where $\Gamma$ is the amount of peptide adsorbed, $\Gamma_\infty$ is the maximum amount of peptide that can adsorb, $\beta$ is the adsorption coefficient, Cs is the sublayer concentration of folded peptide. In the limit of fast diffusion, this leads to a slope of 1 in figure 4-5, where the scaling of the log of $t_{90}$ is $\ln(t_{90}) \sim -\ln(Cs) \sim -\ln(\sigma Co)$.

In the diffusion limited case, the maximum surface concentration, $\Gamma_\infty$, will be obtained at time $t_\infty$, given by $\Gamma_\infty = 2\sigma Co(Dt_\infty)^{1/2}$. This leads to time scales for diffusion

limited adsorption of $t \sim (\Gamma_\infty/\sigma Co)^2/D$. For this case, we would expect to recover kinetics where $\ln(t_{90}) \sim -2 \ln(Co)$. The diffusion-controlled case would yield a slope of 2. In figure 4-5, slopes of one and two are shown with dashed lines. Slope 1.35 indicates that the adsorption of the peptide to the interface dominates the dynamic process. This is in contrast to surfactants where diffusion typically dominates [128].

Applying the assumption that folding kinetics are fast and adsorption kinetics limits the process, we can also evaluate the $t_{95}$ of changing salt concentrations at constant total peptide concentration, figure 4-4B. In this case, we anticipate the rate of adsorption to the interface to increase with increasing salt concentration. This increased rate of adsorption is controlled by an increase in the population of folded peptides at higher salt concentrations, where the assumption of fast diffusion fixes the sublayer concentration to $\sigma Co$. Figure 4-6 shows the $\ln (t_{95})$ plotted against $- \ln (\sigma Co)$, where the $\sigma$ term is determined from figure 4-2B by using equation 5. If the assumptions made regarding diffusion and folding are correct, then the same slope should be recovered in this plot. The slope here is found to be 1.39. These experiments corroborate our central hypothesis that we can dynamically control surface activity by controlling the folded and unfolded states of the peptide. Additionally, this simplistic analysis shows that the pendant bubble can effectively quantify the adsorption dynamics of the peptide system.

A more complete model for the dynamic pendant drop experiment is developed and is discussed in the next section. The model is based on existing models for the diffusion and adsorption of surfactants to the pendant bubble interface [129-131], but it takes into account the dynamics of folding and unfolding. Using this model, we observe that the

non-equilibrium concentrations of folded and unfolded peptides in the depletion layer adjacent to the bubble determine the rate of change of the surface tension.

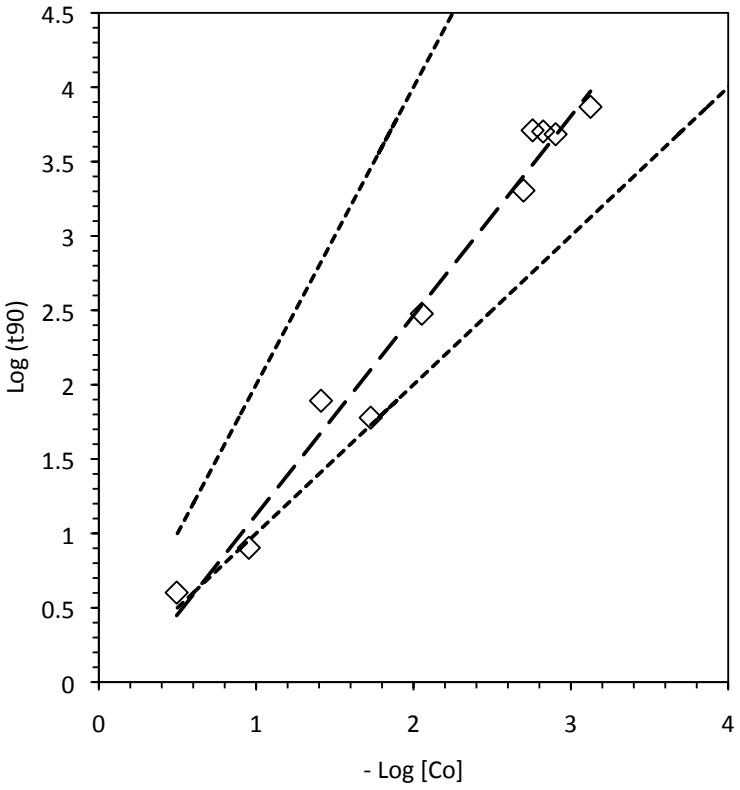


**Figure 4-5**. Values for the time where the surface tension reaches 90% of the minimum surface tension, $t_{90}$, are plotted against the total peptide concentration. The slope is 1.35. Slopes of 1 (adsorption limited) and 2 (diffusion limited) are also plotted.

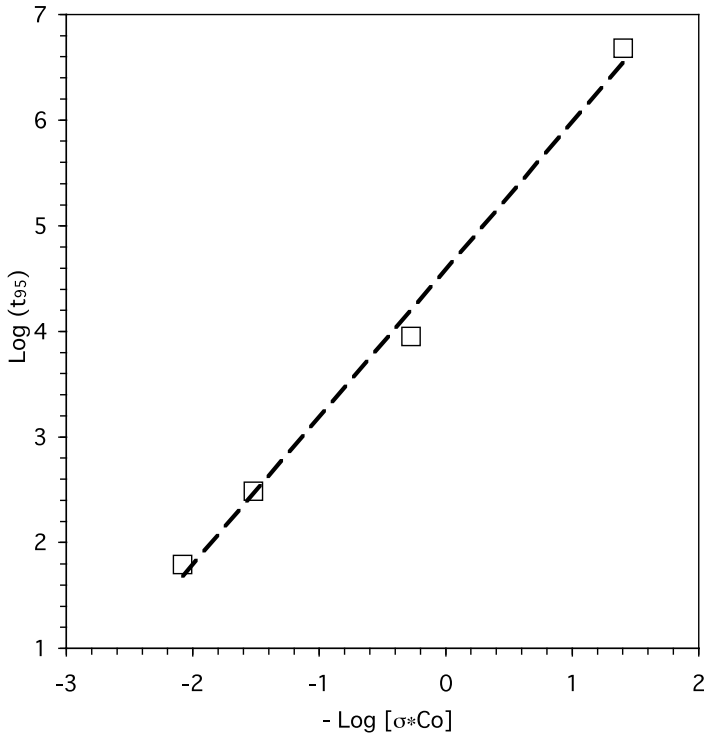


**Figure 4-6**. For various salt concentrations, $t_{95}$ is plotted against the folded peptide population, given by σCo. β represents the adsorption coefficient for langmuir adsorption. The slope of ln ($t_{95}$) vs. - ln (σCo) is 1.39.

# Chapter 5

# Modeling the dynamic folding and surface activity of the helical peptide

In this chapter, to understand the factors influencing the dynamics of the switchability, a model is developed for the transport of the surface-active form of the peptide from the solution onto air–water interface. As is the case with the low molecular weight head–tail surfactants, the transport involves the bulk diffusion of the folded form to the surface and the kinetic adsorption onto the interface. Unlike the head–tail surfactants, the diffusion can be augmented by the kinetics of the folding of the peptide from the unfolded form. The model is formulated within the context of the transport of the peptide from a uniform bulk solution onto an initially clean air–water interface in a pendant bubble system, where the transport rate can be measured by recording the reduction in surface tension using the shape analysis of the bubble. Experiments are undertaken and compared to the predictions of the model simulations of the tension

reduction for a range of values of the kinetic adsorption constant and the folding kinetic constant. The results indicate that the kinetic adsorption rate of the folded peptide onto air–water interface dominates the dynamic process, which contrasts many head–tail surfactants where diffusion typically dominates over kinetics adsorption. Moreover, our 'best-fits' suggest that there is a phase transition at high surface concentrations that slows the long- time adsorption of the peptides to the interface. Finally, the numerical solution is compared with an asymptotic solution, showing agreement with our findings that the fundamental dynamics of the tunable surface-active peptide are indeed controlled by the adsorption step.

The aim of this exercise is to develop to develop a model for transport of the surface-active form of the peptide to an interface to understand the factors controlling the dynamics of switchability [132]. Adsorption of the folded peptide at the air-water interface involves three steps: (1) the folding 'reaction' (2) the diffusion of the folded peptide from the bulk solution to the sublayer surface and (3) the adsorption from the sublayer onto the air-water interface. The diffusion and adsorption equation in the model are based on existing models for surfactants, and adding the dynamic folding and unfolding of the peptide. Unknown parameters involved in the modeling are the folding kinetic constant ($k_1$), adsorption rate constant ($\beta$), desorption rate constant ($\alpha$) and maximum surface packing concentration ($\Gamma_\infty$). We determine folding/unfolding rates and adsorption constants by measuring the reduction in surface tension as the folded peptide diffuses towards the sublayer and, subsequently, adsorbs onto the fresh air-water interface ($\Gamma = 0$ at time = 0). By modeling this folded peptide exchange with diffusion-adsorption equations, surface concentration ($\Gamma$) can be predicted as a function of the

folding rate and adsorption constants. We derive an equation of state by relating surface tension (γ) to surface concentration (Γ). From this equation of state, our model can predict the dynamic reduction in surface tension. Thus, fundamental aspects of the folding rate and adsorption/desorption rates are elucidated by comparing model behavior with experimental results.

In the following section, we describe the modeling of the helical peptide folding, diffusing and adsorbing to an air-water interface. And then, we describe our selection and application of the equation of state, allowing us to compare the experimental results with our transport model.

## 5.1 Model formulation

The following discussion describes our model for the adsorption of the peptide onto the interface. The interface is peptide free initially i.e. surface concentration Γ = 0 at time = 0. Diffusivity of the folded and unfolded peptide is assumed to be same, and convection in the cuvette is taken to be negligible. The unfolded peptide is initially in equilibrium with the folded peptide.

$$C_r \underset{k_{-1}}{\overset{k_1}{\rightleftharpoons}} C_\alpha \qquad [7]$$

$$\sigma = \frac{C_{\alpha\infty}}{C_{r\infty}} = \frac{k_1}{k_{-1}} \qquad [8]$$

The dynamic behavior can be described by coupling a diffusion and kinetic model, which characterizes folding as a function of peptide concentration.

$$\frac{\partial C_\alpha}{\partial t} = D_\alpha \frac{\partial^2 C_\alpha}{\partial x^2} + k_1 C_r - k_{-1} C_\alpha \qquad [9]$$

$$\frac{\partial C_r}{\partial t} = D_r \frac{\partial^2 C_r}{\partial x^2} - k_1 C_r + k_{-1} C_\alpha \qquad [10]$$

$C_\alpha$ is the concentration of the folded peptide, $C_r$ is the concentration of the unfolded peptide, $D_\alpha$, and $D_r$ are the diffusivities of the folded and unfolded peptide, respectively, $k_1$ and $k_{-1}$ are the rate constants, σ is the equilibrium constant, and $C_{\alpha\infty}$ and $C_{r\infty}$ are the equilibrium concentrations of folded and unfolded peptide, respectively. We approximate the diffusion coefficient by assuming the peptide is a cylinder, using an equation from Eimer et al [133].

$$D = \left( \frac{K_B T}{3\pi\eta_0 L} \right) (\ln p + \gamma) \qquad [11]$$

Where, $K_B$ is Boltzmann's constant, $T$ is the absolute temperature, $\eta_0$ is the pure solvent viscosity and $L$ is the length of the folded peptide. $p$ is the ratio of diameter to length of helical peptide and $\gamma$ is the end effect correction.

These equations are similar to the transport equations for surfactants [134-136], and they reduce to the differential equations from Ward-Tordai [137] when the reaction terms are removed. Therefore, we can use the Ward-Tordai result as a limiting condition to validate our numerical solution.

In order to solve equations 9 and 10 to obtain a surface concentration Γ, we need to calculate the sublayer concentration, $C_s$. We apply a Langmuir adsorption isotherm, where the adsorption rate is proportional to the sublayer concentration and the available

surface vacancy ($1-\Gamma/\Gamma_\infty$), and the desorption rate is proportional to the surface coverage $\Gamma$. We have assumed that only folded peptide adsorbs at the air water interface. Therefore, for folded and unfolded peptide we have,

$$\frac{\partial \Gamma_\alpha}{\partial t} = \beta C_\alpha(0,t)\left(\Gamma_\infty - \Gamma_\alpha\right) - \alpha\Gamma_\alpha = D_\alpha\left(\frac{\partial C_\alpha}{\partial x}\right)_{x=0} \qquad [12]$$

$$\frac{\partial \Gamma_r}{\partial t} = D_r\left(\frac{\partial C_r}{\partial x}\right)_{x=0} = 0 \qquad [13]$$

where, $\beta$ and $\alpha$ are the adsorption and desorption constants for the folded peptide. $\Gamma_\alpha$ and $\Gamma_r$ are the surface concentrations for folded and unfolded peptide, respectively. $C_\alpha(0,t)$ is the sublayer concentrations for folded peptide. And $\Gamma_\infty$ is the maximum packing concentration.

Also, from the equilibrium surface tension curve (Figure 5-1), we observe that the process is irreversible i.e. there appears to be no desorption. Therefore, $\alpha=0$ and,

$$\frac{\partial \Gamma_\alpha}{\partial t} = \beta C_\alpha(0,t)\left(\Gamma_\infty - \Gamma_\alpha\right) = D_\alpha\left(\frac{\partial C_\alpha}{\partial x}\right)_{x=0} \qquad [14]$$

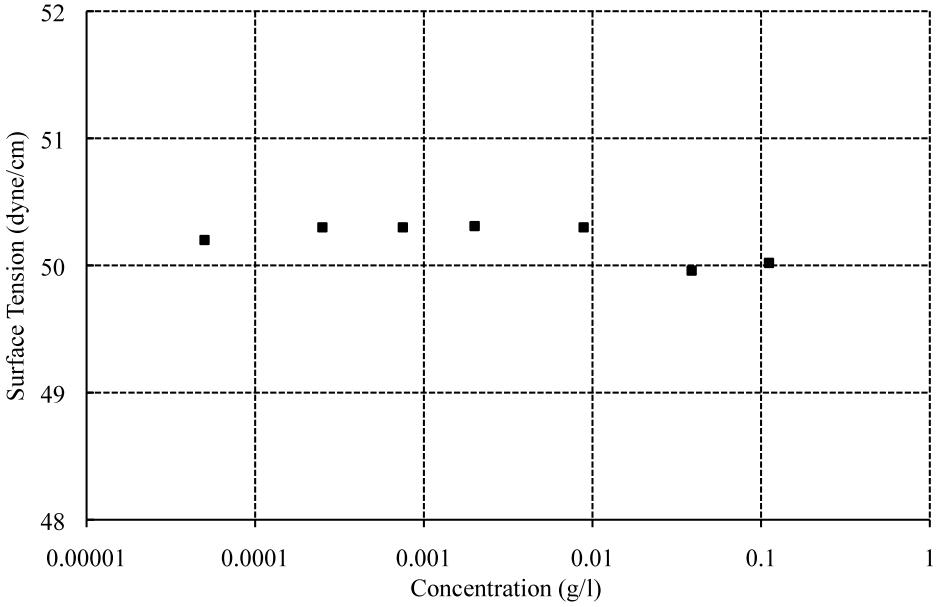


**Figure 5-1.** The equilibrium surface tensions for air/peptide aqueous solution at constant salt concentration 1M.

Additionally, we define the boundary conditions for both folded and unfolded peptide far away from interface as equal to the initial bulk concentration. Equation (13) and (14) are the second boundary condition for the unfolded and folded peptides, respectively. The sublayer concentration is taken to be a function *f(t)*. The initial conditions for both folded and unfolded peptides are defined by the initial bulk concentrations. Lastly, since $\Gamma_r$ i.e. surface concentration of the unfolded peptide is zero, we will represent $\Gamma_\alpha$, the surface concentration of the folded peptide, by $\Gamma$.

The boundary conditions are as follows:

The boundary conditions are as follows:

$$C_\alpha\left(x \to \infty, t\right) = C_{\alpha\infty}$$

$$C_r\left(x \to \infty, t\right) = C_{r\infty} = \frac{1}{\sigma} C_{\alpha\infty} \qquad [15]$$

$$C_\alpha\left(x = 0, t\right) = f(t)$$

$$D_r\left(\frac{\partial C_r}{\partial x}\right)_{x=0} = 0$$

The initial conditions are as follows:

$$C_\alpha\left(x, t = 0\right) = C_{\alpha\infty}$$

$$C_r\left(x, t = 0\right) = C_{r\infty} \qquad [16]$$

To solve the above coupled partial differential equation, we first non-dimensionalize the two differential equation, substituting

$$\eta = \frac{x}{h},\ \tau = \frac{t}{\tau_D},\ \overline{C_\alpha} = \frac{C_\alpha}{C_{\alpha\infty}},\ \overline{C_r} = \frac{C_r}{C_{r\infty}}$$

where, h is the depletion length $h = \frac{\Gamma_\infty}{C_{\alpha\infty}}$, and $\tau_D = \frac{h^2}{D}$ is the diffusivity time scale.

We define ε as inverse of Damkohler number, $\varepsilon = \frac{D}{h^2 k_1}$.

After non-dimensionalizing, we obtain the following governing equations

$$\frac{\partial \overline{C_\alpha}}{\partial \tau} = \frac{\partial^2 \overline{C_\alpha}}{\partial \eta^2} + \frac{1}{\sigma\varepsilon}\left(\overline{C_r} - \overline{C_\alpha}\right) \qquad [17]$$

$$\frac{\partial \overline{C_r}}{\partial \tau} = \frac{\partial^2 \overline{C_r}}{\partial \eta^2} - \frac{1}{\varepsilon}\left(\overline{C_r} - \overline{C_\alpha}\right) \qquad [18]$$

with the boundary conditions given by:

$$\eta \to \infty \quad \overline{C_\alpha} = 1 \text{ and } \overline{C_r} = 1$$

$$\eta \to 0 \quad \overline{C_\alpha} = \frac{f(t)}{C_{\alpha\infty}} \text{ and } \left(\frac{\partial \overline{C_r}}{\partial \eta}\right)_{\eta=0} = 0 \qquad [19]$$

and initial conditions given by:

$$\overline{C_\alpha}(\eta,0) = 1$$

$$\overline{C_r}(\eta,0) = 1 \qquad [20].$$

Taking the Laplace transforms of equations (17) and (18), we get two ordinary differential equations. Applying the boundary conditions to obtain the relevant constants solves these two equations. The final solution is obtained by taking the Laplace inverse.

$$\Gamma(t) = (\sigma+1)\int_0^\tau f(\tau-\tau') \times \left\{ \begin{array}{l} \frac{\sigma}{1-\sigma^2}\left[\frac{1}{\sqrt{\Pi\tau'}} + \frac{\sqrt{a}}{\sigma\sqrt{1-\sigma^2}}\exp\left(\frac{a\sigma^2}{1-\sigma^2}\tau'\right) erf\left(\sqrt{\frac{a\sigma^2\tau'}{1-\sigma^2}}\right)\right] + \\ \frac{1}{\sigma^2-1}\left[\frac{e^{-a\tau'}}{\sqrt{\Pi\tau'}} + \sqrt{a}\sqrt{\frac{1}{1-\sigma^2}}\exp\left(\frac{a\sigma^2}{1-\sigma^2}\tau'\right) erf\left(\sqrt{\frac{a}{1-\sigma^2}\tau'}\right)\right] \end{array} \right\} d\tau' +$$

$$(\sigma+1)\int_0^\tau -1 \times \left\{ \begin{array}{l} \frac{\sigma}{1-\sigma^2}\left[\frac{1}{\sqrt{\Pi\tau'}} + \frac{\sqrt{a}}{\sigma\sqrt{1-\sigma^2}}\exp\left(\frac{a\sigma^2}{1-\sigma^2}\tau'\right) erf\left(\sqrt{\frac{a\sigma^2\tau'}{1-\sigma^2}}\right)\right] + \\ \frac{1}{\sigma^2-1}\left[\frac{e^{-a\tau'}}{\sqrt{\Pi\tau'}} + \sqrt{a}\sqrt{\frac{1}{1-\sigma^2}}\exp\left(\frac{a\sigma^2}{1-\sigma^2}\tau'\right) erf\left(\sqrt{\frac{a}{1-\sigma^2}\tau'}\right)\right] \end{array} \right\} d\tau' \qquad [21]$$

Where, $a = \frac{1}{\varepsilon} + \frac{1}{\sigma\varepsilon}$

Here, if we remove the reaction term (ε→∞) then this equation reduces to the Ward-Tordai equation (figure 5-2).

$$\Gamma(\tau) = 2\sqrt{\frac{\tau}{\Pi}} - \frac{2}{\sqrt{\Pi}}\int_0^{\sqrt{\tau}} f(\tau - \tau')d\sqrt{\tau'} \qquad [22]$$

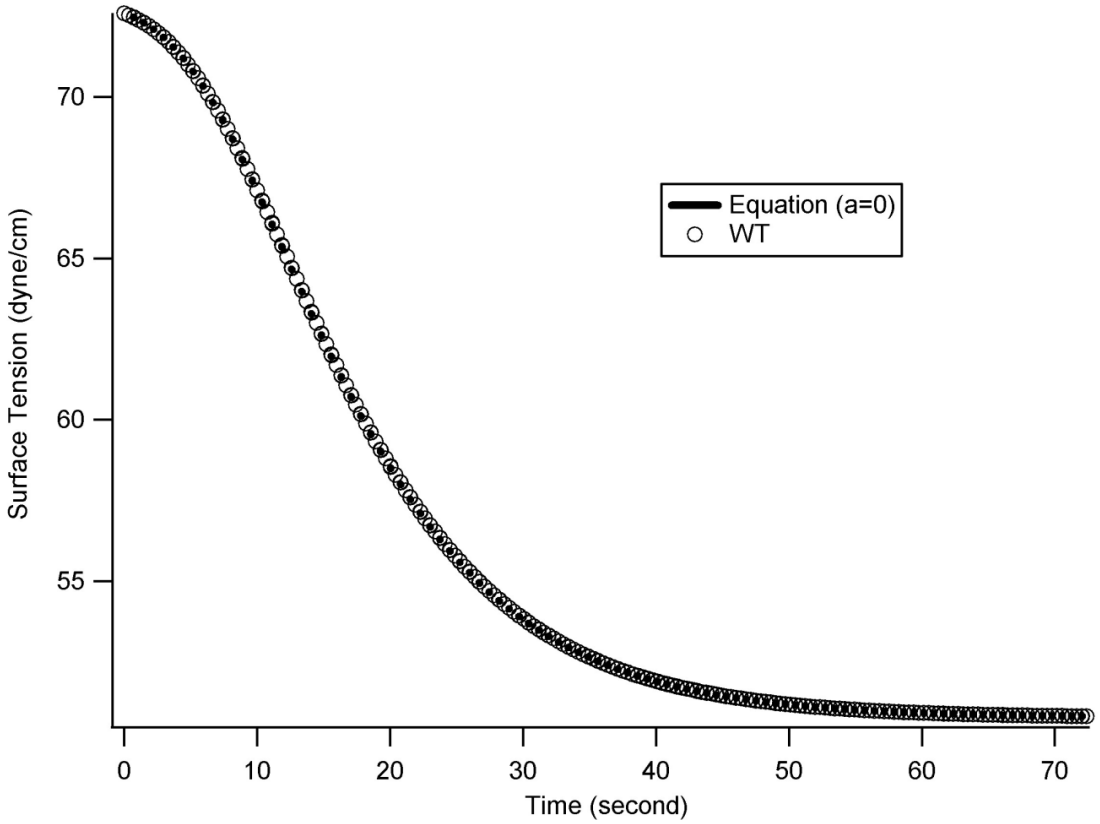


**Figure 5-2.** Validating the analytical solution by comparing it with Ward n Tordai equation when there is no 'reaction' in the system (ε→∞).

Now, we have two equations, equation (14) and (21), and there are two unknowns, Γ and $C_s$. We solve these equations simultaneously giving us the time dependent surface concentration Γ and sublayer concentration $C_s$. Lastly, we relate the surface tension to the

surface concentration using an equation of state derived from iteratively expanding the pendant bubble.

## 5.2. Measurement of the equation of state

We measure a series of expansions with the pendant bubble to obtain an equation of state. The method is described in Pan et al [134], Lin et al [136], and Kumar et al [131]. Briefly, a pendant bubble of diameter 1-3 mm is allowed to reach equilibrium. Subsequently, this bubble is rapidly expanded. Images of the bubble before and after expansions are captured and analyzed. The bubble with known surface area, $A_1$, and surface concentration, $\Gamma_1$, is expanded to a bubble having new surface area, $A_2$, and surface concentration, $\Gamma_2$. As bubble before expansion has reached equilibrium, surface tension for surface concentration $\Gamma_1$ is always equilibrium surface tension ($\gamma_{equilibrium}=\gamma_{reference}=50$ dyne/cm). It is assumed that there is no adsorption of folded peptide during expansion. Therefore, we directly relate surface coverage with area, yielding

$$\frac{\Gamma_2}{\Gamma_1} = \frac{A_1}{A_2}$$

For each expansion, a plot of surface tension (after expansion) as a function of relative surface concentration ($\Gamma_{rel}=\Gamma_2/\Gamma_1$) is drawn. This expansion experiment is repeated for different ratios of $A_1/A_2$ by varying the expansion of the bubble, and each $\Gamma_{rel}$ datum is associated with a given $\gamma$, Figure 5-3. This equation of state is then fit to an empirical equation similar to the equation used by Subramanyam et al [135].

$$\gamma = 72.6 - q_1 \ln\left(1 + \frac{\exp\left(q_3 \Gamma_{rel}\right) - 1}{q_2}\right) \qquad [23]$$

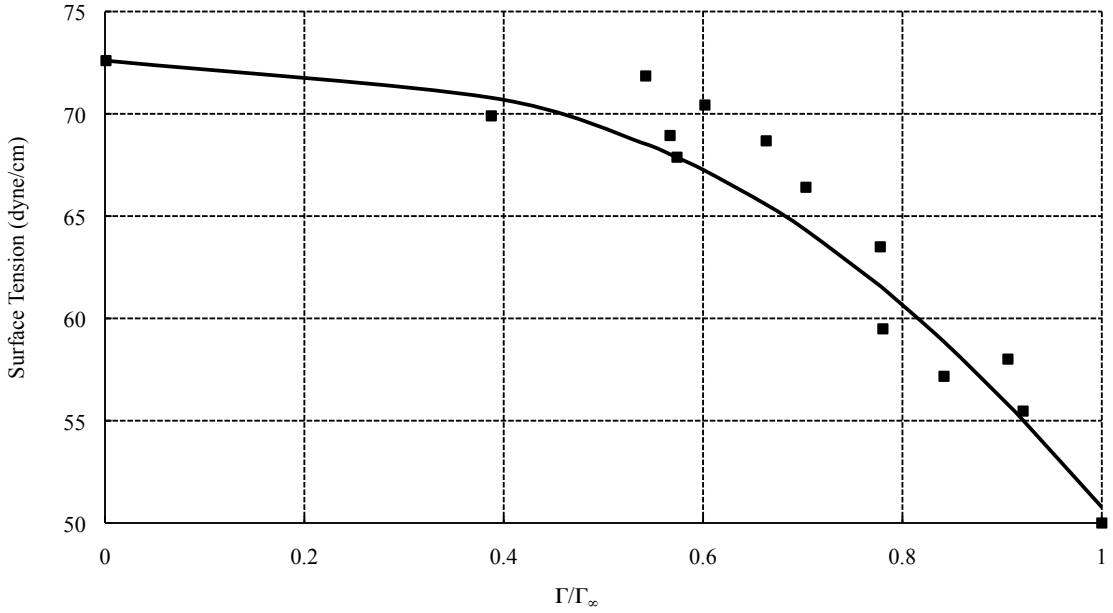


**Figure 5-3.** Surface tension as a function of relative surface concentration for model peptide and empirical fit to the data. For empirical fit, q1= 12.9, q2=45, q3=5.3. Solid line: empirical fit, symbols: experimental data.

## 5.3. Results and Discussion

We use the model to test the relative contributions from our dimensionless parameters. Figures 5-4 and 5-5 show the effect of changes in σ and ω on non-dimensional surface concentration (Γ) and sublayer concentration ($C_s$) for folded peptide. First we discuss the effect of σ as it controls the switchability of our peptide.

### 5.3.1. Effect of σ

In this case, we vary the ratio of the folding and unfolding rates, s. We fix ω and ε to a value of 1, which can be interpreted as a scenario where the diffusion time and adsorption time are equivalent, and the reaction time and diffusion time are also equivalent. From figure 5-4A and 5-4B, we observe that as σ increases, surface concentration and sublayer concentration approaches Ward-Tordai. This is also seen in equation (21) as it reduces to the Ward-Tordai equation when $\sigma \to \infty$. We show that as σ increases, population of folded peptide increases, and, at high values of σ, the system behaves as if there is only folded peptide. At σ=25 (salt concentration=1M) from figure 5-4A and 5-4B, we see that the surface concentration and sublayer concentration approaches the Ward–Tordai solution for surface concentration and sublayer concentration. Interestingly, smaller σ gives faster dynamics because in the non-dimensional form the unfolded population acts as a reservoir. So we believe that when the folded peptide adsorbs at the interface, this unfolded peptide converts to the folded peptide that then adsorbs at the interface resulting in faster dynamics.

A)

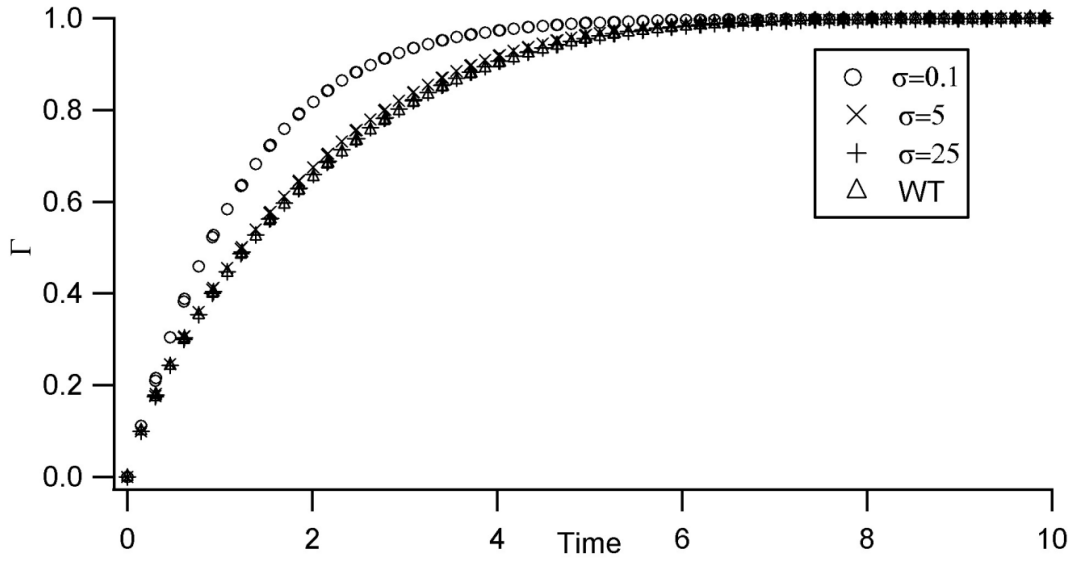


B)

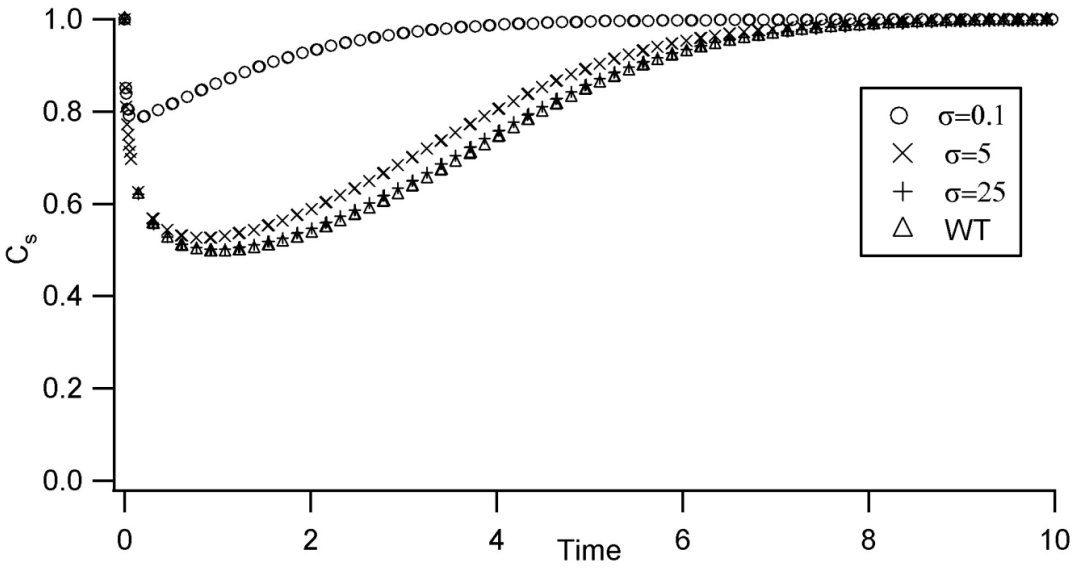


**Figure 5-4.** Effect of σ on A) Surface concentration (Γ) B) Sub-layer concentration ($C_s$).

### 5.3.2. Effect of ω

In this case we vary ω, the ratio of adsorption time to diffusion time. We fix σ=25 (high folded populations) and ε=1. When $\omega < 1$, the process is diffusion controlled i.e. the adsorption step is very fast. Therefore, the drop in the sublayer concentration for low values of ω is greater than the drop in the sublayer concentration at high values of ω as shown in figure 5-5B. Since adsorption is faster than diffusion, surface concentration Γ quickly reaches $\Gamma_\infty$, maximum packing, figure 5-5A. When $\omega > 1$, adsorption becomes the rate determining step i.e. diffusion is faster than adsorption. Thus, sublayer concentration $C_s$ is always near 1 for high values of ω as seen in figure 5-5B. Since adsorption is slow, surface concentration Γ reaches $\Gamma_\infty$ slowly, figure 5-5A.

A)

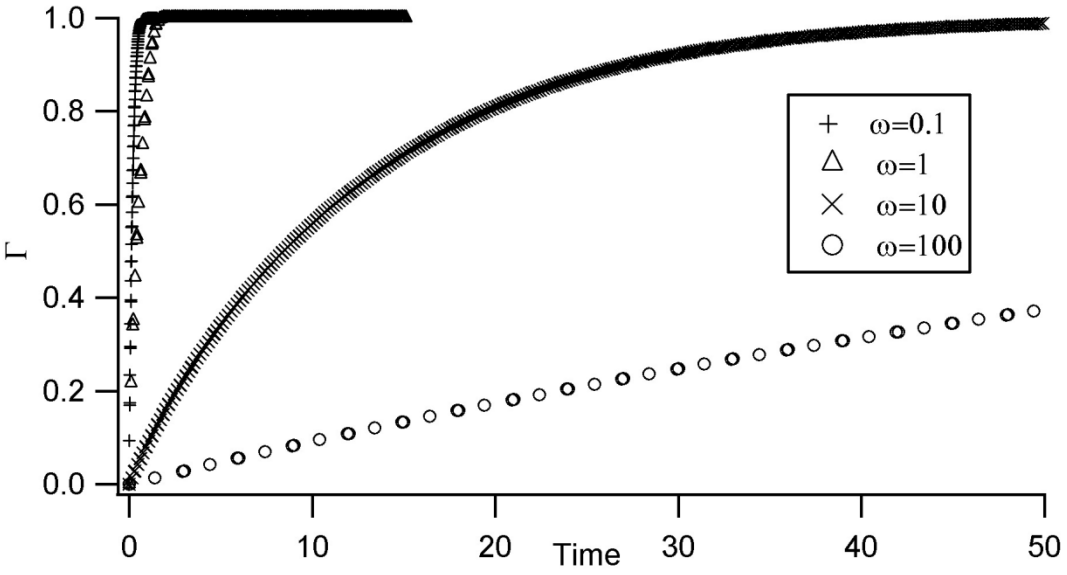


B)

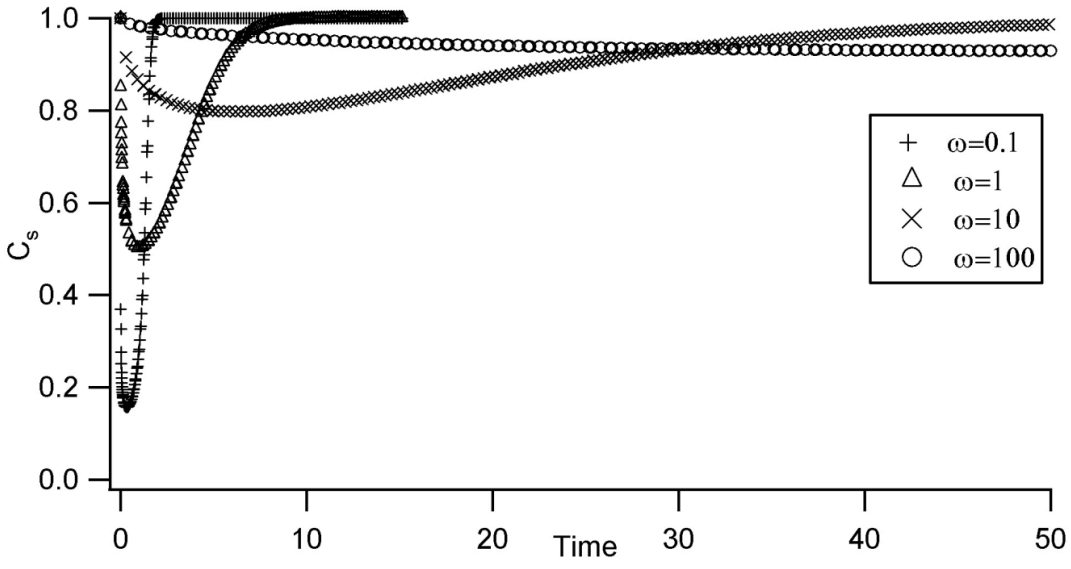


**Figure 5-5.** Effect of ω on A) Surface concentration (Γ) B) Sub-layer concentration ($C_s$)

### 5.3.3. Effect of ε

We did not see a significant effect of ε (Figure 5-6), the Damkohler number, on surface concentration and sublayer concentration at σ=25 and ω=1. From our discussion on the effect of σ on surface concentration and sublayer concentration, we have shown that at high values of σ equation (21) reduces to Ward – Tordai equation. As a result, we believe, ε has little effect on surface concentration and sublayer concentration. To validate this assumption, we will analyze the effect of ε by asymptotic method in which we consider the case ε→0 (very fast reaction case).

A)

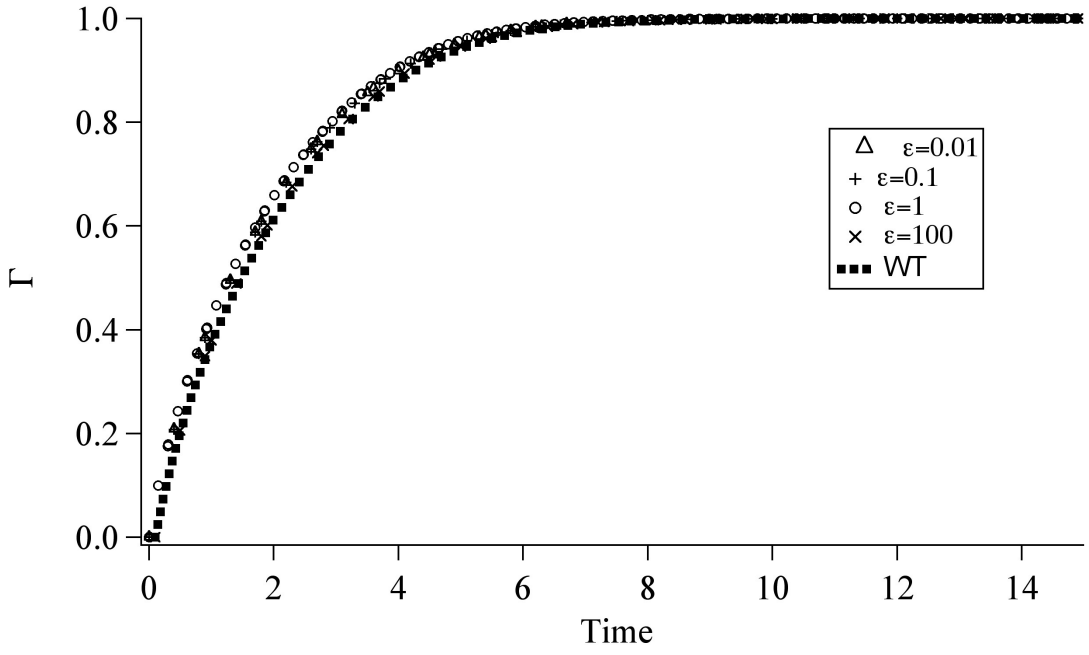


B)

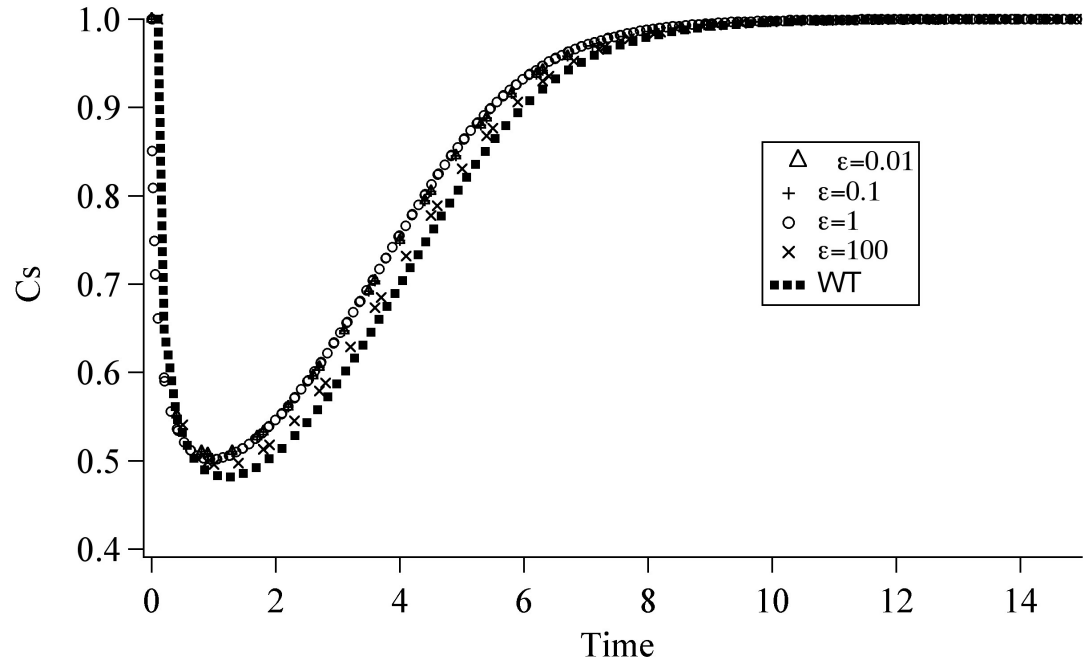


**Figure 5-6**. Effect of ε on A) Surface concentration (Γ) B) Sub-layer concentration ($C_s$)

## 5.4 Asymptotic Solution

In the asymptotic method, we consider very fast reaction case, ε→0, and we divide the interfacial region in two parts. The inner region is the region very close to the interface, and the outer region is the represents the bulk aqueous phase, figure 5-7. We consider the two regions separately.

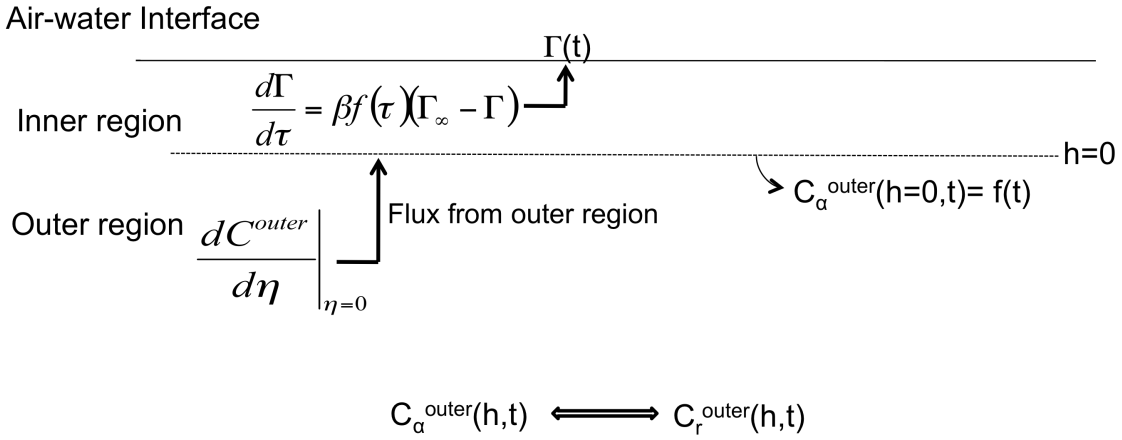


**Figure 5-7.** Schematic diagram for asymptotic solution showing inner and outer region.

### 5.4.1 Outer region

For outer region from equation (17) and (18) we have,

$$\frac{\partial \overline{C_\alpha}}{\partial \tau} = \frac{\partial^2 \overline{C_\alpha}}{\partial \eta^2} + \frac{1}{\sigma\varepsilon}\left(\overline{C_r} - \overline{C_\alpha}\right)$$

$$\frac{\partial \overline{C_r}}{\partial \tau} = \frac{\partial^2 \overline{C_r}}{\partial \eta^2} - \frac{1}{\varepsilon}\left(\overline{C_r} - \overline{C_\alpha}\right)$$

The boundary conditions are as follows:

$$\eta \to \infty \quad \overline{C_\alpha} = 1 \text{ and } \overline{C_r} = 1$$

$$\eta \to 0 \quad \overline{C_\alpha} = f(\tau) \text{ and } \left(\frac{\partial \overline{C_r}}{\partial \eta}\right)_{\eta=0} = 0 \qquad [24]$$

The initial conditions are as follows:

$$\overline{C_\alpha}(\eta,0) = 1$$

$$\overline{C_r}(\eta,0) = 1 \qquad [25]$$

Since reaction between folded and unfolded peptide is very fast, folded and unfolded peptide are assumed to be in equilibrium. Therefore, in the outer region, a quasi-steady state approximation is assumed.

$$C_\alpha^{\ outer}(\eta,\tau) \rightleftharpoons C_r^{\ outer}(\eta,\tau)$$

$$C_\alpha = \sigma C_r \qquad [26]$$

Now multiplying equation (17) by σ and adding the resulting equation to equation (18) and then using equation (26) we get,

$$\frac{\partial \overline{C_\alpha}}{\partial \tau} = \frac{\partial^2 \overline{C_\alpha}}{\partial \eta^2} \qquad [27]$$

To solve this, we take the Laplace transform of this partial differential equation. We solve this equation and apply the boundary conditions. Taking Laplace inverse, we get

$$C_\alpha^{\ outer} = 1 - erfc\left(\frac{\eta}{2\sqrt{\tau}}\right) + \int_0^\tau f(\tau - \tau') \frac{\eta}{2\sqrt{\Pi}} \tau'^{-3/2} \exp\left(\frac{\eta^2}{4\tau'}\right) d\tau' \quad [28]$$

From quasi-steady state approximation we have,

$$C_r^{\,outer} = \frac{1}{\sigma}\left(1 - erfc\left(\frac{\eta}{2\sqrt{\tau}}\right) + \int_0^{\tau} f(\tau - \tau')\frac{\eta}{2\sqrt{\Pi}}\tau'^{-3/2}\exp\left(\frac{\eta^2}{4\tau'}\right)d\tau'\right) \qquad [29]$$

The total flux of the peptide (folded and unfolded) from outer region to the boundary of the inner region is given by

$$\left.\frac{dC^{outer}}{d\eta}\right|_{\eta=0} = \left.\frac{dC_\alpha^{\,outer}}{d\eta}\right|_{\eta=0} + \left.\frac{dC_r^{\,outer}}{d\eta}\right|_{\eta=0} \qquad [30]$$

$$\left.\frac{dC^{outer}}{d\eta}\right|_{\eta=0} = \frac{\sigma}{\sigma+1}\left(\frac{1}{\sqrt{\Pi\tau}} + \int_0^{\tau}\frac{f(\tau-\tau')}{2\sqrt{\Pi}}\tau'^{-3/2}\,d\tau'\right) \qquad [31]$$

## 5.4.2 Inner region

In the inner region, adsorption of folded peptide onto the air water interface is the dominating step, and the reaction rate between the folded and unfolded peptide is fast. Consequently, their concentrations are independent of time. Equation (17) and (18) becomes,

$$\frac{\partial^2\overline{C_\alpha}}{\partial\eta^2} + \frac{1}{\sigma\varepsilon}\left(\overline{C_r} - \overline{C_\alpha}\right) = 0 \qquad [32]$$

$$\frac{\partial^2\overline{C_r}}{\partial\eta^2} - \frac{1}{\varepsilon}\left(\overline{C_r} - \overline{C_\alpha}\right) = 0 \qquad [33]$$

We solve this partial differential equation and use Van dyke matching condition to get the constants (solution not shown). The flux of peptide from the inner region to interface is defined by Langmuir adsorption.

$$\frac{d\Gamma}{d\tau} = \beta f(\tau)\left(\Gamma_\infty - \Gamma\right) \qquad [34]$$

And the overall mass balance defines the fluxes of the peptide from outer region to the boundary of the inner region and from inner region to the interface to be equal:

$$\frac{d\Gamma}{d\tau} = \left.\frac{dC^{outer}}{d\eta}\right|_{\eta=0} \qquad [35]$$

And therefore,

$$\frac{d\Gamma}{d\tau} = \frac{\sigma}{\sigma+1}\left(\frac{1}{\sqrt{\Pi\tau}} + \int_0^\tau \frac{f(\tau-\tau')}{2\sqrt{\Pi}}\tau'^{-3/2}\,d\tau'\right) \qquad [36]$$

Solving equation (36) for Γ we get,

$$\Gamma(\tau) = \frac{\sigma}{\sigma+1}\left(2\sqrt{\frac{\tau}{\Pi}} - \frac{2}{\sqrt{\Pi}}\int_0^\tau \frac{f(\tau-\tau')}{\sqrt{\Pi\tau'}}d\tau'\right) \qquad [37]$$

Above equation is similar to the Ward – Tordai equation except for the σ terms outside the brackets. This shows that when σ is large, the system is populated with the folded peptide, and the adsorbing peptide behaves as a single component system. Again, we have two equations (37 & 34). We solve them simultaneously, using our equation of state to get surface tension as a function of time.

## 5.5 Comparison of experimental data with numerical and asymptotic solution

In this section, we compare the experimental data with the numerical solution and determine the unknown constants in the modeling (Figure 5-8). We only need to determine two unknowns, $\beta$ and $\Gamma_\infty$. Diffusion co-efficient used for this comparison is $2.175 \times 10^{-10}$ $m^2/s$. To ensure that the system does not vary with $\varepsilon$ (i.e. $k_1$), we compare our numerical solution with the asymptotic solution. From figure 5-9, we observe that at high values of $\sigma$, the reaction between folded peptide and unfolded peptide behaves as a single component system. We also check the significance of values obtained for the different parameters, comparing the non-dimensional parameters used in the numerical solution, $\varepsilon$ and $\omega$.

In our system, we expect that $\varepsilon$ will always be of the order 0 since the folding time (~1 us to 1 ms) is much smaller than the diffusion time (1000sec). $\omega$, the ratio of adsorption time to diffusion time, is dependent on the concentration of the peptide. For concentrations of peptide from 1 g/l -0.001 g/l, $\omega$ is large, and adsorption is the rate-determining step. This supports the result of our 'simple' analysis described in Jain et al [6]. Additionally, we observe that this model is insufficient to fit the long time dynamics of peptide adsorption. We believe this will require the addition of terms that account for phase behavior at the interface. The model teaches us that the fundamental behavior of the peptide at the air-water interface will likely require a more complex equation of state expression. Modifications to the equation of state will require additional experimental work to characterize the condensed phases of a highly populated interface. Other future work will examine the design of novel peptides where selective binding is coupled to surface activity, serving as a platform for next generation materials and separation tools.

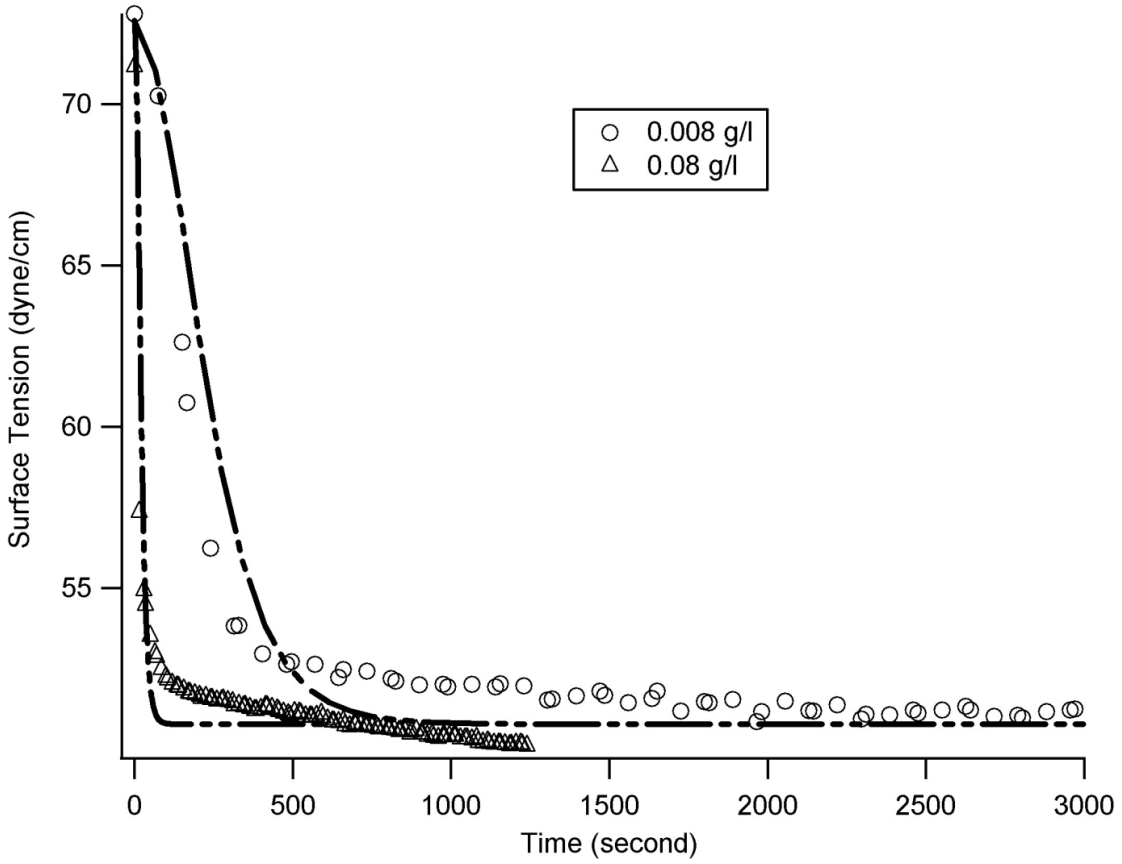


**Figure 5-8.** Experimental data is fitted by numerical solution with $\beta = 2.85\ m^3/mol\ s$ and $\Gamma_\infty = 10^{-7}\ mol/m^2$

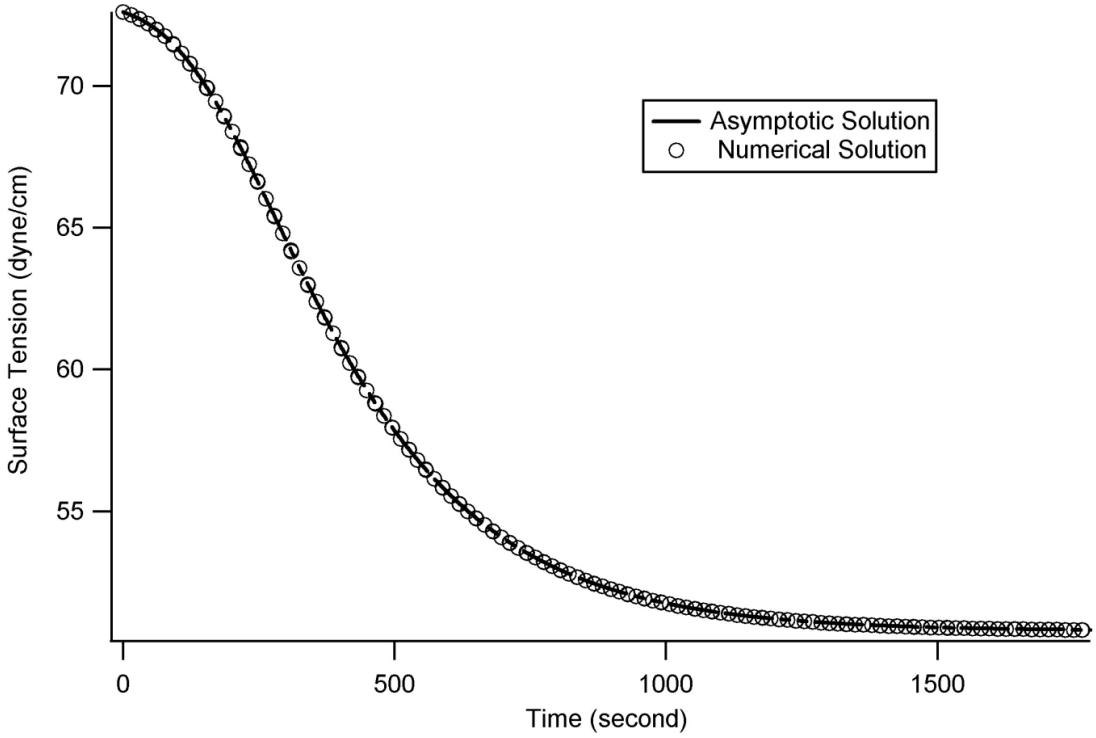


**Figure 5-9.** Comparison between asymptotic and numerical solution for 0.08g/l peptide solution in 1M NaCl.

# Chapter 6

# Liquid Crystal experiments

In this chapter, we will look at the use of dynamic molecules like our model peptide as a viable sensing tool. In the previous section, we have shown that one can use pendant bubble technique to examine the dynamics associated with the model peptide where surface-active form of the peptide (folded) adsorbs at the interface. Here, we will use the technique pioneered by Abbott lab [8] where a thermotropic liquid crystal is used to visualize the adsorption of peptide to an interface. The dynamics of this process mirror the pendant bubble, but there are three key advantages to the technique. First, the method is simple and inexpensive to execute. Second, the method requires very small sample volumes (~ 5μL). Third, preliminary work suggests that the method is very sensitive to the adsorption of amphiphilic helical peptides.

Liquid crystals are well suited for low concentration detection because cooperative orientational dynamics inherently leads to signal amplification. In order to make these new dynamic molecules into a viable sensing tool, we use this robust and flexible system

to measure the folding and unfolding behavior. Future work will involve in engineering the peptide sequence where the dynamic behavior of folding and unfolding is coincident with the target binding.

Figure 6-1 shows the different alignments (planar and homeotropic) of the liquid crystal under the polarized light. Figure 6-2 is the schematic representation of our hypothesis, model peptide responding to environmental stimuli. An external stimulus, NaCl or DNA, induces folding in the peptide resulting in a surface-active state. Here, our assumptions are similar to those made in the pendant bubble experiments: (1) the folded peptide is in equilibrium with the unfolded peptide in the bulk phase and (2) only the folded peptide (surface active/amphiphilic) adsorbs at the interface. So, when unfolded peptide interacts with the surface, liquid crystal remains in a planar arrangement (Figure 6-1 A and B). When the folded peptide adsorbs to the interface, the amphiphilic nature causes the liquid crystal to transition into the homeotropic phase, removing the bright pattern (Figure 6-1 C and D).

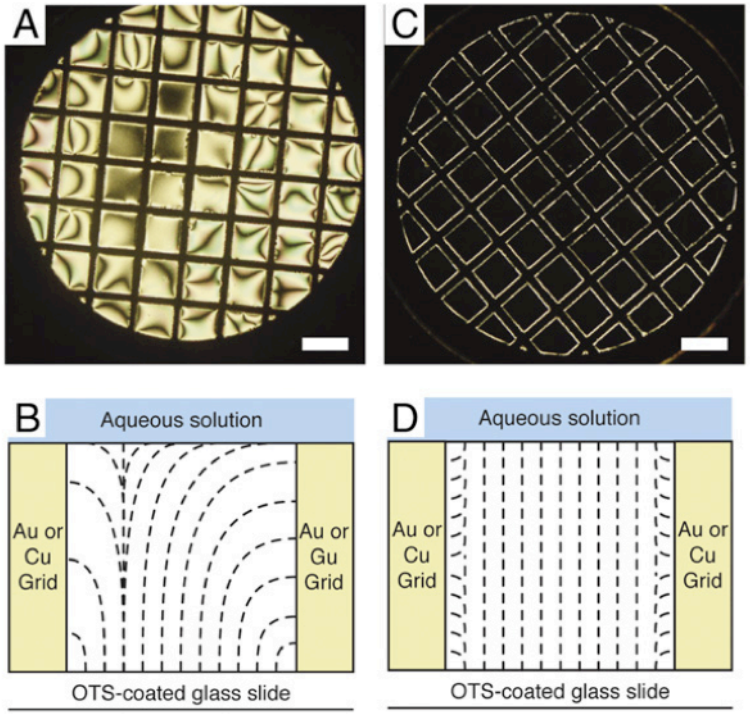


**Figure 6-1.** Appearance and orientation of liquid crystals with different surface anchoring conditions. Optical images (crossed polars, A, C) and schematic illustrations of the director profiles (B, D) of the liquid crystal 5CB hosted in a gold grid and under conditions leading to planar (A–B) and homeotropic (C–D).

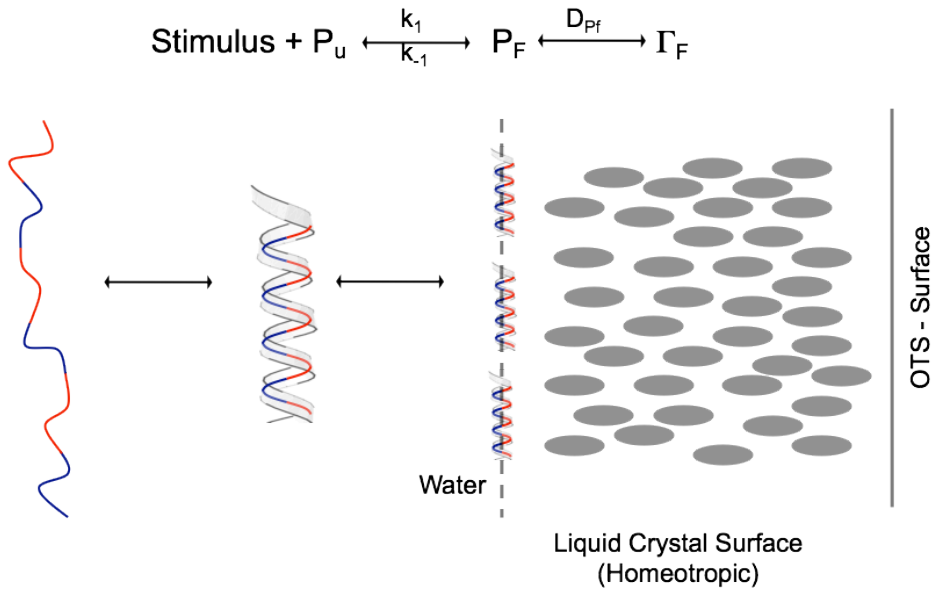


**Figure 6-2:** Schematic representation of the model peptide responding to the external stimuli resulting in dynamic folding and amphiphilicity. Adsorption of the folded peptide at the liquid crystal-aqueous interface causes the liquid crystal transition into the hemeotropic phase.

## 6.1 Experimental set-up

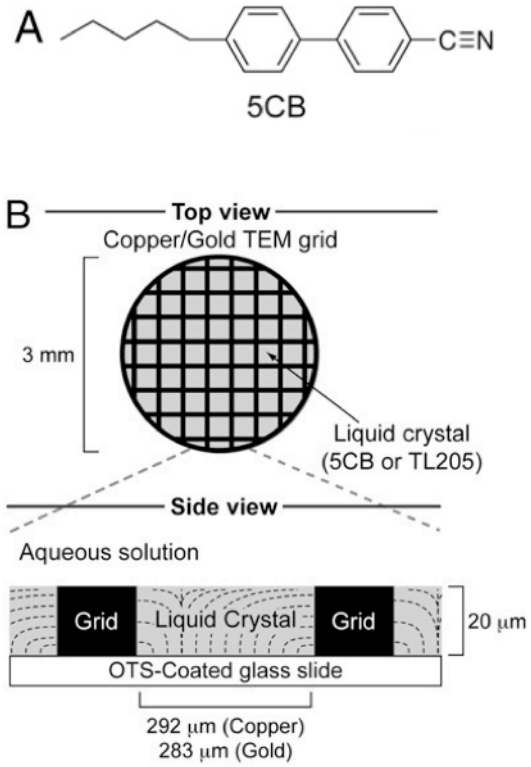


**Figure 6-3**: A) Molecular structure of 5CB. B) Schematic representation of the experimental setup used for the study of adsorption of amphiphilic helical peptide at the aqueous-liquid crystal interface.

Experimental setup used for the liquid crystal experiments is as follows (figure 6-3B): A glass microscope slide is treated with octadecyltrichlorosilane (OTS) to make the glass surface hydrophobic (contact angle ~ 103°). A SEM copper grid is placed on the pre-treated glass slide and 5CB liquid crystal (figure 6-3A) fills the pores of the grid. When the aqueous solution is added to this setup, it forms a stable interface between

aqueous surface and liquid crystal and the resulting images are captured under polarized light.

## 6.2 Results and discussion

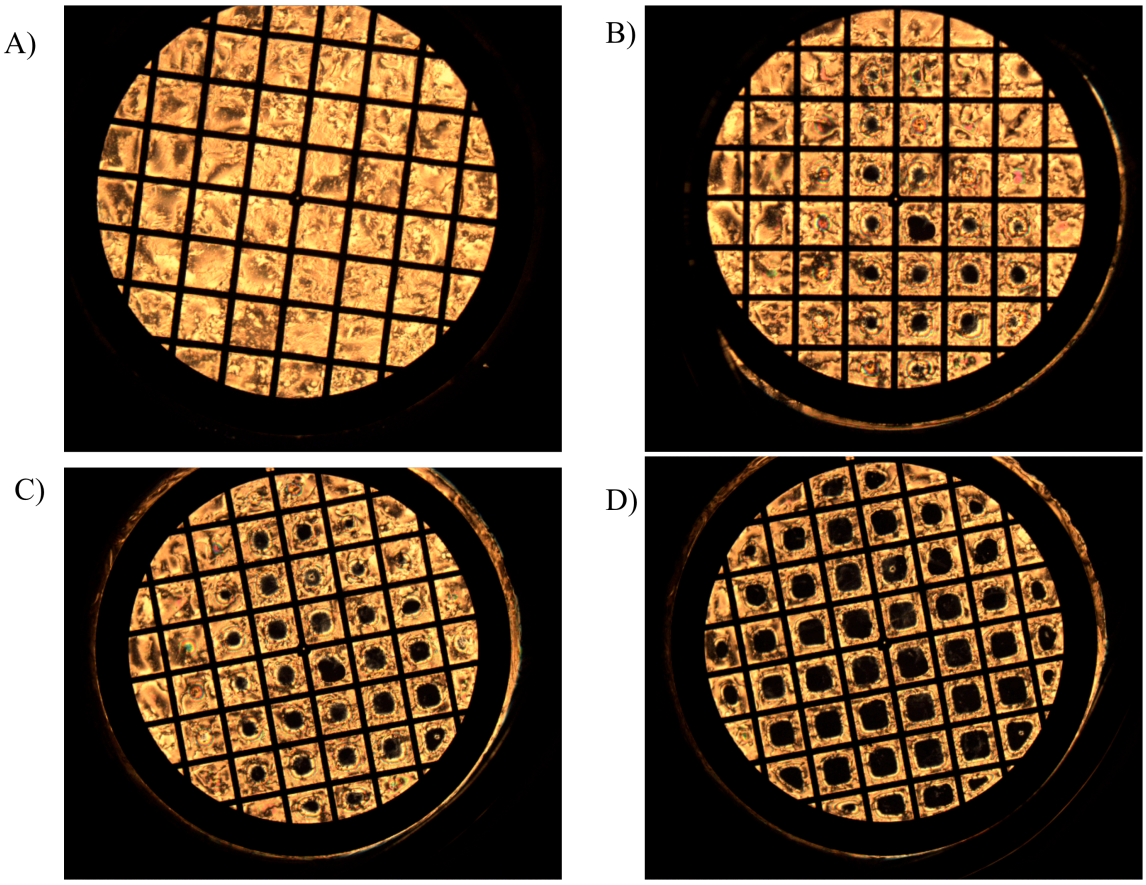


**Figure 6-4.** A) Liquid crystal. B) Aqueous peptide solution is added to the liquid crystal. C) DNA is introduced in the system. D) Image captured after 30 min (equilibrium image).

In figure 6-4A, the submerged liquid crystal image serves as the baseline for the other images before peptide and DNA are added to the experimental system. In the case of peptide aqueous solution in DI water, we know from the CD experiments that the

solution consist primarily of unfolded peptide that is not amphiphilic. When the model peptide aqueous solution is added to the liquid crystal setup, the liquid crystal remains in planar arrangement and the resulting image is bright (figure 6-4B). When DNA is introduced in the same system, the DNA induces the folding of the peptide, making an amphiphilic complex. Now, this amphiphilic nature of the peptide:DNA causes change in the alignment (homeotropic) of the liquid crystal (figure 6-4C). After 30 min, equilibrium is reached and the whole image has darkened indicating the homeotropic alignment of the liquid crystal caused by the adsorption of the amphiphilic helical peptide at the aqueous liquid crystal interface (figure 6-4D).

We have showed that this liquid crystal method can be used to measure the folding and unfolding behavior of the model peptide. To use this technique in the biosensor application, next step is to design the peptide sequence that shows this dynamic behavior and binds selectively to target site.

# Chapter 7

# Investigating kinetics of DNA condensation

The main objective of this chapter is to discuss our study of the DNA condensation kinetics by using rationally designed peptide with transient secondary structure and amphiphilicity. We can control the spatial, chemical and physical properties of peptide, allowing us to investigate the influence of cooperative structure formation associated with the DNA condensation. As discussed before, synthetic peptides can be designed in the laboratory with well-controlled secondary structure by proper selection and positioning of amino acids [3, 4, 85-88, 138]. The model peptide used in this study is designed based on the phenomenon observed in nature where folding is coupled to binding. We investigate the dynamics of the DNA-condensation by using our model peptide where the interaction between DNA and peptide is non-specific. We compare the DNA condensation with our model peptide with another well-studied condensing agent, Spermidine. We have used circular dichroism to show the folding of the peptide in presence of DNA at different salt concentrations and Multi angle light scattering (MALS)

for the time-resolved study of DNA-peptide complex formation. The circular dichroism experiment shows that when DNA is introduced in the system, an increase in helicity is observed, validating that the peptide binds to DNA in the folded form.

The MALS experiments are used to explore the rate of formation of the DNA:peptide complex. We apply a Composition Gradient (CG) apparatus that allows us to simultaneously control the concentration of peptide, DNA and also the surrounding conditions (salt concentration, pH). This allows us to investigate their effects on the complex formed and also monitor the size and molecular weight of the complex, which are essential for the efficient transport across cell membranes in gene delivery.

## 7.1. Materials and methods

### Materials

The model peptide sequence is synthesized and purified with HPLC by The Rockefeller University Proteomics Resource Center is stored at –20 °C. The peptide is used without any further modification. All aqueous solutions are prepared using clean water from a Milli-Q water purification system. Sodium chloride (>=990 ppm and <= 1010ppm Na) obtained from Fisher Scientific (NJ) is used for preparing peptide solution in salt. All peptide solutions are prepared freshly for each experiment.

### DNA purification

DNA (herring sperm) from Sigma (St. Louis, MO) is purified by dissolving it in ethanol and centrifuging the solution at -40 °C for 20 min. This cycle is repeated 3 times,

and the resulting pellet is dried in vacuum oven. To check the purity of DNA, size exclusion experiment is conducted, and a single flat peak is observed as compared to multiple small peaks for the unpurified DNA.

## Circular dichroism

Circular dichroism spectrophotometer experiments are conducted to see if the introduction of DNA induces the folding in the peptide. These experiments are carried out at two different NaCl concentration, 1mM and 100mM. We assume that the unfolded peptide is in equilibrium with the folded peptide in the solution, and we have shown that we can shift the equilibrium by controlling the salt concentration [6]. Circular dichroism experiments are performed at low DNA concentrations and at high concentration where the complex begins to precipitate out of the solution, resulting in an overall decrease in the intensity (data not shown).

## Multi angle light scattering

Multi angle light scattering (MALS) measurements are carried out with a DAWN DSP Laser Photometer (Wyatt Technology Inc., Santa Barbara, CA). Detecting the intensity of light at different angles (in this case 18 different angles) can be used to measure the size (radius of gyration) and molecular weight of the particle. In light scattering, there are two non-ideal effects: large particle size effect and non-ideal solutions. Non-ideality allows us to determine the second virial coefficient. Overall, Multi angle light scattering can be used to measure average number molecular weight ($M_w$), radius of gyration ($<s^2>$) and the second virial coefficient ($A_2$).

$$\frac{Kc}{R_\theta} = \left(\frac{1}{M_w} + 2A_2c\right)\left(1 + \frac{16\pi^2}{3\lambda^2}\left\langle s^2\right\rangle_\omega \sin^2\frac{\theta}{2}\right)$$

where, $R_\theta$ is the excess Rayleigh ratio of the solution, θ is the scattering angle and $c$ is the concentration. The Rayleigh ratio is directly proportional to the intensity of the scattered light in excess of the light scattered by the pure solvent. $K$ is constant that depends on the solvent properties, and $K$ is calculated using the following equation:

$$K = \frac{4\pi^2 n_0{}^2}{N_A\lambda^4}\left(\frac{dn}{dc}\right)^2$$

where, λ is the wavelength, $M_w$ is the weighted average molecular weight of the particle, $<s^2>_w$ is the radius of gyration of the particle, $A_2$ is the second virial coefficient in the virial expansion of the osmotic pressure, $n_0$ is the index of refraction of the solvent, and $N_A$ is Avogadro's number.

The light scattering experiments consists of measuring $Kc/R_\theta$ for various concentrations and at various scattering angles. To calculate the molecular weight of the particle, first, we plot $K_c/R_\theta$ as a function of $\sin^2(\theta/2)$ at constant concentration to give a straight line with the following slope and intercept:

$$\text{Slope: } \left(\frac{1}{M_w} + 2A_2c\right)\frac{16\pi^2}{3\lambda^2}\left\langle s^2\right\rangle_\omega$$

$$\text{Intercept: } \left(\frac{1}{M_w} + 2A_2c\right)$$

Next step is to plot the intercept as a function of concentration. The resulting plot should be a straight with slope= $2A_2$ and intercept= $1/M_w$. Substituting these values in the slope of the first plot will give us radius of gyration $\langle s^2 \rangle$.

We use MALS to monitor both the DNA peptide complex as a function of time and the effect of peptide concentration, DNA concentration and electrolytes on the complex formation. Experiments are performed at two different salt concentrations, 1mm NaCl and 100mM NaCl, where the peptide is mostly random coil and helical, respectively.

## 7.2 Circular dichroism

As the DNA is added to the peptide solution, we observe that our model peptide is capable of condensing the DNA. The DNA-peptide complex precipitates out and can be seen by the naked eye. Here, the interaction between the peptide and DNA is non-specific. These preliminary experiments were performed at high concentration of peptide and DNA (data not shown). As the DNA concentration is increased, a decrease in the overall intensity of the CD spectrum is observed. This suggests that the peptide, after forming complex with DNA, precipitates out, and there is decrease in peptide concentration in the solution.

a)

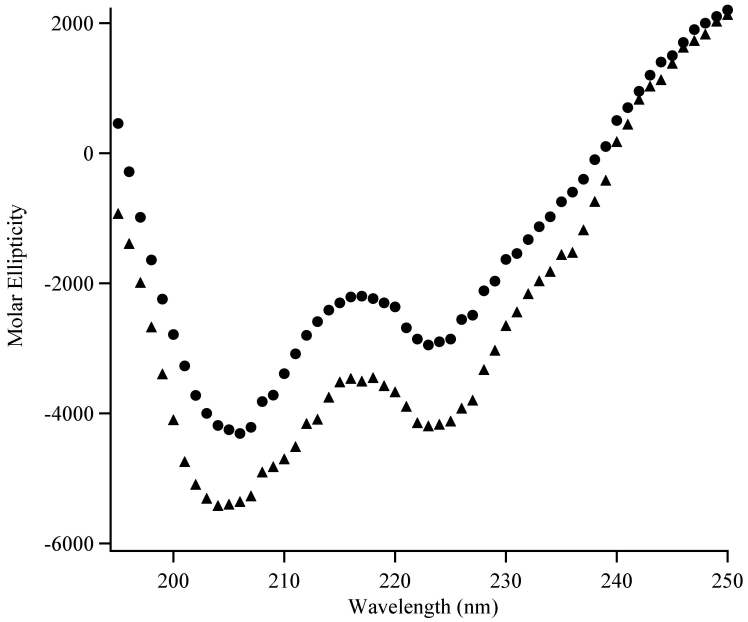


b)

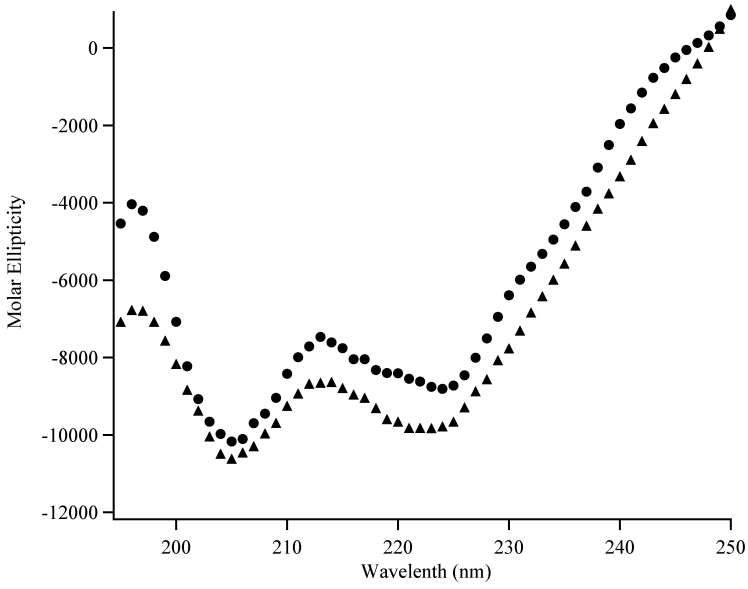


**Figure 7-1.** Circular dichroism for the model peptide in presence of DNA in a) 1mmNaCl b) 100mM NaCl. ●:- Peptide. ▲:- Peptide + DNA

However, when low concentration DNA (~ 0.001 g/l) is added to the peptide solution, the resulting solution is clear and circular dichroism shows an increase in helicity. This increase in helicity is the result of fishing mechanism. At low salt concentration (1mM and 100mM, figure 7-1), we observe that the solution consist of primarily unfolded peptide. When DNA is added to the solution, the unfolded peptide forms an α-helix and then binds to the DNA, increasing the observed helicity. For both salt concentrations, 1mM and 100mM, peptide binds to DNA in the folded form.

## 7.3 Multi angle light scattering

Kinetic of DNA peptide complex are studied by using multi angle light scattering (MALS). Experiments are performed at two different salt concentration, 1mM and 100mM, and also at different DNA and peptide concentrations. In this section, we will compare the DNA condensation by our model peptide and other well studied condensing agent, Spermidine. We will also look at the DNA condensation by the unfolded and partially folded model peptide. We know from our circular dichroism experiments that the helicity of our model peptide increases with increase in salt concentration. At 1mM NaCl concentration, solution primarily consists of unfolded peptide while at 100mM NaCl concentration, it consist of folded peptide. We observe faster condensation kinetics at 1mM NaCl concentration, suggesting that the binding kinetics is enhanced due to cooperative folding and binding process.

### 7.3.1 Comparing DNA condensation by model peptide and spermidine

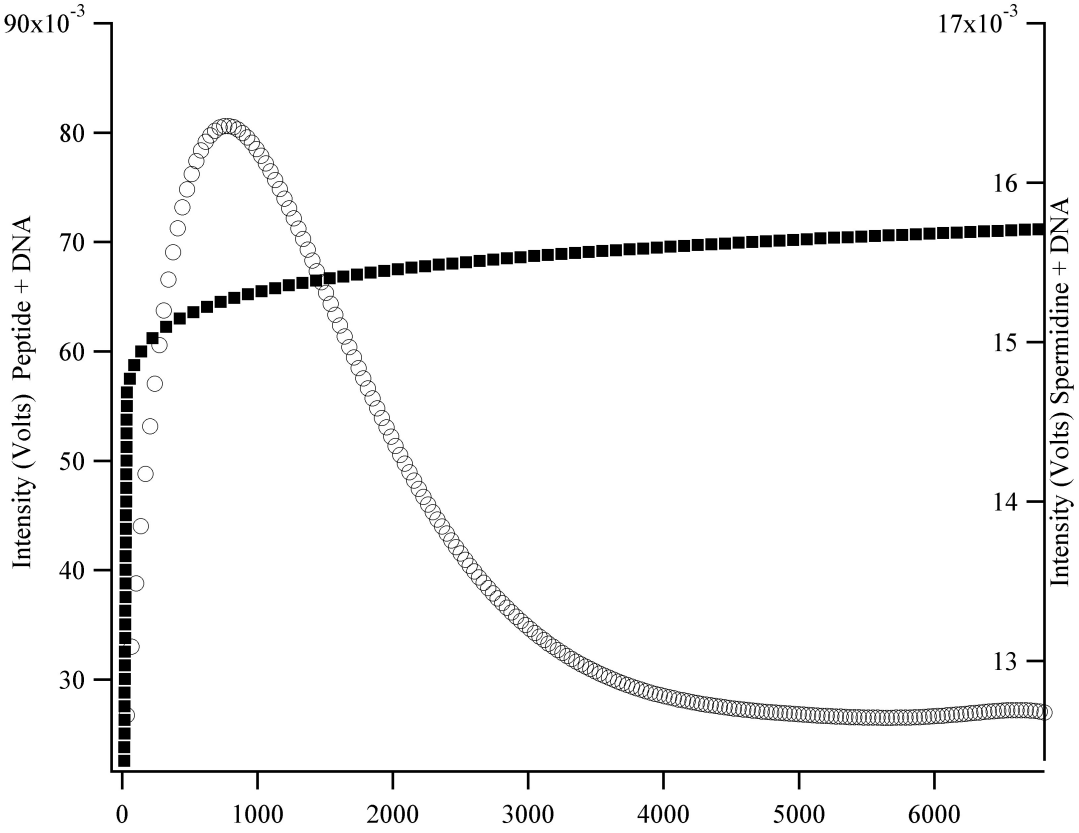


**Figure 7-2.** Comparing DNA condensation using our model peptide and Spermidine. ■:- Spermidine + DNA and ○:- Model peptide + DNA.

Figure 7-2 compares the two condensing agent, our model peptide and Spermidine. In both cases, initially rise in intensity is observed which suggest that the size of the complex is increasing. In case of spermidine, this rise in intensity is continuous and in the end it reaches the equilibrium value. This trend is observed in other condensing agents such as poly L-lysine and cobalt hexamine. In case of our model peptide, after initial rise in intensity, the scattering reaches a maximum value and, subsequently, the signal decreases to a significantly lower equilibrium value. This drop in intensity is unique in

our system, and we believe it is the re-arrangement with in the DNA:peptide complex. This re-arrangement behavior is observed in our system at different salt concentrations.

## 7.3.2 Effect of salt concentration

### 7.3.2.1 Comparing dynamics at 1mM and 100mM NaCl concentration

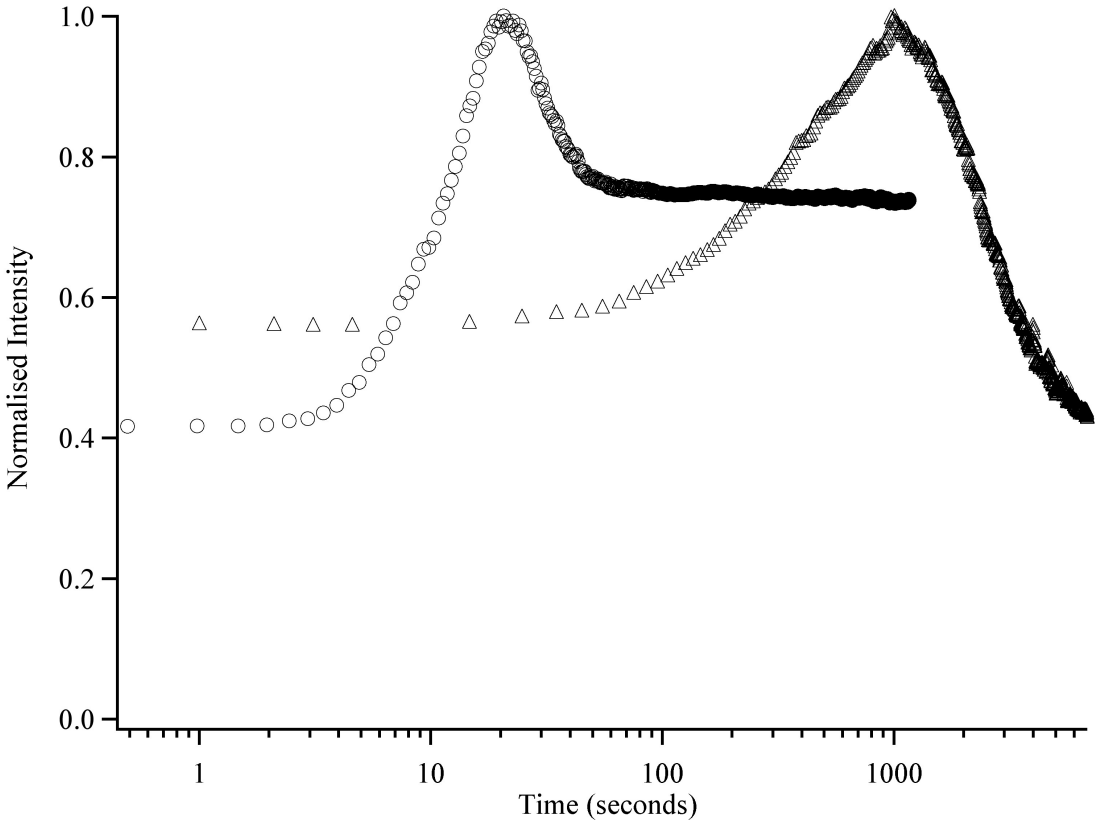


**Figure 7-3**. Comparing dynamics at 1mM and 100mM salt concentration. △: 100mM NaCl and ○: 1mM NaCl.

By comparing the time scales with 100mM NaCl concentration (figure 7-3), we see that the DNA peptide complex reaches equilibrium very quickly in 1mM NaCl solution. For 1mM NaCl solution, equilibrium time scales are in the order 100 seconds. For

100mM NaCl equilibrium time scales are in the order of 5000-7500 seconds (Figure 7-3). Thus, significantly faster kinetics are observed when the unfolded peptide interacts with the DNA (at the same peptide and DNA concentrations). This observation suggests that faster dynamics are promoted by the cooperative folding and binding mechanism. As stated earlier, the CD experiments show that the 1mM NaCl peptide solutions consist primarily of unfolded peptides and, when the DNA is introduced in the system, peptide folds and binds to DNA resulting in faster kinetics. In case of 100mM NaCl, solution consists of folded peptide and hence slower dynamics are observed as compared to 1mM NaCl solution. The following sections are an effort to elucidate the underlying mechanism for this observation.

#### 7.3.2.2 Determination of Critical Aggregation Concentration (CAC)

In this section, we determine the Critical Aggregate Concentration (CAC) of the model peptide that is the minimum concentration required to condense the DNA. We find that the CAC is different at different salt concentration. First we will look at 100mM NaCl concentration.

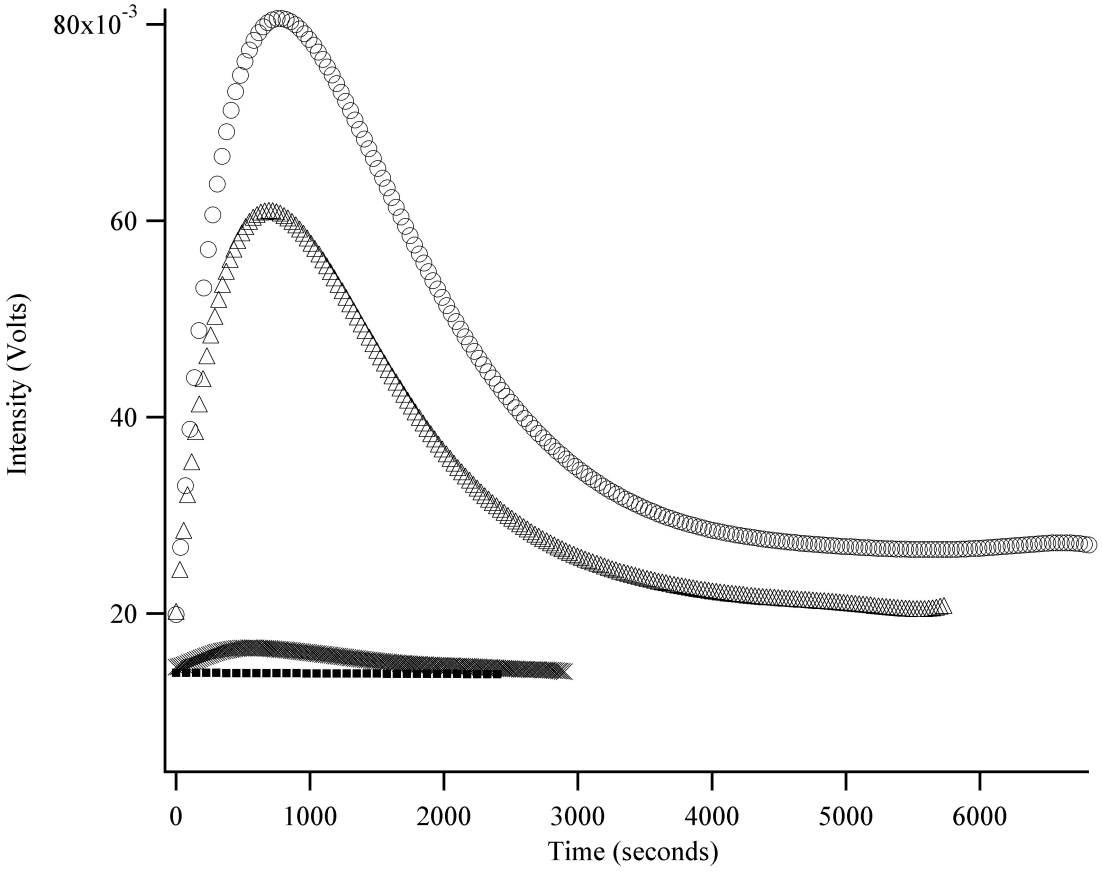


**Figure 7-4.** Critical Aggregate Concentration for 100mM NaCl. Legend represents peptide concentration. DNA concentration is kept constant 0.001 g/l. Different markers are peptide concentration: ○:- 7.5mg/l, △:-6.5mg/l, ×:-4.5mg/l, ■:-baseline.

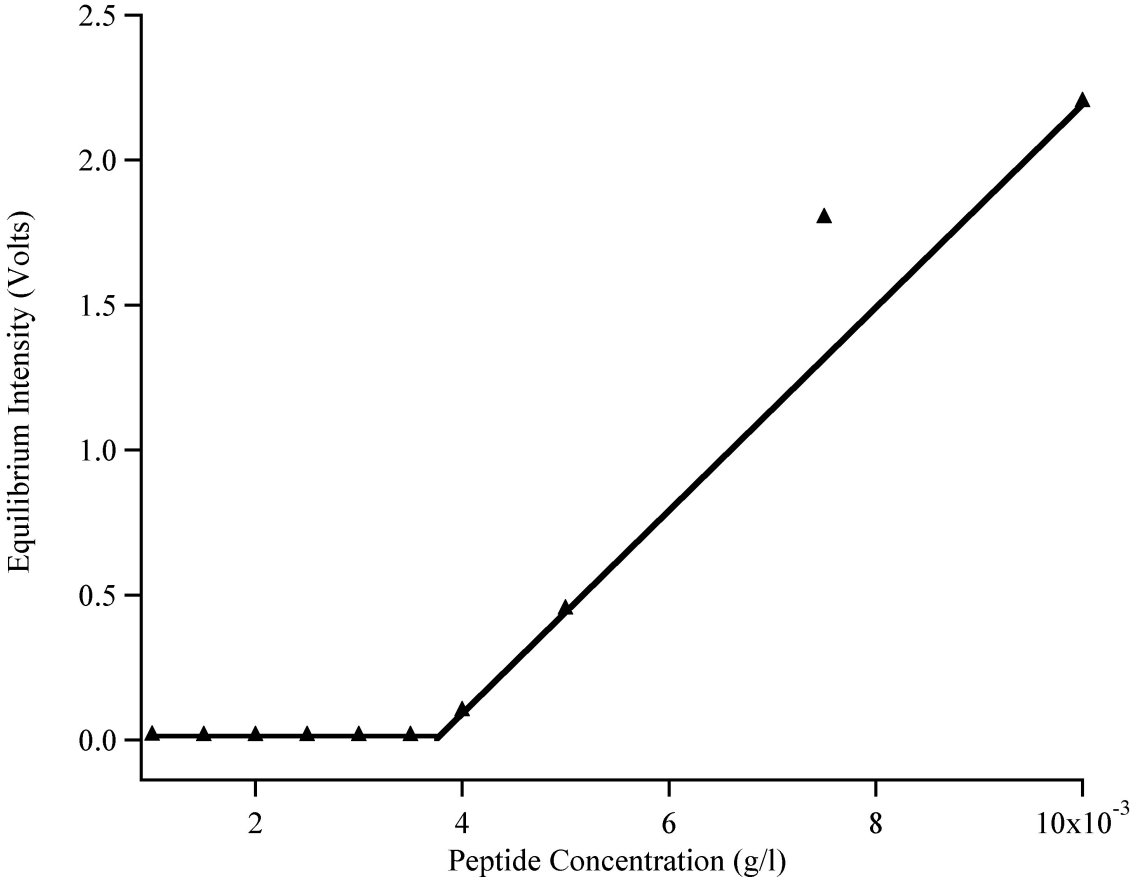


**Figure 7-5.** Determining Critical Aggregate Concentration at 100mM NaCl. DNA concentration is kept constant 0.005 g/l.

In the figure 7-4, DNA concentration is kept constant while peptide concentration is changed. The experiments are performed at 100mM NaCl Concentration. The DNA:peptide complex is detected only above certain peptide concentration (4mg/l), Critical Aggregate Concentration (CAC). We performed experiments at different DNA concentration (0.0005g/l to 0.1g/l), and we found that the CAC of the model peptide are the same in this range of concentrations. This is unique to our system (at 100mM NaCl) as others have reported decreasing CAC with increasing DNA concentrations using condensing agent such as spermidine or cobalt hexamine. In addition, we see that the

equilibrium intensity of the complex increases with increased peptide concentrations at fixed DNA concentration (figure 7-5). But after the peptide concentration reaches the saturation concentration there is no rise in the equilibrium intensity, which we discuss in detail in section 7.3.3.

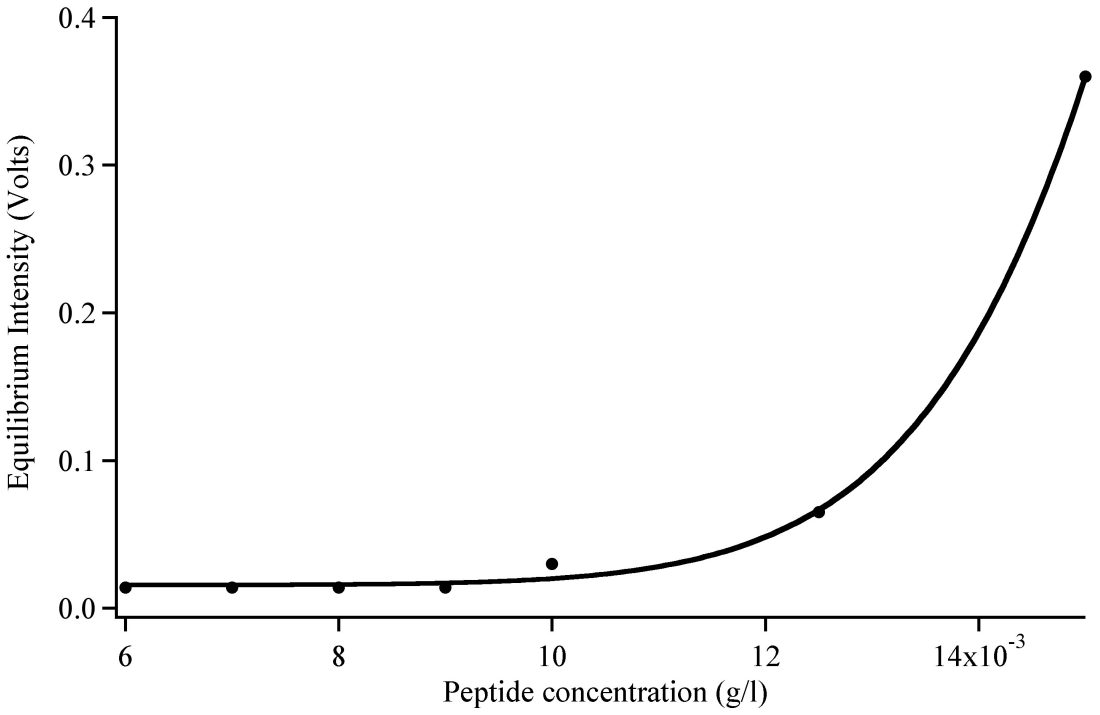


**Figure 7-6.** Determining Critical Aggregate Concentration for 1mM NaCl. DNA concentration is kept constant (0.005 g/l)

As is the case with the 100mM NaCl solution, we observe complexes in 1mM solution only above the threshold CAC peptide concentration (figure 7-6). Unlike the 100mM NaCl experiments, the CAC at 1mM NaCl does varies with the DNA concentration. CAC is different for DNA concentrations below and above 0.01g/l. However, a similar re-arrangement phase is seen at 1mM NaCl concentration. For low DNA concentration (< 0.01g/l), results similar to the case with 100mM NaCl

concentration are observed and the equilibrium time scales are of the order 1000 seconds. But for high DNA concentration (>0.01g/l), different time scales are observed and they are of the order of 100-200 seconds.

### 7.3.3 Determination of saturation concentration

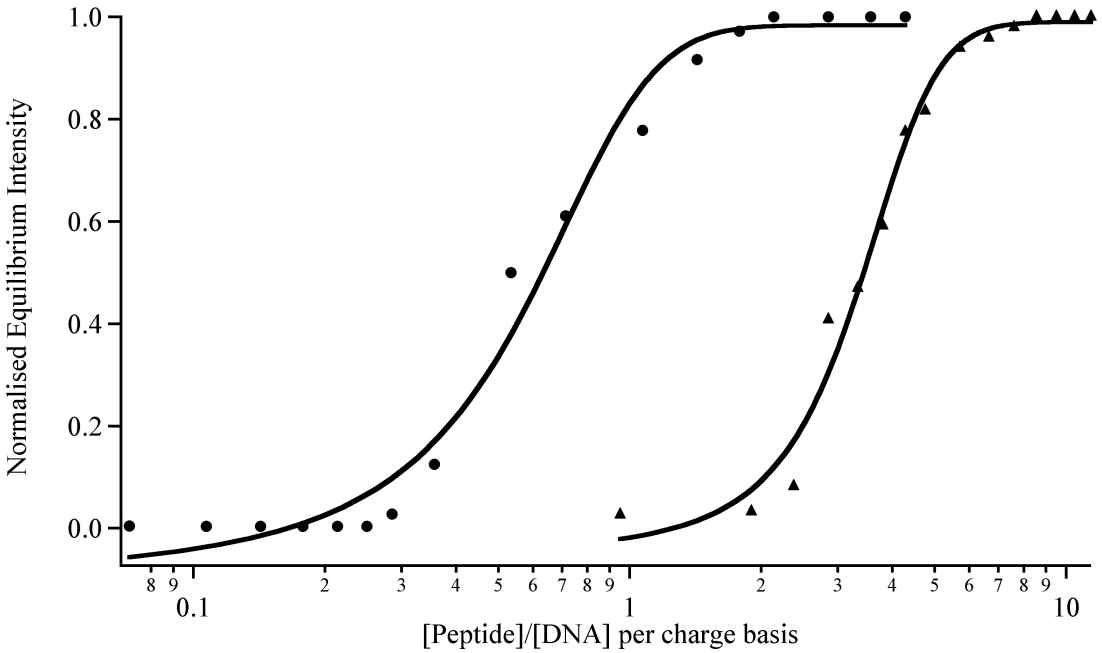


**Figure 7-7.** Normalized equilibrium intensity as a function of peptide concentration at a fixed DNA concentration (100mM NaCl concentration). Legends represents DNA concentration ● :- 0.005 g/l ▲ :- 0.00075 g/l.

In this section, we determine the saturation concentration of the model peptide, which will provide us the information about the mechanism of DNA condensation. We have conducted experiments in the limit of low DNA concentration and also in the limit of high DNA concentration. These experiments are performed at 100mM NaCl concentration. In these experiments, DNA concentration was kept constant and peptide

concentration was increased till there was no increase in equilibrium intensity is observed i.e. there is no further increase in the size and the molecular weight of the complex even if peptide concentration is increased. At that particular DNA concentration, the complex has reached its saturation point.

In low DNA concentration case (0.00075 g/l), peptide saturation concentration is 0.0104 g/l (figure 7-7) and the ratio on per charge basis with DNA is 4:1 which suggest that the complex formation is driven by the self-assembly process and not by electrostatics. When similar experiments were performed at high DNA concentration (0.005 g/l), as expected the peptide saturation concentration increased. But in this case, the peptide (saturation concentration) to DNA ratio on per charge basis is 1:1. This tells us that at high DNA concentration, even though we observe the re-arrangement phase, the complex formation is driven solely by the electrostatics.

Overall, these results show that the initial folded state of the peptide has a profound effect on the kinetics of DNA condensation. Further work is required to explore this self-assembly and also the re-arrangement phase. However, this model peptide serves as a template for our future design of peptides where folding is coupled to selective binding.

# Chapter 8

# Conclusion

We have successfully engineered the synthetic peptide with well-controlled secondary structure and amphiphilicity by using two rules, intrinsic propensity and periodicity. We have shown using circular dichroism and dynamic pendant bubble experiments that our rationally designed model peptide exhibits dynamic surface activity that is coupled to the folding of the peptide into an amphiphilic helix. We also show that the peptide folding can be controlled by an environmental cue, namely, changes in the salt concentration. We have characterized the dynamic surface activity of a tunably surface-active peptide. We have developed the model that quantitatively captures and predicts several aspects of the experimental system. By comparing the numerical solution to experimental data, adsorption constant ($\beta$) and maximum packing concentration ($\Gamma_\infty$) are determined. We have also shown that adsorption is the rate determining step, which is in agreement with order of magnitude analysis of the experimental results. Additionally, we have illustrated the fundamental effects of different parameters such as $\sigma$, $\omega$ and $\varepsilon$ on

surface concentration and sublayer concentration. Finally, we find agreement between our model in the limit of very fast reaction, $\varepsilon \rightarrow 0$, and the asymptotic solution that is based on the same assumption. This work provides a framework for the fundamental analysis of peptides with selective binding coupled to surface activity.

Our next set of findings are centered around the ability for our peptide system to interact with other biological molecules, namely DNA. Our model peptide is capable of condensing DNA, and we observe that the peptide binds to the DNA in the folded form. Faster dynamics are observed at low salt concentration (1mM) as compared with the high salt concentration (100mM). At 100mM salt concentration and low DNA concentration, the complex formation is driven by self-assembly. In contrast, at lmM salt concentration the fundamental mechanism of condensation changes. We observe a change in the time scale of condensation from ~1000 seconds to ~100 seconds when folding and assembly become a cooperatively controlled process. The difference in time scales of two orders of magnitude mirrors natural systems where folding dynamics play a significant role in DNA binding processes.

We have shown that we can engineer biomolecular systems where surface activity/amphiphilicity is coupled to folding of the peptide. We have successfully modeled the dynamic folding and the dynamic surface activity. This model peptide system can be extended to study other systems such as the adsorption of protein at the air-water interface, where the model peptide adsorption behavior stand in contrast to the paradigmatic protein adsorption behavior in which surface adsorption is associated with protein unfolding. Additionally, these peptides also can teach us about the mechanism of adsorption of biomolecules at the air-water interface, where complex biomolecular

interaction is different from both regular surfactant systems and high molecular weight proteins.

We have also shown that we can use the dynamic behavior of such peptides for biosensing applications and to control the fundamental mechanisms of DNA condensation. Kinetic studies by MALS shows that there are two time-scales associated with folding and self-assembly in the DNA-peptide complex formation. To investigate the morphology of the DNA:peptide complex, SAXS experiments are to be conducted. These experiments will give us an idea about the re-arrangement of the phases observed in our multi-angle light scattering studies, focusing on the non-specific interaction between peptide and DNA. This model peptide serves as a template for the future design of biological molecules that can be used for various applications ranging from gene therapy to DNA separations.

The next step is to design a set of peptides capable of binding selectively to the target site. We have designed the peptide sequence based on the natural structural motif basic leucine zipper. This motif is particularly interesting because of its modular nature, possessing two distinct regions: a leucine zipper that nucleates assembly and a basic binding region that binds to a specific sequence of DNA.

Ala-Leu-Lys-Arg-Ala-Arg-Asn-THr-Glu-Ala-Ala-Arg-Arg-Ser-Arg-Ala-Arg-Lys-Leu-Gln-Arg-Met-Lys-Gln-Gly-Gly-Cys-$NH_2$ (1)
Ala-Leu-Lys-Arg-Ala-Arg-Asn-THr-Leu-Ala-Ala-Leu-Arg-Ser-Arg-Ala-Arg-Lys-Leu-Gln-Arg-Met-Lys-Gln-Gly-Gly-Cys-$NH_2$ (2)
Ala-Leu-Lys-Arg-Leu-Arg-Asn-THr-Glu-Ala-Ala-Arg-Arg-Ser-Arg-Leu-Arg-Lys-Leu-Gln-Arg-Met-Lys-Gln-Gly-Gly-Cys-$NH_2$ (3)
Ala-Leu-Lys-Arg-Leu-Arg-Asn-THr-Leu-Ala-Ala-Leu-Arg-Ser-Arg-Leu-Arg-Lys-Leu-Gln-Arg-Met-Lys-Gln-Gly-Gly-Cys-$NH_2$ (4)

**Figure 8-1:** Peptide sequence based on basic binding region of the basic leucine zipper (bZIP). GGC linker is at the N-terminal that will take care of the dimerization. Red color represents the amino acid to be replaced by leucine in the next sequence. Green color represents the leucine amino acids already present in the basic region.

Figure 8-1 shows four-peptide sequences that we designed based on the basic region of the GCN4 motif. The background section discusses the GCN4 motif describing how selectivity of the binding region is retained even when the leucine zipper is replaced with the GGC dimerization motif at the N-terminal. The first sequence is the basic region of the GCN4 motif and as we go from sequence one to four, we have replaced the colored amino acids with leucines, a more hydrophobic amino acid. Selectivity is examined by using the target DNA (-GGATGACGTCATCC-) and the scrambled version of the target DNA (-GGATCTCGAGATCC-).

We propose to characterize the folding, binding and surface-activity of these peptides by using combination of circular dichroism, multi angle light scattering and liquid crystal experiments. These techniques will allow us to characterize the selectivity and kinetics of the cooperative folding and binding process. This will help us in understanding the fundamental kinetics of the binding process and can be directly translated into new dynamic architectures for viable sensing technologies.

# Appendix

**Table 1**. The values in this table are normalized so that the most hydrophobic residue is given value of 100 relative to glycine, which is considered neutral (0 value) [86].

| pH 2±1 | | pH 7±2 | |
|---|---|---|---|
| Very Hydrophobic | | | |
| Leu | 100 | Phe | 100 |
| Ile | 100 | Ile | 99 |
| Phe | 92 | Trp | 97 |
| Trp | 84 | Leu | 97 |
| Val | 79 | Val | 76 |
| Met | 74 | Met | 74 |
| Hydrophobic | | | |
| Cys | 52 | Tyr | 63 |
| Tyr | 49 | Cys | 49 |
| Ala | 47 | Ala | 41 |

| Neutral | | | |
|---|---|---|---|
| Thr | 13 | Thr | 13 |
| Glu | 8 | His | 8 |
| Gly | 0 | Gly | 0 |
| Ser | -7 | Ser | -5 |
| Gln | -18 | Gln | -10 |
| Asp | -18 | | |
| Hydrophilic | | | |
| Arg | -26 | Arg | -14 |
| Lys | -37 | Lys | -23 |
| Asn | -41 | Asn | -28 |
| His | -42 | Glu | -31 |
| Pro | -46 | Pro | -46 |
| | | Asp | -55 |

## Detailed Solution for modeling part

$$\frac{\partial \overline{C_\alpha}}{\partial \tau} = D\frac{\partial^2 \overline{C_\alpha}}{\partial \tau^2} + \frac{1}{\sigma\varepsilon}\left(\overline{C_r} - \overline{C_\alpha}\right)$$

$$\frac{\partial \overline{C_r}}{\partial \tau} = D\frac{\partial^2 \overline{C_r}}{\partial \tau^2} - \frac{1}{\varepsilon}\left(\overline{C_r} - \overline{C_\alpha}\right)$$

Boundary Condition:

$$\eta \to \infty \quad \overline{C_\alpha} = 1 \text{ and } \overline{C_r} = 1$$

$$\eta \to 0 \quad \overline{C_\alpha} = \frac{f(t)}{C_{\alpha\infty}} \text{ and } \left(\frac{\partial \overline{C_r}}{\partial \eta}\right)_{\eta=0} = 0$$

Initial condition:

$$\overline{C_\alpha}(\eta,0) = 1$$

$$\overline{C_r}(\eta,0) = 1$$

Now taking Laplace transform of the two non-dimensional partial differential equation,

$$L\left[\frac{\partial \overline{C_\alpha}}{\partial \tau}\right] = sL\left\{\overline{C_\alpha}\right\} - \overline{C_\alpha}(\eta,0)$$

Here, $C_\alpha(\eta,0) = 1$ from initial condition

And we assume that $L\left\{\overline{C_\alpha}\right\} = \overline{C_\alpha}'$ and $L\left\{\overline{C_r}\right\} = \overline{C_r}'$

$$L\left\{\frac{\partial^2 \overline{C_\alpha}}{\partial \eta^2}\right\} = \frac{\partial^2}{\partial \eta^2} L\left\{\overline{C_\alpha}(\eta,\tau)\right\} = \frac{\partial^2 \overline{C_\alpha}'}{\partial \eta^2}$$

By substituting, we get for the folded peptide

$$\frac{d^2 \overline{C_\alpha}'}{d\eta^2} + \frac{\overline{C_r}'}{\sigma\varepsilon} - \left(s + \frac{1}{\sigma\varepsilon}\right)\overline{C_\alpha}' + 1 = 0$$

Similarly, taking Laplace transform for the other equation, we get

$$\frac{d^2\overline{C_r}'}{d\eta^2}+\frac{\overline{C_\alpha}'}{\varepsilon}-\left(s+\frac{1}{\varepsilon}\right)\overline{C_r}'+1=0$$

Boundary condition:

$$\eta\to\infty\ \ \overline{C_\alpha}'=\frac{1}{s}\text{ and }\overline{C_r}'=\frac{1}{s}$$

$$\eta\to 0\quad \overline{C_\alpha}'=\frac{f(s)}{C_{\alpha\infty}}\text{ and }\left(\frac{\partial\overline{C_r}'}{\partial\eta}\right)_{\eta=0}=0$$

So, we have two non-dimensional ordinary non-homogenous differential equation. Final solution will be combined of homogenous part and the particular solution.

We first find the homogenous solution

$$\frac{d^2\overline{C_\alpha}'}{d\eta^2}+\frac{\overline{C_r}'}{\sigma\varepsilon}-\left(s+\frac{1}{\sigma\varepsilon}\right)\overline{C_\alpha}'=0$$

$$\frac{d^2\overline{C_r}'}{d\eta^2}+\frac{\overline{C_\alpha}'}{\varepsilon}-\left(s+\frac{1}{\varepsilon}\right)\overline{C_r}'=0$$

Substitute, $\overline{C_\alpha}'=ae^{\lambda_1\eta}$ and $\overline{C_r}'=ce^{\lambda_1\eta}$

We will get two equations, which we solve simultaneously by writing the equation in matrix form. Determinant of that matrix should be equal to zero. From this, we get four eigenvalues. The eigenvalues and the corresponding eigenvector are:

| Eigenvalues | Eigenvector |
|---|---|
| $\lambda_1=\sqrt{s+\frac{1}{\varepsilon}+\frac{1}{\sigma\varepsilon}}$ | $\begin{bmatrix}1\\-\sigma\end{bmatrix}$ |
| $\lambda_2=-\sqrt{s+\frac{1}{\varepsilon}+\frac{1}{\sigma\varepsilon}}$ | $\begin{bmatrix}1\\-\sigma\end{bmatrix}$ |
| $\lambda_3=\sqrt{s}$ | $\begin{bmatrix}1\\1\end{bmatrix}$ |

| | |
|---|---|
| $\lambda_4 = -\sqrt{s}$ | $\begin{bmatrix}1\\1\end{bmatrix}$ |

$$\begin{bmatrix}\overline{C_\alpha}'\\ \overline{C_r}'\end{bmatrix} = a\begin{bmatrix}1\\-\sigma\end{bmatrix}e^{\sqrt{s+\frac{1}{\varepsilon}+\frac{1}{\sigma\varepsilon}}\eta} + b\begin{bmatrix}1\\-\sigma\end{bmatrix}e^{-\sqrt{s+\frac{1}{\varepsilon}+\frac{1}{\sigma\varepsilon}}\eta} + c\begin{bmatrix}1\\1\end{bmatrix}e^{-\sqrt{s}\eta} + d\begin{bmatrix}1\\1\end{bmatrix}e^{\sqrt{s}\eta}$$

where *a*, *b*, *c*, and *d* are the arbitrary constant.

As $\eta\to\infty$, the solution should be bounded. So we can safely neglect *a* and *d*.

$$\begin{bmatrix}\overline{C_\alpha}'\\ \overline{C_r}'\end{bmatrix} = b\begin{bmatrix}1\\-\sigma\end{bmatrix}e^{-\sqrt{s+\frac{1}{\varepsilon}+\frac{1}{\sigma\varepsilon}}\eta} + c\begin{bmatrix}1\\1\end{bmatrix}e^{-\sqrt{s}\eta}$$

Writing them separately,

$$\overline{C_\alpha}' = be^{-\sqrt{s+\frac{1}{\varepsilon}+\frac{1}{\sigma\varepsilon}}\eta} + ce^{-\sqrt{s}\eta}$$

$$\text{and } \overline{C_r}' = -b\sigma e^{-\sqrt{s+\frac{1}{\varepsilon}+\frac{1}{\sigma\varepsilon}}\eta} + ce^{-\sqrt{s}\eta}$$

These are the homogenous solution. Now we find the particular solution by using method of undetermined coefficient and for both folded and unfolded peptide it turns out to be $\frac{1}{s}$.

So, final solution is

$$\overline{C_\alpha}' = be^{-\sqrt{s+\frac{1}{\varepsilon}+\frac{1}{\sigma\varepsilon}}\eta} + ce^{-\sqrt{s}\eta} + \frac{1}{s}$$

$$\overline{C_r}' = -b\sigma e^{-\sqrt{s+\frac{1}{\varepsilon}+\frac{1}{\sigma\varepsilon}}\eta} + ce^{-\sqrt{s}\eta} + \frac{1}{s}$$

Now, we apply the boundary condition to get the constants *b* and *c*.

We found out,

$$b = \frac{sf(s) - C_{\alpha\infty}}{C_{\alpha\infty}\sqrt{s}\left[\sqrt{s} + \sigma\sqrt{s + \frac{1}{\varepsilon} + \frac{1}{\sigma\varepsilon}}\right]}$$

$$c = \frac{\left[sf(s) - C_{\alpha\infty}\right]\sigma\sqrt{s + \frac{1}{\varepsilon} + \frac{1}{\sigma\varepsilon}}}{C_{\alpha\infty}s\left[\sqrt{s} + \sigma\sqrt{s + \frac{1}{\varepsilon} + \frac{1}{\sigma\varepsilon}}\right]}$$

$$\overline{C_\alpha}' = \frac{sf(s) - C_{\alpha\infty}}{C_{\alpha\infty}\sqrt{s}\left[\sqrt{s} + \sigma\sqrt{s + \frac{1}{\varepsilon} + \frac{1}{\sigma\varepsilon}}\right]} e^{-\sqrt{s + \frac{1}{\varepsilon} + \frac{1}{\sigma\varepsilon}}\eta} + \frac{\left[sf(s) - C_{\alpha\infty}\right]\sigma\sqrt{s + \frac{1}{\varepsilon} + \frac{1}{\sigma\varepsilon}}}{C_{\alpha\infty}s\left[\sqrt{s} + \sigma\sqrt{s + \frac{1}{\varepsilon} + \frac{1}{\sigma\varepsilon}}\right]} e^{-\sqrt{s}\eta} + \frac{1}{s}$$

$$\overline{C_r}' = -\sigma\frac{sf(s) - C_{\alpha\infty}}{C_{\alpha\infty}\sqrt{s}\left[\sqrt{s} + \sigma\sqrt{s + \frac{1}{\varepsilon} + \frac{1}{\sigma\varepsilon}}\right]} e^{-\sqrt{s + \frac{1}{\varepsilon} + \frac{1}{\sigma\varepsilon}}\eta} + \frac{\left[sf(s) - C_{\alpha\infty}\right]\sigma\sqrt{s + \frac{1}{\varepsilon} + \frac{1}{\sigma\varepsilon}}}{C_{\alpha\infty}s\left[\sqrt{s} + \sigma\sqrt{s + \frac{1}{\varepsilon} + \frac{1}{\sigma\varepsilon}}\right]} e^{-\sqrt{s}\eta} + \frac{1}{s}$$

Now for the folded peptide,

$$\frac{\partial\Gamma}{\partial t} = D\left(\frac{\partial C_\alpha}{\partial x}\right)_{x=0}$$

Non-dimensionalizing the above equation,

$$\frac{\partial\Gamma}{\partial\tau} = \left(\frac{\partial\overline{C_\alpha}}{\partial\eta}\right)_{\eta=0}$$

Taking Laplace transform,

$$s\Gamma(s) - \Gamma(0) = \left(\frac{\partial\overline{C_\alpha}'}{\partial\eta}\right)_{\eta=0}$$

Assuming that at time $t = 0$ there is no adsorption,

$$\Gamma`(0)=0.$$

After taking the derivative of $C_\alpha$` with respect to η at η=0, we get

$$\Gamma(s)=\left[\frac{(sf(s)-C_{\alpha\infty})\sqrt{s+\frac{1}{\varepsilon}+\frac{1}{\sigma\varepsilon}}}{C_{\alpha\infty}s\left[\sqrt{s}+\sigma\sqrt{s+\frac{1}{\varepsilon}+\frac{1}{\sigma\varepsilon}}\right]}\right]\frac{(\sigma+1)}{\sqrt{s}}$$

Now, we take the Laplace inverse of the above equation and final solution is:

$$\Gamma(t)=(\sigma+1)\int_0^{\tau}\frac{f(\tau-\tau')}{C_{\alpha\infty}}\times\left\{\begin{array}{l}\frac{\sigma}{1-\sigma^2}\left[\frac{1}{\sqrt{\Pi\tau}}+\frac{\sqrt{a}}{\sigma\sqrt{1-\sigma^2}}e^{\frac{a\sigma^2}{1-\sigma^2}\tau}erf\left(\sqrt{\frac{a\sigma^2\tau}{1-\sigma^2}}\right)\right]+\\ \frac{1}{\sigma^2-1}\left[\frac{e^{-a\tau}}{\sqrt{\Pi\tau}}+\sqrt{a}\sqrt{\frac{1-2\sigma^2}{1-\sigma^2}}e^{\frac{a\sigma^2}{1-\sigma^2}\tau}erf\left(\sqrt{\frac{a-2a\sigma^2}{1-\sigma^2}\tau}\right)\right]\end{array}\right\}d\tau+$$

$$(\sigma+1)\int_0^{\tau}-1\times\left\{\begin{array}{l}\frac{\sigma}{1-\sigma^2}\left[\frac{1}{\sqrt{\Pi\tau}}+\frac{\sqrt{a}}{\sigma\sqrt{1-\sigma^2}}e^{\frac{a\sigma^2}{1-\sigma^2}\tau}erf\left(\sqrt{\frac{a\sigma^2\tau}{1-\sigma^2}}\right)\right]+\\ \frac{1}{\sigma^2-1}\left[\frac{e^{-a\tau}}{\sqrt{\Pi\tau}}+\sqrt{a}\sqrt{\frac{1-2\sigma^2}{1-\sigma^2}}e^{\frac{a\sigma^2}{1-\sigma^2}\tau}erf\left(\sqrt{\frac{a-2a\sigma^2}{1-\sigma^2}\tau}\right)\right]\end{array}\right\}d\tau$$

Where, $a=\frac{1}{\varepsilon}+\frac{1}{\sigma\varepsilon}$.

# Bibliography

1. Luo, D.; Saltzman, W.M. Synthetic DNA delivery systems. *Nat Biotech* **2000**, *18*, 33-37.

2. Shoemaker, B.A.; Portman, J.J.; Wolynes, P.G. Speeding molecular recognition by using the folding funnel: The fly-casting mechanism. *Proceedings of the National Academy of Sciences of the United States of America* **2000**, *97*, 8868-8873.

3. Xiong, H.; Buckwalter, B.L.; Shieh, H.M.; Hecht, M.H. Periodicity of polar and nonpolar amino acids is the major determinant of secondary structure in self-assembling oligomeric peptides. *Proceedings of the National Academy of Sciences of the United States of America* **1995**, *92*, 6349-6353.

4. DeGrado, W.F.; Lear, J.D. Induction of peptide conformation at apolar water interfaces. 1. A study with model peptides of defined hydrophobic periodicity. *Journal of the American Chemical Society* **1985**, *107*, 7684-7689.

5. Parente, R.A.; Nadasdi, L.; Subbarao, N.K.; Szoka, F.C. Association of a pH-sensitive peptide with membrane vesicles: role of amino acid sequence. *Biochemistry* **1990**, *29*, 8713-8719.

6. Jain, V.; Jimenez, A.; Maldarelli, C.; Tu, R.S. Dynamic surface activity by folding and unfolding an amphiphilic α-helix. *Langmuir* **2008**, *24*, 9923-9928.

7. Fields, G.B.; Noble, R.L. Solid phase peptide synthesis utilizing 9-fluorenylmethoxycarbonyl amino acids. *International Journal of Peptide and Protein Research* **1990**, *35*, 161-214.

8. Lockwood, N.A.; Gupta, J.K.; Abbott, N.L. Self-assembly of amphiphiles, polymers and proteins at interfaces between thermotropic liquid crystals and aqueous phases. *Surface Science Reports* **2008**, *63*, 255-293.

9. Dyson, H.J.; Wright, P.E. Coupling of folding and binding for unstructured proteins. *Current Opinion in Structural Biology* **2002**, *12*, 54-60.

10. Dunker, A.K.; Brown, C.J.; Lawson, J.D.; Iakoucheva, L.M.; Obradović, Z. Intrinsic disorder and protein function. *Biochemistry* **2002**, *41*, 6573-6582.

11. Dunker, A.K.; Lawson, J.D.; Brown, C.J.; Williams, R.M.; Romero, P.; Oh, J.S.; Oldfield, C.J.; Campen, A.M.; Ratliff, C.M.; Hipps, K.W.; Ausio, J.; Nissen, M.S.; Reeves, R.; Kang, C.; Kissinger, C.R.; Bailey, R.W.; Griswold, M.D.; Chiu, W.; Garner, E.C.; Obradovic, Z. Intrinsically disordered protein. *Journal of Molecular Graphics and Modelling* **2001**, *19*, 26-59.

12. Sugase, K.; Dyson, H.J.; Wright, P.E. Mechanism of coupled folding and binding of an intrinsically disordered protein. *Nature* **2007**, *447*, 1021-1025.

13. Tsai, C.-J.; Kumar, S.; Ma, B.; Nussinov, R. Folding funnels, binding funnels, and protein function. *Protein Science* **1999**, *8*, 1181-1190.

14. Wright, P.E.; Dyson, H.J. Intrinsically unstructured proteins: Re-assessing the protein structure-function paradigm. *Journal of Molecular Biology* **1999**, *293*, 321-331.

15. Wright, P.E.; Dyson, H.J. Linking folding and binding. *Current Opinion in Structural Biology* **2009**, *19*, 31-38.

16. Miller, R.; Fainerman, V.B.; Makievski, A.V.; Kragel, J.; Grigoriev, D.O.; Kazakov, V.N.; Sinyachenko, O.V. Dynamics of protein and mixed protein/surfactant adsorption layers at the water/fluid interface. *Advances in Colloid and Interface Science* **2000**, *86*, 39-82.

17. Bloomfield, V.A. DNA condensation by multivalent cations. *Biopolymers* **1997**, *44*, 269-282.

18. Bloomfield, V.A. Condensation of DNA by multivalent cations: Considerations on mechanism. *Biopolymers* **1991**, *31*, 1471-1481.

19. Riemer, S.C.; Bloomfield, V.A. Packaging of DNA in bacteriophage Heads: Some considerations on energetics. *Biopolymers* **1978**, *17*, 785-794.

20. Marquet, R.; Houssier, C. Thermodynamics of cation-induced DNA condensation. *J. Biomol. Struct. Dyn.* **1991**, *9*, 159-167.

21. DeHaseth, P.L.; Gross, C.A.; Burgess, R.R.; Record, M.T. Measurement of binding constants for protein-DNA interactions by DNA-cellulose chromatography. *Biochemistry* **1977**, *16*, 4777-4783.

22. Gelbart, W.M.; Bruinsma, R.F.; Pincus, P.A.; Parsegian, V.A. DNA-Inspired Electrostatics. *Physics Today* **2000**, *53*, 38.

23. Lau, A.W.C.; Pincus, P. Counterion condensation and fluctuation-induced attraction. *Physical Review E* **2002**, *66*, 041501.

24. Safinya, C.R. Structures of lipid-DNA complexes: supramolecular assembly and gene delivery. *Current Opinion in Structural Biology* **2001**, *11*, 440-448.

25. Koltover, I.; Salditt, T.; Safinya, C.R. Phase Diagram, Stability, and Overcharging of Lamellar Cationic Lipid-DNA Self-Assembled Complexes. *Biophysical Journal* **1999**, *77*, 915-924.

26. Lai, E.; van Zanten, J.H. Real time monitoring of lipoplex molar mass, size and density. *Journal of Controlled Release* **2002**, *82*, 149-158.

27. Felgner, P.L.; Gadek, T.R.; Holm, M.; Roman, R.; Chan, H.W.; Wenz, M.; Northrop, J.P.; Ringold, G.M.; Danielsen, M. Lipofection: a highly efficient, lipid-mediated DNA-transfection procedure. *Proceedings of the National Academy of Sciences of the United States of America* **1987**, *84*, 7413-7417.

28. Rädler, J.O.; Koltover, I.; Salditt, T.; Safinya, C.R. Structure of DNA-Cationic Liposome Complexes: DNA Intercalation in Multilamellar Membranes in Distinct Interhelical Packing Regimes. *Science* **1997**, *275*, 810-814.

29. Matulis, D.; Rouzina, I.; Bloomfield, V.A. Thermodynamics of Cationic Lipid Binding to DNA and DNA Condensation: Roles of Electrostatics and Hydrophobicity. *Journal of the American Chemical Society* **2002**, *124*, 7331-7342.

30. Wilson, R.W.; Bloomfield, V.A. Counterion-induced condensation of deoxyribonucleic acid. A light-scattering study. *Biochemistry* **1979**, *18*, 2192-2196.

31. Vijayanathan, V.; Thomas, T.; Shirahata, A.; Thomas, T.J. DNA Condensation by Polyamines: A Laser Light Scattering Study of Structural Effects. *Biochemistry* **2001**, *40*, 13644-13651.

32. Matulis, D.; Rouzina, I.; Bloomfield, V.A. Thermodynamics of DNA binding and condensation: isothermal titration calorimetry and electrostatic mechanism. *Journal of Molecular Biology* **2000**, *296*, 1053-1063.

33. Tecle, M.; Preuss, M.; Miller, A.D. Kinetic Study of DNA Condensation by Cationic Peptides Used in Nonviral Gene Therapy: Analogy of DNA Condensation to Protein Folding. *Biochemistry* **2003**, *42*, 10343-10347.

34. Lai, E.; van Zanten, J.H. Monitoring DNA/Poly-l-Lysine Polyplex Formation with Time-Resolved Multiangle Laser Light Scattering. *Biophysical Journal* **2001**, *80*, 864-873.

35. Dyson, H.J.; Wright, P.E. Intrinsically unstructured proteins and their functions. *Nat Rev Mol Cell Biol* **2005**, *6*, 197-208.

36. Fuxreiter, M.; Tompa, P.; Simon, I.; Uversky, V.N.; Hansen, J.C.; Asturias, F.J. Malleable machines take shape in eukaryotic transcriptional regulation. *Nat Chem Biol* **2008**, *4*, 728-737.

37. Iakoucheva, L.M.; Brown, C.J.; Lawson, J.D.; Obradovic, Z.; Dunker, A.K. Intrinsic disorder in cell-signaling and cancer-associated proteins. *Journal of Molecular Biology* **2002**, *323*, 573-584.

38. Iakoucheva, L.M.; Radivojac, P.; Brown, C.J.; O'Connor, T.R.; Sikes, J.G.; Obradovic, Z.; Dunker, A.K. The importance of intrinsic disorder for protein phosphorylation. *Nucleic Acids Research* **2004**, *32*, 1037-1049.

39. Dames, S.A.; Martinez-Yamout, M.; De Guzman, R.N.; Dyson, H.J.; Wright, P.E. Structural basis for Hif-1α/CBP recognition in the cellular hypoxic response. *Proceedings of the National Academy of Sciences of the United States of America* **2002**, *99*, 5271-5276.

40. Creighton, T.E. Protein folding. *Biochemical journal* **1990**, *270*, 1-16.

41. Pérez-Payà, E.; Houghten, R.; Blondelle, S. The role of amphipathicity in the folding, self-association and biological activity of multiple subunit small proteins. *Journal of Biological Chemistry* **1995**, *270*, 1048.

42. Kaiser, E.; Kezdy, F. Amphiphilic secondary structure: Design of peptide hormones. *Science* **1984**, *223*, 249-255.

43. Kaiser, E.T.; Kezdy, F.J. Secondary structures of proteins and peptides in amphiphilic environments. (A review). *Proceedings of the National Academy of Sciences of the United States of America* **1983**, *80*, 1137-1143.

44. von Hippel, P.H. From "simple" DNA-protein interactions to the macromolecular machines of gene expression. *Annual Review of Biophysics and Biomolecular Structure* **2007**, *36*, 79-105.

45. Verkhivker, G.M.; Bouzida, D.; Gehlhaar, D.K.; Rejto, P.A.; Freer, S.T.; Rose, P.W. Simulating disorder-order transitions in molecular recognition of unstructured proteins: Where folding meets binding. *Proceedings of the National Academy of Sciences of the United States of America* **2003**, *100*, 5148-5153.

46. Slutsky, M.; Mirny, L.A. Kinetics of protein-DNA interaction: facilitated target location in sequence-dependent potential. *Biophysical Journal* **2004**, *87*, 4021-4035.

47. Spolar, R.S.; Record, M.T., Jr. Coupling of local folding to site-specific binding of proteins to DNA. *Science* **1994**, *263*, 777-784.

48. Huang, Y.; Liu, Z. Kinetic advantage of intrinsically disordered proteins in coupled folding-binding process: A critical assessment of the "Fly-Casting" mechanism. *Journal of Molecular Biology* **2009**, *393*, 1143-1159.

49. Landschulz, W.H.; Johnson, P.F.; McKnight, S.L. The leucine zipper: a hypothetical structure common to a new class of DNA binding proteins. *Science* **1988**, *240*, 1759-1764.

50. O'Shea, E.K.; Rutkowski, R.; Kim, P.S. Evidence that the leucine zipper is a coiled coil. *Science* **1989**, *243*, 538-542.

51. O'Neil, K.T.; Shuman, J.D.; Ampe, C.; DeGrado, W.F. DNA-induced increase in the alpha-helical content of C/EBP and GCN4. *Biochemistry* **1991**, *30*, 9030-9034.

52. O'Neil, K.; Hoess, R.; DeGrado, W. Design of DNA-binding peptides based on the leucine zipper motif. *Science* **1990**, *249*, 774-778.

53. Talanian, R.; McKnight, C.; Kim, P. Sequence-specific DNA binding by a short peptide dimer. *Science* **1990**, *249*, 769-771.

54. Talanian, R.V.; McKnight, C.J.; Rutkowski, R.; Kim, P.S. Minimum length of a sequence-specific DNA binding peptide. *Biochemistry* **1992**, *31*, 6871-6875.

55. Kim, Y.-G.; Park, H.-J.; Kim, K.K.; Lowenhaupt, K.; Rich, A. A peptide with alternating lysines can act as a highly specific Z-DNA binding domain. *Nucl. Acids Res.* **2006**, *34*, 4937-4942.

56. Tu, R.S.; Marullo, R.; Pynn, R.; Bitton, R.; Bianco-Peled, H.; Tirrell, M.V. Cooperative DNA binding and assembly by a bZip peptide-amphiphile. *Soft Matter* **2010**, *6*, 1035-1044.

57. Kokkoli, E.; Mardilovich, A.; Wedekind, A.; Rexeisen, E.L.; Garg, A.; Craig, J.A. Self-assembly and applications of biomimetic and bioactive peptide-amphiphiles. *Soft Matter* **2006**, *2*, 1015-1024.

58. Cui, H.; Webber, M.J.; Stupp, S.I. Self-Assembly of peptide amphiphiles: From molecules to nanostructures to biomaterials. *Biopolymers* **2010**, *94*, 1-18.

59. Leulliot, N.; Varani, G. Current topics in RNA-protein recognition: control of specificity and biological function through induced fit and conformational capture. *Biochemistry* **2001**, *40*, 7947-7956.

60. Williamson, J.R. Proteins that bind RNA and the labs who love them. *Nat Struct Mol Biol* **2001**, *8*, 390-391.

61. Agalarov, S.C.; Prasad, G.S.; Funke, P.M.; Stout, C.D.; Williamson, J.R. Structure of the S15,S6,S18-rRNA complex: Assembly of the 30S ribosome central domain. *Science* **2000**, *288*, 107-112.

62. Henkels, C.H.; Kurz, J.C.; Fierke, C.A.; Oas, T.G. Linked folding and anion binding of the bacillus subtilis ribonuclease P protein. *Biochemistry* **2001**, *40*, 2777-2789.

63. Bouvet, P.; Allain, F.H.T.; Finger, L.D.; Dieckmann, T.; Feigon, J. Recognition of pre-formed and flexible elements of an RNA stem-loop by nucleolin. *Journal of Molecular Biology* **2001**, *309*, 763-775.

64. Mogridge, J.; Legault, P.; Li, J.; Van Oene, M.D.; Kay, L.E.; Greenblatt, J. Independent ligand-induced folding of the RNA-binding domain and two functionally distinct antitermination regions in the phage lambda N protein. *Molecular Cell* **1998**, *1*, 265-275.

65. Allain, F.H.T.; Bouvet, P.; Dieckmann, T.; Feigon, J. Molecular basis of sequence-specific recognition of pre-ribosomal RNA by nucleolin. *EMBO J* **2000**, *19*, 6870-6881.

66. Bloomer, A.C.; Champness, J.N.; Bricogne, G.; Staden, R.; Klug, A. Protein disk of tobacco mosaic virus at 2.8Å resolution showing the interactions within and between subunits. *Nature* **1978**, *276*, 362-368.

67. Champness, J.N.; Bloomer, A.C.; Bricogne, G.; Butler, P.J.G.; Klug, A. The structure of the protein disk of tobacco mosaic virus to 5Å resolution. *Nature* **1976**, *259*, 20-24.

68. Jardetzky, O.; Akasaka, K.; Vogel, D.; Morris, S.; Holmes, K.C. Unusual segmental flexibility in a region of tobacco mosaic virus coat protein. *Nature* **1978**, *273*, 564-566.

69. Stubbs, G.; Warren, S.; Holmes, K. Structure of RNA and RNA binding site in tobacco mosaic virus from 4Å map calculated from X-ray fibre diagrams. *Nature* **1977**, *267*, 216-221.

70. Mattaj, I.W. RNA recognition: A family matter? *Cell* **1993**, *73*, 837-840.

71. Burd, C.G.; Dreyfuss, G. Conserved structures and diversity of functions of RNA-binding proteins. *Science* **1994**, *265*, 615-621.

72. Lazinski, D.; Grzadzielska, E.; Das, A. Sequence-specific recognition of RNA hairpins by bacteriophage antiterminators requires a conserved arginine-rich motif. *Cell* **1989**, *59*, 207-218.

73. Daly, T.J.; Rusche, J.R.; Maione, T.E.; Frankel, A.D. Circular dichroism studies of the HIV-1 Rev protein and its specific RNA binding site. *Biochemistry* **1990**, *29*, 9791-9795.

74. Tan, R.; Chen, L.; Buettner, J.A.; Hudson, D.; Frankel, A.D. RNA recognition by an isolated alpha helix. *Cell* **1993**, *73*, 1031-1040.

75. Tan, R.; Frankel, A.D. Costabilization of peptide and RNA structure in an HIV Rev peptide-RRE complex. *Biochemistry* **1994**, *33*, 14579-14585.

76. Kjems, J.; Calnan, B.J.; Frankel, A.D.; Sharp, P.A. Specific binding of a basic peptide from HIV-1 REV. *Embo Journal* **1992**, *11*, 1119-1129.

77. DeGrado, W.; Wasserman, Z.; Lear, J. Protein design, a minimalist approach. *Science* **1989**, *243*, 622-628.

78. Kamtekar, S.; Schiffer, J.; Xiong, H.; Babik, J.; Hecht, M. Protein design by binary patterning of polar and nonpolar amino acids. *Science* **1993**, *262*, 1680-1685.

79. Bryson, J.W.; Betz, S.F.; Lu, H.S.; Suich, D.J.; Zhou, H.X.; O'Neil, K.T.; DeGrado, W.F. Protein design: A hierarchic approach. *Science* **1995**, *270*, 935-941.

80. Beasley, J.; Hecht, M. Protein design: the choice of de novo sequences. *Journal of Biological Chemistry* **1997**, *272*, 2031.

81. Tu, R.S.; Tirrell, M. Bottom-up design of biomimetic assemblies. *Advanced Drug Delivery Reviews* **2004**, *56*, 1537-1563.

82. Zhou, N.; Kay, C.; Hodges, R. Synthetic model proteins. Positional effects of interchain hydrophobic interactions on stability of two-stranded alpha-helical coiled-coils. *Journal of Biological Chemistry* **1992**, *267*, 2664.

83. Lear, J.; Wasserman, Z.; DeGrado, W. Synthetic amphiphilic peptide models for protein ion channels. *Science* **1988**, *240*, 1177-1181.

84. Aurora, R.; Creamer, T.; Srinivasan, R.; Rose, G. Local interactions in protein folding: lessons from the alpha-helix. *Journal of Biological Chemistry* **1997**, *272*, 1413.

85. Chou, P.Y.; Fasman, G.D. Conformational parameters for amino acids in helical, beta-sheet, and random coil regions calculated from proteins. *Biochemistry* **1974**, *13*, 211-222.

86. Monera, O.D.; Sereda, T.J.; Zhou, N.E.; Kay, C.M.; Hodges, R.S. Relationship of sidechain hydrophobicity and alpha-helical propensity on the stability of the single-stranded amphipathic alpha-helix. *Journal of Peptide Science* **1995**, *1*, 319-329.

87. O'Neil, K.; DeGrado, W. A thermodynamic scale for the helix-forming tendencies of the commonly occurring amino acids. *Science* **1990**, *250*, 646-651.

88. Lyu, P.; Liff, M.; Marky, L.; Kallenbach, N. Side chain contributions to the stability of alpha-helical structure in peptides. *Science* **1990**, *250*, 669-673.

89. Narita, M.; Tomotake, Y.; Isokawa, S.; Matsuzawa, T.; Miyauchi, T. Syntheses and properties of resin-bound oligopeptides. 2. Infrared spectroscopic conformational analysis of cross-linked polystyrene resin bound oligoleucines in the swollen state. *Macromolecules* **1984**, *17*, 1903-1906.

90. McLachlan, A.D. Repeated helical pattern in apolipoprotein-A-I. *Nature* **1977**, *267*, 465-466.

91. Fukushima, D.; Kupferberg, J.P.; Yokoyama, S.; Kroon, D.J.; Kaiser, E.T.; Kezdy, F.J. A synthetic amphiphilic helical docosapeptide with the surface properties of plasma apolipoprotein A-I. *Journal of the American Chemical Society* **1979**, *101*, 3703-3704.

92. Yokoyama, S.; Fukushima, D.; Kupferberg, J.; Kezdy, F.; Kaiser, E. The mechanism of activation of lecithin: cholesterol acyltransferase by apolipoprotein AI and an amphiphilic peptide. *Journal of Biological Chemistry* **1980**, *255*, 7333.

93. Raghuraman, H.; Chattopadhyay, A. Melittin: a membrane-active peptide with diverse functions. *Biosci Rep* **2007**, *27*, 189-223.

94. Blondelle, S.E.; Houghten, R.A. Hemolytic and antimicrobial activities of the twenty-four individual omission analogs of melittin. *Biochemistry* **1991**, *30*, 4671-4678.

95. DeGrado, W.F.; Kezdy, F.J.; Kaiser, E.T. Design, synthesis, and characterization of a cytotoxic peptide with melittin-like activity. *Journal of the American Chemical Society* **1981**, *103*, 679-681.

96. DeGrado, W.F.; Musso, G.F.; Lieber, M.; Kaiser, E.T.; Kezdy, F.J. Kinetics and mechanism of hemolysis induced by melittin and by a synthetic melittin analogue. *Biophysical Journal* **1982**, *37*, 329-338.

97. Li, W.; Nicol, F.; Szoka, F.C. GALA: a designed synthetic pH-responsive amphipathic peptide with applications in drug and gene delivery. *Advanced Drug Delivery Reviews* **2004**, *56*, 967-985.

98. Subbarao, N.K.; Parente, R.A.; Szoka, F.C.; Nadasdi, L.; Pongracz, K. The pH-dependent bilayer destabilization by an amphipathic peptide. *Biochemistry* **1987**, *26*, 2964-2972.

99. Parente, R.; Nir, S.; Szoka, F. pH-dependent fusion of phosphatidylcholine small vesicles. Induction by a synthetic amphipathic peptide. *Journal of Biological Chemistry* **1988**, *263*, 4724.

100. Fattal, E.; Nir, S.; Parente, R.A.; Szoka, F.C. Pore-forming peptides induce rapid phospholipid flip-flop in membranes. *Biochemistry* **1994**, *33*, 6721-6731.

101. Nicol, F.; Nir, S.; Szoka Jr, F.C. Effect of cholesterol and charge on pore formation in bilayer vesicles by a pH-sensitive peptide. *Biophysical Journal* **1996**, *71*, 3288-3301.

102. Nicol, F.; Nir, S.; Szoka, F.C. Orientation of the pore-forming peptide GALA in POPC vesicles determined by a BODIPY-avidin/biotin binding assay. **1999**, *76*, 2121-2141.

103. Shlomo N, Nicol, F, Szoka, F.C. Surface aggregation and membrane penetration by peptides: Relation to pore formation and fusion. *Molecular Membrane Biology* **1999**, *16*, 95-101.

104. Parente, R.A.; Nir, S.; Szoka, F.C. Mechanism of leakage of phospholipid vesicle contents induced by the peptide GALA. *Biochemistry* **1990**, *29*, 8720-8728.

105. Nicol, F.; Nir, S.; Szoka Jr, F.C. Effect of phospholipid composition on an amphipathic peptide-mediated pore formation in bilayer vesicles. *Biophysical Journal* **2000**, *78*, 818-829.

106. Plank, C.; Oberhauser, B.; Mechtler, K.; Koch, C.; Wagner, E. The influence of endosome-disruptive peptides on gene transfer using synthetic virus-like gene transfer systems. *Journal of Biological Chemistry* **1994**, *269*, 12918.

107. Haensler, J.; Szoka, F.C. Polyamidoamine cascade polymers mediate efficient transfection of cells in culture. *Bioconjugate Chemistry* **1993**, *4*, 372-379.

108. Simoes, S.; Slepushkin, V.; Gaspar, R.; De Lima, M.; Duzgunes, N. Gene delivery by negatively charged ternary complexes of DNA, cationic liposomes and transferrin or fusigenic peptides. *Gene therapy* **1998**, *5*, 955.

109. Simoes, S.; Slepushkin, V.; Pretzer, E.; Dazin, P.; Gaspar, R.; Pedroso de Lima, M.C.; Duzgunes, N. Transfection of human macrophages by lipoplexes via the combined use of transferrin and pH-sensitive peptides. *Journal of Leukocyte Biology* **1999**, *65*, 270-279.

110. Simoes, S.; Slepushkin, V.; Pires, P.; Gaspar, R.; de Lima, M.; Dsuzgunes, N. Mechanisms of gene transfer mediated by lipoplexes associated with targeting ligands or pH-sensitive peptides. *Gene therapy* **1999**, *6*, 1798.

111. Wyman, T.B.; Nicol, F.; Zelphati, O.; Scaria, P.V.; Plank, C.; Szoka, F.C. Design, synthesis, and characterization of a cationic peptide that binds to nucleic acids and permeabilizes bilayers. *Biochemistry* **1997**, *36*, 3008-3017.

112. Plank, C.; Tang, M.X.; Wolfe, A.R.; Szoka, F.C. Branched cationic peptides for gene delivery: Role of type and number of cationic residues in formation and in vitro activity of DNA polyplexes. *Human Gene Therapy* **2004**, *10*, 319-332.

113. Rosslee, C.A.; Abbott, N.L. Principles for Microscale Separations Based on Redox-Active Surfactants and Electrochemical Methods. *Analytical Chemistry* **2001**, *73*, 4808-4814.

114. Hays, M.E.; Jewell, C.M.; Lynn, D.M.; Abbott, N.L. Reversible Condensation of DNA Using a Redox-Active Surfactant. *Langmuir* **2007**, *23*, 5609-5614.

115. Jewell, C.M.; Hays, M.E.; Kondo, Y.; Abbott, N.L.; Lynn, D.M. Ferrocene-containing cationic lipids for the delivery of DNA: Oxidation state determines transfection activity. *Journal of Controlled Release* **2006**, *112*, 129-138.

116. Bennett, D.E.; Gallardo, B.S.; Abbott, N.L. Dispensing Surfactants from Electrodes:‚Äâ Marangoni Phenomenon at the Surface of Aqueous Solutions of (11-Ferrocenylundecyl)trimethylammonium Bromide. *Journal of the American Chemical Society* **1996**, *118*, 6499-6505.

117. Gallardo, B.S.; Metcalfe, K.L.; Abbott, N.L. Ferrocenyl Surfactants at the Surface of Water:‚Äâ Principles for Active Control of Interfacial Properties. *Langmuir* **1996**, *12*, 4116-4124.

118. Shin, J.Y.; Abbott, N.L. Using Light to Control Dynamic Surface Tensions of Aqueous Solutions of Water Soluble Surfactants. *Langmuir* **1999**, *15*, 4404-4410.

119. Eastoe, J.; Dominguez, M.S.; Wyatt, P.; Beeby, A.; Heenan, R.K. Properties of a Stilbene-Containing Gemini Photosurfactant:‚Äâ Light-Triggered Changes in Surface Tension and Aggregation. *Langmuir* **2002**, *18*, 7837-7844.

120. Shang, T.; Smith, K.A.; Hatton, T.A. Self-Assembly of a Nonionic Photoresponsive Surfactant under Varying Irradiation Conditions: A Small-Angle Neutron Scattering and Cryo-TEM Study. *Langmuir* **2006**, *22*, 1436-1442.

121. Cicciarelli, B.A.; Elia, J.A.; Hatton, T.A.; Smith, K.A. Temperature Dependence of Aggregation and Dynamic Surface Tension in a Photoresponsive Surfactant System. *Langmuir* **2007**, *23*, 8323-8330.

122. Cicciarelli, B.A.; Hatton, T.A.; Smith, K.A. Dynamic Surface Tension Behavior in a Photoresponsive Surfactant System. *Langmuir* **2007**, *23*, 4753-4764.

123. Shai, Y. Molecular recognition between membrane-spanning polypeptides. *Trends in Biochemical Sciences* **1995**, *20*, 460-464.

124. Han, X.; Bushweller, J.H.; Cafiso, D.S.; Tamm, L.K. Membrane structure and fusion-triggering conformational change of the fusion domain from influenza hemagglutinin. *Nat Struct Mol Biol* **2001**, *8*, 715-720.

125. Garnier, J.; Gibrat, J.F.; Robson, B. GOR method for predicting protein secondary structure from amino acid sequence. *Computer Methods for Macromolecular Sequence Analysis* **1996**, *266*, 540-553.

126. Meiler, J.; Baker, D. Coupled prediction of protein secondary and tertiary structure. *Proc. Natl. Acad. Sci. U. S. A.* **2003**, *100*, 12105-12110.

127. Lednev, I.K.; Karnoup, A.S.; Sparrow, M.C.; Asher, S.A. α-Helix Peptide Folding and Unfolding Activation Barriers: A Nanosecond UV Resonance Raman Study. *Journal of the American Chemical Society* **1999**, *121*, 8074-8086.

128. Chang, C.-H.; Franses, E. Adsorption dynamics of surfactants at the air/water interface: a critical review of mathematical models, data, and mechanisms.

*Colloids and Surfaces A: Physicochemical and Engineering Aspects* **1995**, *100*, 1-45.

129. Lin, S.-Y.; McKeigue, K.; Maldarelli, C. Diffusion-controlled surfactant adsorption studied by pendant drop digitization. *AIChE Journal* **1990**, *36*, 1785-1795.

130. Song, Q.; Couzis, A.; Somasundaran, P.; Maldarelli, C. A transport model for the adsorption of surfactant from micelle solutions onto a clean air/water interface in the limit of rapid aggregate disassembly relative to diffusion and supporting dynamic tension experiments. *Colloids and Surfaces A: Physicochemical and Engineering Aspects* **2006**, *282-283*, 162-182.

131. Kumar, N.; Couzis, A.; Maldarelli, C. Measurement of the kinetic rate constants for the adsorption of superspreading trisiloxanes to an air/aqueous interface and the relevance of these measurements to the mechanism of superspreading. *Journal of Colloid and Interface Science* **2003**, *267*, 272-285.

132. Jain, V.P.; Maldarelli, C.; Tu, R.S. Modeling the dynamic folding and surface-activity of a helical peptide adsorbing to a pendant bubble interface. *Journal of Colloid and Interface Science* **2009**, *331*, 364-370.

133. Eimer, W.; Pecora, R. Rotational and translational diffusion of short rodlike molecules in solution: Oligonucleotides. *The Journal of Chemical Physics* **1991**, *94*, 2324-2329.

134. Pan, R.; Green, J.; Maldarelli, C. Theory and Experiment on the Measurement of Kinetic Rate Constants for Surfactant Exchange at an Air/Water Interface. *Journal of Colloid and Interface Science* **1998**, *205*, 213-230.

135. Subramanyam, R.; Maldarelli, C. Fluorescence Evidence That a Phase Transition Causes the Induction Time in the Reduction in Dynamic Tension during Surfactant Adsorption to a Clean Air/Water Interface and a Kinetic-Diffusive Transport Model for the Phase-Induced Induction. *Journal of Colloid and Interface Science* **2002**, *253*, 377-392.

136. Lin, S.-Y.; Tsay, R.-Y.; Lin, L.-W.; Chen, S.-I. Adsorption Kinetics of C12E8 at the Air-Water Interface: Adsorption onto a Clean Interface. *Langmuir* **1996**, *12*, 6530-6536.

137. Ward, A.F.H.; Tordai, L. Time-Dependence of Boundary Tensions of Solutions I. The Role of Diffusion in Time-Effects. *The Journal of Chemical Physics* **1946**, *14*, 453-461.

138. Jain, V.P.; Tu, R.S. Coupled Folding and Specific Binding: Fishing for Amphiphilicity. *International Journal of Molecular Sciences* **2011**, *12*, 1431-1450.